Anthropogenic input of heavy metals to near-coastal sediment depocenters in the eastern North Sea and the Hauraki Gulf in historical times

Dissertation zur Erlangung des Doktorgrades der Naturwissenschaften (**Dr. rer. nat.)**

am Fachbereich Geowissenschaften der Universität Bremen

vorgelegt von

Florian Boxberg

Bremen, November 2017

Universität Bremen

INTERCOAST

marum
Zentrum für Marine Umweltwissenschaften

Tag des öffentlichen Kolloquiums

29.01.2018

Gutachter der Dissertation

Prof. Dr. Dierk Hebbeln

Prof. Dr. Anne Bernhardt

Weiter Mitglieder des Prüfungsausschusses

Prof. Dr. Tobias Mörz

Prof. Dr. Michal Kucera

Dr. Gerhard Bartzke

Laura Belter

Versicherung an Eides Statt

Ich,

_____

(Vorname, Name, Anschrift)

versichere an Eides Statt durch meine Unterschrift, dass ich die vorstehende Arbeit selbständig und ohne fremde Hilfe angefertigt und alle Stellen, die ich wörtlich dem Sinne nach aus Veröffentlichungen entnommen habe, als solche kenntlich gemacht habe, mich auch keiner anderen als der angegebenen Literatur oder sonstiger Hilfsmittel bedient habe.

Ich versichere an Eides Statt, dass ich die vorgenannten Angaben nach bestem Wissen und Gewissen gemacht habe und dass die Angaben der Wahrheit entsprechen und ich nichts verschwiegen habe.

Die Strafbarkeit einer falschen eidesstattlichen Versicherung ist mir bekannt, namentlich die Strafandrohung gemäß § 156 StGB bis zu drei Jahren Freiheitsstrafe oder Geldstrafe bei vorsätzlicher Begehung der Tat bzw. gemäß § 161 Abs. 1 StGB bis zu einem Jahr Freiheitsstrafe oder Geldstrafe bei fahrlässiger Begehung.

_____ _____

Ort, Datum Unterschrift

Danksagung

Zunächst einmal möchte ich mich herzlich bei Prof. Dr. Dierk Hebbeln für die Vergabe der Arbeit sowie die sehr gute Betreuung und die sehr angenehme Atmosphäre während der ganzen Zeit bedanken. Ich danke Dr. Willem de Lange und Dr. Bethany Fox für die hilfreichen Diskussionen und Ratschlage während der gesamten Zeit und speziell während meines Neuseeland-Aufenthaltes.

Ich danke Prof. Dr. Anne Bernhardt für die Erstellung des Zweitgutachtens.

Des Weiteren danke ich den restlichen Co-Autoren meiner Manuskripte für die Zusammenarbeit: Prof. Dr. Bernhard Schnetger, Dr. Alexander Bartholomä, Brice Blossier und Sanja Asendorf.

Ein großer Dank geht an die AG Hebbeln für die allzeit tolle Stimmung, für die großartige Unterstützung und natürlich für die tollen Stunden während der morgendlichen Kaffee-Pause.

Mein herzlichster Dank gilt meinen tollen Zimmerkollegen Conny Kwiatkowski, Sandy Boehnert und Jens Weiser, die für jeden Spaß zu haben waren und so für eine allzeit tolle Atmosphäre im Büro gesorgt haben.

Für die Unterstützung im Labor an der Universität Bremen danke ich Dr. Jürgen Titschack und Dr. Daniela Pittauer.

Für die tolle Unterstützung während der Feld- und Laborarbeiten in Neuseeland danke ich herzlich Annette Rodgers, Janine Ryburn, Dirk Immenga und Dr. Vicky Moon von der University of Waikato. Vielen Dank für den IT-Support von Jutta Bülten und die Hilfe bei administrativen Belangen von Carmen Murken und Nicole Bammann.

Weiterhin danke ich der Deutschen Forschungsgemeinschaft für die Finanzierung des INTERCOAST-Programms, welches diese einzigartige und schöne Gelegenheit ermöglicht hat.

Ich danke der ganzen INTERCOAST-Familie für die tolle Zeit an diesem und am anderen Ende der Welt.

Ganz besonders danke ich meiner Familie: meinen Eltern Martina und Theo Boxberg sowie meinen Geschwistern Daniel, Nina, Leonie und Rebecca.

Mein größter Dank gilt meiner besseren Hälfte, Julia Fuchs, die in der ganzen Zeit immer für mich da war und mir in dieser Zeit das größte Glück überhaupt beschert hat: unsere wundervolle Tochter Ida.

Abstract

Since the beginning of the industrial revolution, or even earlier, near-coastal marine ecosystems are affected by various anthropogenic influences. One important example for such influences is the enhanced local or regional input of heavy metals to the marine realm. Anthropogenic sources for such heavy metal inputs are diverse including industrial, agricultural, and pharmaceutical ones, amongst others. One of the biggest sources of anthropogenic heavy metal releases to the environment are mining and smelting of metal ores. The atmospheric and fluvial transports of such emissions can lead to the accumulation of anthropogenically mobilised heavy metals in near-coastal sediment depocenters like the ones studied here: the Helgoland mud area in the German Bight, the Skagerrak in the north-eastern North Sea, and the central Hauraki Gulf on the northeast coast of New Zealand`s North Island. Near-coastal sediment depocenters often provide long, undisturbed sediment records in high-resolution and, thus, are a crucial tool for the reconstruction of anthropogenic heavy metal inputs through time.

In contrast to the largest parts of the North Sea, which are marked by high tidal- and wave-energy levels and continuous sediment redistribution, the Helgoland mud area is characterised by the continuous deposition of fine sediments. Based on the analysis of six sediments cores from the Helgoland mud area, new insights in the spatial and temporal development of anthropogenic heavy metal inputs to the area have been obtained. The anthropogenic induced zinc (Zn) and lead (Pb) inputs, dating back to an onset at ~AD 750, reach back significantly longer than previously estimated. These early heavy metal inputs are attributed to medieval mining and smelting activities in the Harz Mountains and the Erzgebirge. Since the onset of anthropogenic heavy metal inputs, approximately 12,000 tons of zinc and 4,000 tons of lead have accumulated in the Helgoland mud area.

The Helgoland mud area is connected to the Skagerrak, the most prominent sediment depocenter in the North Sea, through the South- and North Jutland Currents. The analysis of three high-resolution sediment cores from the southern flank of the Skagerrak, likewise indicate elevated heavy metal levels (zinc, lead, copper (Cu)) in their uppermost layers. However, the heavy metal enrichment factors (modern vs. background values) indicate generally lower enrichments in the Skagerrak sediments (enrichments factors between ~ 1.25 and 1.5) compared to the sediments of the Helgoland mud area (enrichment factors between

~ 2.0 and 2.9). Early Cu and Pb enrichments beginning at ~AD 1230 probably reflect medieval mining and smelting activities in the Falun copper mining district in central Sweden. Heavy metal inputs originating in the Falun area reach the Skagerrak via direct atmospheric transport and an additional fluvial and marine transport through the northern Kattegat. Enhanced zinc inputs to the southern flank of the Skagerrak only commenced at ~AD 1660 and might be attributed to a long-distance transport of heavy metals from the south-eastern North Sea (incl. the Helgoland mud area) with the South- and North Jutland Currents along the Danish west coast.

On the other side of the globe, sediments from the central Hauraki Gulf, a semi-enclosed coastal embayment on the northeast coast of New Zealand's North Island, do not reveal any signal of anthropogenic heavy metal inputs to the Hauraki Gulf due to the generally low sediment input and the continuous reworking of the sediments. However, the analysis of 14 sediment cores from the central Hauraki Gulf provides new insights in the deposition and reworking of surficial sediments as a consequence of the interactions of wind-generated waves and the modern hydrodynamic regime. Especially under strong meteorological forcing, the hydrodynamic regime is responsible for a N-S gradient in sediment texture and elemental concentrations in the central Hauraki Gulf sediments. In contrast to previous findings described in the literature, the central Hauraki Gulf does not act as a modern sediment depocenter.

The findings of this work generally underline the importance of near-costal sediment depocenters for the reconstruction of historic anthropogenic impacts on the environment and provide new insights in the general sedimentary systems and processes in the studied depocenters.

Zusammenfassung

Küstennahe marine Ökosysteme unterliegen, spätestens seit dem Beginn der industriellen Revolution, großen menschlichen Einflüssen. Ein Aspekt dieser vom Menschen verursachten Veränderungen betrifft den lokalen bzw. regionalen verstärkten Eintrag von Schwermetallen in die marine Umwelt. Anthropogene Quellen von Schwermetallen sind unter anderem industrieller, landwirtschaftlicher und pharmazeutischer Natur. Eine wichtige Quelle gerade für Schwermetalle ist der Abbau sowie die Verhüttung von Metallerzen. Durch atmosphärischen und/oder fluviatilen Transport können Schwermetalle dann in küstennahe marine Sedimentakkumulationszentren gelangen, wie z.B. die hier untersuchten Gebiete: das Helgoländer Schlickgebiet in der Deutschen Bucht, das Skagerrak in der nordöstlichen Nordsee sowie der Hauraki Golf im Norden von Neuseelands Nordinsel. Küstennahe Sedimentakkumulationszentren zeichnen sich insbesondere durch oftmals ungestörte Sedimentabfolgen in hoher Auflösung aus und sind deshalb ein wichtiges Werkzeug für die Rekonstruktion von anthropogenen Schwermetalleinträgen in historischen Zeiten.

Im Gegensatz zu weiten Teilen der Nordsee, die durch starke Gezeiten- und Wellenenergien und eine stetige Sedimentumverteilung geprägt sind, ist das Helgoländer Schlickgebiet gekennzeichnet durch die kontinuierliche Ablagerung von feinkörnigen Sedimenten. Die Ergebnisse aus der Analyse von sechs Sedimentkernen aus dem Helgoländer Schlickgebiet geben neue Erkenntnisse über die räumliche und zeitliche Entwicklung des menschlichen Schwermetalleintrags in das Schlickgebiet. Der menschliche Eintrag von Zink und Blei reicht dabei viel länger zurück als bisher angenommen. Der frühe Eintrag von Zink und Blei seit ca. AD 750 geht vermutlich auf den mittelalterlichen Bergbau im Harz und im Erzgebirge zurück. Seit dem Beginn des anthropogenen Schwermetalleintrags wurden ca. 12.000 t Zink und ca. 4.000 t Blei im Helgoländer Schlickgebiet abgelagert.

Durch den südlichen und nördlichen Jütland-Strom ist das Helgoländer Schlickgebiet mit dem Skagerrak, dem bedeutendsten Sedimentakkumulationszentrum der Nordsee, verbunden. Bei der Analyse von drei hochaufgelösten Sedimentkernen aus dem südlichen Skagerrak zeigt sich ebenfalls eine Schwermetallanreicherung (Zink, Blei, Kupfer) in den obersten Schichten mit Anreicherungsfaktoren (moderne vs. Hintergrund-Werte) von ~ 1.27 bis 1.4, die jedoch geringer ausfällt als die Anreicherung im Helgoländer Schlickgebiet mit Anreicherungsfaktoren von ~ 2.0 bis 2.9. Die frühen anthropogenen Blei- und Kupfer-Einträge beginnen ca. AD 1230

und reflektieren vermutlich den mittelalterlichen Abbau und die Verhüttung von Erzen im Bergwerk von Falun in Mittelschweden. Diese erhöhten Schwermetallkonzentrationen gelangen durch direkten atmosphärischen Transport sowie durch zusätzlichen fluviatilen Transport in das nördliche Kattegat und gelangen auf dem weiteren Weg zur Ablagerung im Skagerrak. Erst ab ca. AD 1660 kommt es auch dort zu einer erhöhten Ablagerung von Zink, die vermutlich aus der südöstlichen Nordsee (inkl. des Helgoländer Schlickgebiets) gespeist wird, von wo ein Transport mit dem Jütland-Strom entlang der dänischen Westküste zum Skagerrak stattgefunden haben kann.

Im Hauraki Golf, einer teilweise abgeschlossenen Bucht im Norden der neuseeländischen Nordinsel, können aufgrund des generell sehr geringem Sedimenteintrags sowie der kontinuierlichen Sedimentumlagerung keine auf anthropogene Einwirkungen zurückzuführenden Schwermetallanreicherungen nachgewiesen werden. Die Analyse von 14 Sedimentkernen aus dem mittleren Hauraki Golf geben hingegen neue Einblicke in die generelle Ablagerung und Umlagerung der Oberflächensedimente als Folge des Zusammenspiels von winderzeugten Wellen und der vorherrschenden Meeresströmungen. Insbesondere während großer Sturmereignisse verursacht die Hydrodynamik einen ausgeprägten N-S Gradienten in der Sedimentzusammensetzung (Korngröße, Elementzusammensetzung) des mittleren Hauraki Golfs. Anders als in der Literatur beschrieben, handelt es sich beim untersuchten Gebiet nicht um ein modernes Sedimentakkumulationszentrum.

Insgesamt unterstreichen die Ergebnisse dieser Arbeit die Bedeutung von küstennahen, marinen Sedimentakkumulationszentren für der Rekonstruktion historischer anthropogener Einflüsse auf die marine Umwelt und geben neue, wichtige Einblicke in die sedimentären Prozesse in den untersuchten Akkumulationszentren.

Table of Contents

List of Figures

List of Tables

1. Introduction

1.1 Motivation

Since the increasing interactions of humans with the environment, humans have increasingly impacted the environment in many ways by utilization and exploiting of its natural resources. One important step in the development of human societies was the utilization and processing of metals as tools and weapons (e.g. Kieinlin et al., 2006; Costa Caramé et al., 2010). First evidences of mining and processing of metals date back to the Copper and Early Bronze Age ~ 4,500 BP (e.g. Leblanc et al., 2000; Kienlin et al., 2006). Traces of mining and smelting of (heavy) metals soon became widespread in the environment due to long-range transports in the atmosphere and in the fluvial and marine realm, with traces of Roman (~ 2,500-1,500 years BP) and Medieval Times (~1,200-600 years BP) coming from Europe even found in Greenland ice cores (Hong et al., 1994; Hong et al., 1996).

Heavy metals are defined as naturally occurring metallic elements with high atomic weight and a density at least five times greater than water (Fergusson, 1990). The group of heavy metals include lead, zinc, cadmium, chromium, copper, nickel, amongst others (Fergusson, 1990). Heavy metals form a group of persistent pollutants; i.e. they cannot be degraded or destroyed potentially leading to irreversible harmful effects on living organisms. Additionally, heavy metals can be subdivided into essential and non-essential heavy metals (Tchounwou et al., 2012). Elements such as copper, chromium, and zinc are essential nutrients necessary for various biochemical and physiological functions, whereas heavy metals such as arsenic, lead, and mercury are considered as non-essential heavy metals. Excess supply of essential and non-essential heavy metals to an organism can result in cellular and tissue damage leading to diseases (Tchounwou et al., 2012). There is a narrow range of concentrations related to beneficial as well as to toxic effects. The toxicity depends on several factors including the dose and route of exposure (Tchounwou et al., 2012).

Human exposure to heavy metals has risen significantly since the industrial revolution due to the significantly increasing use of heavy metals in several industrial, agricultural, domestic, and technological applications and, thus, the release of huge amounts of heavy metals into the air, soils, and the aquatic environment (e.g. Bradl et al., 2012). Environmental problems as a result of the enhanced heavy metal emissions include, e.g., the pollution of soils and the contamination (pollution) of fresh water as possible sources of drinking water. High levels of

heavy metals in the marine environments can likewise impact human health. When heavy metals, buried in sediments, get mobilized they have the potential to harm marine organisms and, thus, negatively influence the marine food chain (Förstner and Müller, 1973). Several studies indicated increased amounts of heavy metals in shellfish and fish potentially affecting human health (e.g. Copat et al., 2013; Leung et al., 2014; Dhanakumar et al., 2015).

A multitude of natural and anthropogenic sources release heavy metals to the environment. The primary natural source is the Earth`s crust. Heavy metals are either weathered or eroded from crustal material or are injected into the atmosphere by volcanic activity (Callender, 2003). A significantly lower amount of heavy metals is released to the environment through forest fires and biogenic sources (Nriagu, 1990). However, since the increasing human usage of the environment, anthropogenic induced heavy metals emissions generally exceed heavy metal emissions that are attributed to natural processes (e.g. Adriano, 1986). Anthropogenic sources are manifold. including industrial, agricultural, pharmaceutical, and domestic effluents, amongst other (He et al., 2005). One of the biggest sources of anthropogenic heavy metal releases to the environment are mining and smelting activities (Alloway, 2013). Other important industrial sources include the burning of fossil fuels, paper procession plants, and industrial sewage systems (Alloway, 2013). Heavy metal sources can generally be subdivided into point sources and non-point/diffuse sources (e.g. Vink et al., 1999a; Salomons et al., 2012). A point source release of heavy metals can be traced back to a single source. Areas located in close proximity to point sources (e.g. mining areas, foundries, smelters, sewage plants) are often marked by environmental pollution (e.g. Candeias et al., 2014; Li et al., 2014). Non-point pollution, however, has rather diffuse sources and cannot be attributed to a specific location or time (e.g. widespread atmospheric emissions, urban storm water runoff) (Salomons et al., 2012).

The two major pathways for heavy metals for-long range transport before eventually becoming incorporated into soils and sediments are via the atmosphere and the aquatic realm (Kersten et al., 1993) (Fig. 1.1). For instance, mining releases heavy metals to the aquatic environments (rivers, lakes, and the sea) as tailings and to the atmosphere as heavy metal enriched dust. Smelting of heavy metals releases metals to the atmosphere as a result of high-temperature refining processes (Callender, 2003). Heavy metals in the aquatic systems are either transported in a dissolved form or in a particulate form as suspended load or bedload and can be transported over long distances. Besides the incorporation in abiotic

compartments (atmosphere, water, sediment), heavy metals can also be distributed into biotic compartments as, e.g., seston and benthic organisms (Fig. 1.1). Heavy metal enriched sediments are preferably deposited in areas close to the point source or in near-coastal areas of sediment deposition, where the marine settings provide less energy than river flow. Heavy metal concentrations generally decrease with distance from the source (e.g. Ek and Renberg, 2001). During the atmospheric transport heavy metals are diluted with increasing distance from the source (e.g. Ek and Renberg, 2001). However, the atmospheric transport is highly dependent on wind direction and strength prior to the wet and/or dry atmospheric deposition (Fig. 1.1). Airborne heavy metals can be transported over thousands of kilometres. Evidences of early smelting activities in Europe could even be observed in Greenland ice cores (Hong et al., 1994; Hong et al., 1996). Fig. 1.1 illustrates a schematic model of major pathways of heavy metals in the marine environment from emission sources to removal processes.

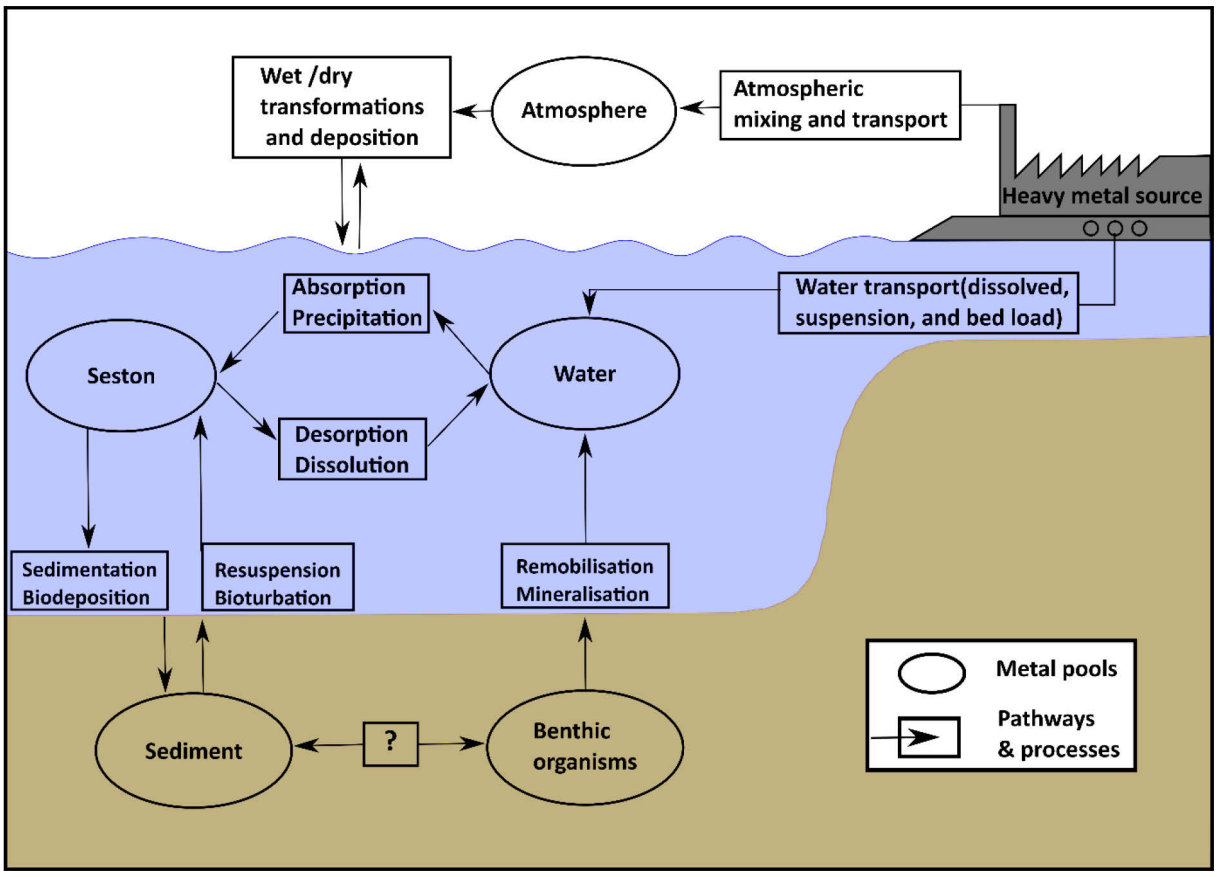

Fig. 1.1 *Schematic figure of major pathways and pools of heavy metals in the marine realm (modified after Kersten et al., 1993). Heavy metals initially reach the environment through atmospheric or water transport (as suspension load, bedload or in a dissolved form). Heavy metical can generally be distributed into biotic (seston, benthic organisms) and abiotic (atmosphere, water, sediment) compartments.*

Even though environmental heavy metal pollution is commonly thought to have commenced as a consequence of increasing heavy metal emissions during the ongoing industrialization, several recent studies found evidences of heavy metal pollution reaching back a lot further than previously thought. Anthropogenic heavy metal enrichments (pollution) in the environment are likely to have started with first mining and smelting activities during the Copper and Early Bronze Age ~ 4,500 BP (e.g. Leblanc et al., 2000; Kielnin et al., 2006; Cortizas et al., 2016). However, small-scale mining and smelting probably only had local environmental impacts. With the increasing need of metals in medieval times, the exploitation of the surficial deposits exponentially increased and, consequently, resulted in larger environmental impacts (Brännvall et al., 2001). With the onset of industrialisation in Europe in the mid-18th century, the exposure to heavy metals became increasingly important, leading to ecological and global public health concerns in recent years. As a result, many efforts were made to decrease heavy metal releases to the environment and to decrease human exposure to heavy metals. Governmental regulations as well as international conventions such as the OSPAR convention (the Convention for the Protection of the Marine Environment of the North-East Atlantic) resulted in first successes of decreased heavy metal inputs into the environment with the ban of leaded gasoline in North America and Western Europe in the early 1990s as the most prominent example (e.g. von Storch et al., 2003). In recent times, heavy metal emissions indicate a decreasing trend in many highly developed countries (e.g. Vink et al., 1999b).

Besides the analysis of ice-cores, which are limited to only few areas on Earth, the study of (marine) sediments is the most common tool for reconstructing anthropogenic induced heavy metal inputs in high-resolution of annual- to decadal-scale (e.g. Lee and Cundy, 2001; Pinedo et al., 2014; Xu et al., 2014). Heavy metals buried in sediments can comprise heavy metals both atmospherically as well as fluvial transported and, hence, can reflect heavy metals of a variety of sources. Especially sedimentary archives in areas of high and continuous sediment inputs as, e.g., near-coastal sediment depocenters, can provide high-resolution paleo-records of historical heavy metal inputs potentially covering the entirety of human impacts on the environment. Furthermore, sediments cover vast areas and, hence, cannot solely be used for reconstructing temporal developments of heavy metal inputs, but also for the reconstruction of the spatial distribution pattern of heavy metals (e.g. Irion et al., 1987). The spatial distribution of heavy metals in sedimentary archives generally provides evidence of transport mechanism and pathways.

Consequently, studying the spatial and temporal evolution of anthropogenic induced heavy metal inputs into near-coastal sediment depocenters is important because it does not only provide insights into the timing of human interactions with the environment, but also helps to improve the general understanding of the sedimentary setting of those environments. In recent times, where the sustainable use of these coastal ecosystems and also their protection has become increasingly important, the detailed knowledge of the sedimentary setting and the processes controlling it is essential, underlining the importance of studying these environments.

1.2 Scientific Objectives and Approach

The abundance of heavy metals in different paleo archives and their spatial and temporal distribution has been subject to many studies in the last decades as a result of increasing concerns caused by significant anthropogenic induced releases of heavy metals to the environment.

These studies are based on different environmental archives, such as water (e.g. Smolders et al., 2003), soil (e.g. Li et al., 2007), marine and lacustrine sediments (e.g. Renberg et al., 2000; Hebbeln et al., 2003), and ice cores (Hong et al., 1994; Hong et al., 1996; Hong et al., 1997). Besides the monitoring of air and water quality in highly industrialized areas, the historic development of anthropogenic induced heavy metal pollution has been subject to several studies. Paleo archives such as marine and lacustrine sediment cores can provide high-resolution paleoenvironmental records and, thus, are suited to study long-term developments of heavy metal inputs to the marine environment (e.g. Lee and Cundy, 2001; Pinedo et al., 2014; Xu et al., 2014).

This thesis focuses on the temporal development of anthropogenic induced heavy metal inputs to three near-coastal sediment depocenters: the Helgoland mud area in the south-eastern North Sea, the Skagerrak in the north-eastern North Sea, and the Hauraki Gulf on the northeast coast of the North Island of New Zealand. Today, the three study sites are bordered by human-impacted, highly industrialized areas. Consequently, the sediment depocenters potentially retrieved anthropogenic induced heavy metal inputs since the onset of industrialisation, or even before. However, huge differences in the long-term development of the catchment areas of the North Sea and the Hauraki Gulf are obvious. While the human interaction with the environment in the North Sea region is ongoing since >7,500 BC (Lotze et al., 2000), New Zealand became the last major landmass to be settled by humans at ~ AD 1,200 (Sutton, 1994). Thus, the North Sea environment has been impacted by humans for about 10,000 yrs, whereas the human development in New Zeeland has a comparatively short history of less than a millennium.

Heavy metals in the Helgoland mud area have already been subject to earlier studies (e.g. Irion et al., 1987; Hebbeln et al., 2003), which drew a coherent picture of Zn-enrichment in near-surface sediments. However, the spatial pattern of the heavy metal enriched sediments, the temporal developments of heavy metal inputs, and the source of the heavy metals remained

uncertain or were controversially discussed. Also heavy metal contents in surface sediments in the Skagerrak have been subject of studies in the past (Zöllmer and Irion, 1993; Kuijpers et al., 1993a), but little is known about the historical development of heavy metal inputs in preindustrial to modern times. However, the close connection between the Helgoland mud area in the south-eastern North Sea and the Skagerrak in the north-eastern North Sea through the Jutland Current suggests a similar development of heavy metal inputs (Fig. 2.1). Likewise, the development of heavy metal inputs to the central Hauraki Gulf has not been studied before. Studies dealing with the long-term anthropogenic heavy metal enrichments focused on estuarine sediments and sediments in natural harbours located around the city of Auckland (Glasby et al., 1988; Abrahim and Parker, 2002). The close proximity to the highly industrialized city of Auckland and the Coromandel Peninsula with its mining history (Clement et al., 2017), however, suggests the central Hauraki Gulf to be a suitable site for the reconstruction of historical anthropogenic induced heavy metal inputs to the marine environment.

This study intends to investigate the long-term developments of anthropogenic induced heavy metal inputs in the three near-coastal marine sediment depocenters. The previous works performed in the study areas resulted in the following objectives of this thesis:

1. Deciphering the historical, anthropogenic induced, heavy metal input to sediments in two key regions of anthropogenic impact on coastal systems, the North Sea (Helgoland mud area and the Skagerrak) and the Hauraki Gulf in New Zealand.

2. Identification of possible heavy metal source areas.

3. Understanding the transport mechanisms of sediments and heavy metals in the study areas.

4. Comparing the presumably long-term human impact on the marine environments in the North Sea with the rather short-term human impacts in the Hauraki Gulf.

The research strategy to address the scientific objectives is to analyse the heavy metal contents in sediment cores of the three study sites. In total 23 sediment cores were retrieved

(6 gravity cores from the Helgoland mud area, 3 gravity cores from the Skagerrak, and 14 Rumohr cores from the Hauraki Gulf; see chapter 3.1) and serve as a base for these analyses.

1.3 Note on Intercoast

The thesis is part of the interdisciplinary International Research Training Group INTERCOAST – “Integrated Coastal Zone and Shelf-Sea Research”, a collaborative project between the Universities of Bremen, Germany, and Waikato, New Zealand that on the German side is funded by the German Research Foundation (DFG). The overall aim of this International Research Training Group is to provide fundamental knowledge on oceanographic, sedimentological, biological, and chemical processes as well as socio-economic interactions and legal effects to support the understanding of coastal and shelf-sea areas for sustainable usage . PhD students with various backgrounds (geosciences, marine biology, social sciences, and legal sciences) are trained to work in an interdisciplinary environment. Furthermore, each Bremen PhD student undertakes a research stay between 6 and 12 months at the partner university to work on the New Zealand-part of the dissertation. Consequently, the field work, laboratory analyses, and interpretations of the “New Zealand data” was conducted at the University of Waikato.

2. Regional setting

To answer the research questions outlined in chapter 1.2, this study focuses on the two key regions of INTERCOAST: the eastern North Sea and the Hauraki Gulf, a semi-enclosed coastal embayment on the northeast coast of the North Island of New Zealand. More specifically the thesis deals with sediments from near-coastal marine sediment depocenters in the North Sea, the Helgoland mud area and the Skagerrak, and in the central Hauraki Gulf. Even though the study areas area separated by nearly 18,000 km of land and ocean, the Helgoland mud area and the Skagerrak show similarities to the Hauraki Gulf, as e.g. relatively high sedimentation rates in close proximity to highly industrialized areas allowing for tracing anthropogenic impacts on the sedimentary system back in time (Knudsen et al., 1996; Manighetti and Carter, 1999; Hebbeln et al.; 2003).

The long-term development of the near-coastal marine ecosystems and sedimentary systems in the study regions is closely related to the human settlement history and their interaction with and modification of the environment and the usage of its natural resources. However, significant differences arise due to the different time scales of human impacts in the two regions. While New Zealand was first settled by Polynesians in the 12th century (Lowe et al., 2000), human footprints in the North Sea region date back to >7,500 BC (Lotze et al., 2000). Consequently, the North Sea region is severely longer impact by humans than the Hauraki Gulf region, which might be visible in the sedimentary records studied in this thesis.

2.1 North Sea

The North Sea in general is a very shallow, semi-enclosed marginal sea of the North Atlantic, located on the European shelf, and widely open to the north (Fig. 2.1). It stretches from 51°N to 61°N (~ 970 km) and from 4°E to 9°E (~ 580 km) covering an area of approximately 750,000 km^2. On average less than 100 m in water depth, the North Sea is characterized by high tidal- and wave- energy levels and the sediment redistribution as a predominating process in shaping the sedimentary environment. Hence, modern-day sediment accumulation is limited to a small number of areas (Lohse et al., 1995) with the Skagerrak being the most prominent depocenter.

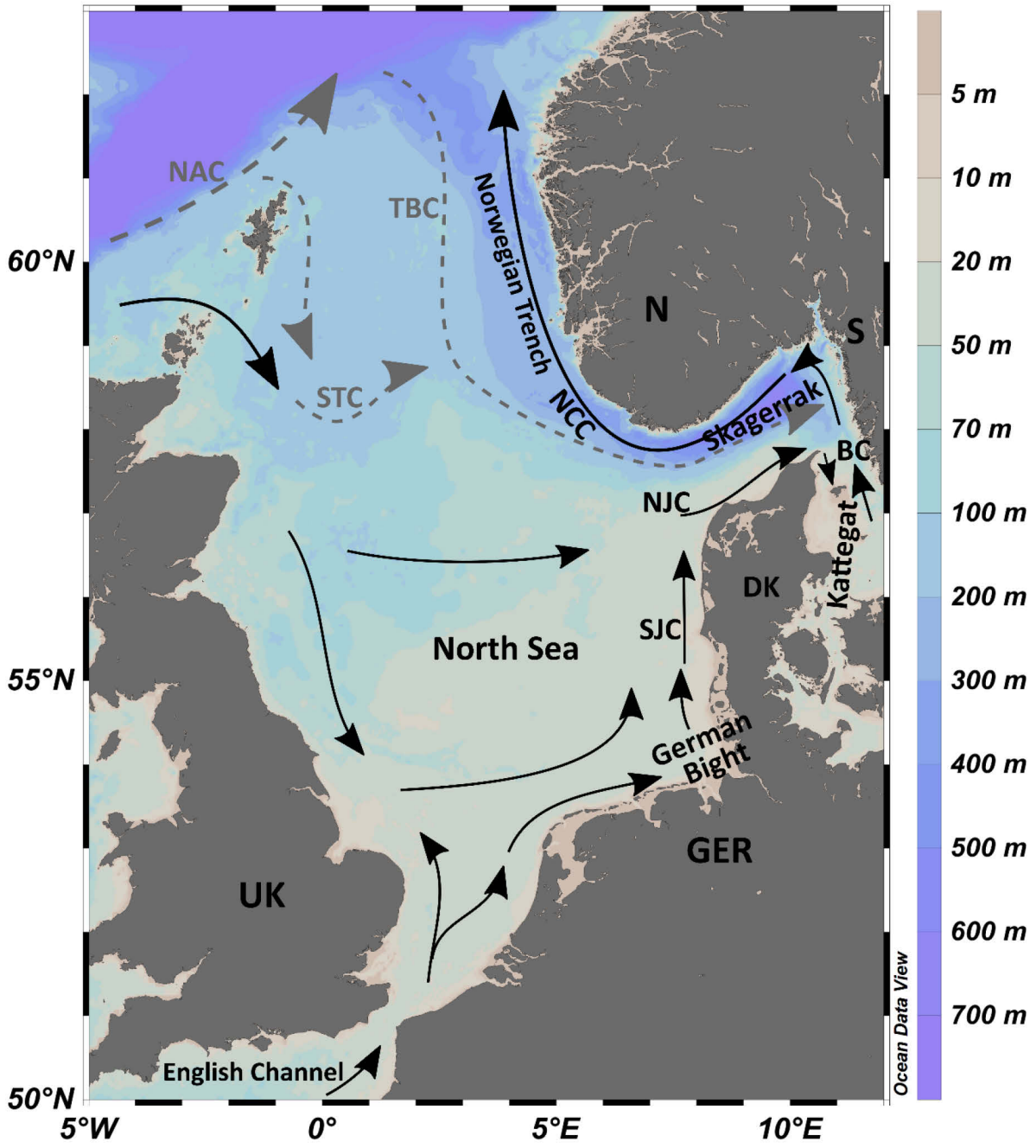

Fig. 2.1 *Bathymetric map of the North Sea showing the prevailing surface currents. Water masses from the North Atlantic directly flowing into the Skagerrak are shown by grey-stippled arrows. Modified water from the North Atlantic is indicated by black arrows. Abbreviations: GER, Germany; DK, Denmark; UK, United Kingdom; S, Sweden; N, Norway; SJJ, South Jutland Current; NJC, North Jutland Current; BC, Baltic Current; NCC, Norwegian Coastal Current; STC, Southern Trench Current; TBC, Tampen Bank Current; NAC, North Atlantic Current. Modified from Danielssen et al. (1991) and Nordberg (1991).*

The North Sea can be subdivided into three main regions according to water depths: the Southern Bight, the Central North Sea, and the Northern North Sea. Water depths in the Southern Bight, covering the area between 51°N and 54°N, are generally low with values of

less than 40 m. The German Bight with a mean water depth of 22.5 m as well as the Helgoland mud area are located in its southern part. The central North Sea is generally deeper with water depths between 40 and 100 m, except for the Dogger Bank and along the western coastline of Denmark. The northern North Sea includes the area north of 57°N with significantly higher water depths of up to > 700 m in the Skagerrak between Denmark and Norway.

The general surface water circulation in the North Sea is anti-clockwise, dominated by three main inflows: North Atlantic waters entering between Scotland and Norway, North Atlantic waters entering via the English Channel between France and Great Britain and less saline Baltic Sea waters entering via Kattegat and Skagerrak (Fig. 2.1) (Rodhe, 1998). The largest amount of water masses entering the North Sea is directly transported eastwards from the North Atlantic into the Skagerrak, mainly following the 100 m contour line. A significantly smaller amount flows from the NW North Sea in southern direction along the British East Coast. Further south, these water masses are complemented by North Atlantic waters entering through the English Channel. On its way along the coasts of Belgium, the Netherlands, Germany, and Denmark in north-eastern direction these waters are strongly modified by freshwater inputs of several large rivers (e.g. Humber, Thames, Rhine, Meuse, Weser, and Elbe) (Rodhe, 1998). These major rivers influence both the chemical composition and the suspension load of the water and contribute significantly to the suspension load of the North Sea waters (e.g. Eisma and Kalf, 1987). On its course further north, these water masses get mixed with those waters entering the North Sea along the 100 m isobath from the North Atlantic and flow into the Skagerrak. In the eastern Skagerrak, these waters get mixed with less saline Baltic Sea outflows and eventually leave the North Sea in eastern direction along the northern slope of the Norwegian Trench. This general circulation pattern can be largely affected by atmospheric forcing (e.g. wind stress and heat flux). For example, the strength of the South Jutland Current and, thus, the supply of North Sea suspended matter to the Skagerrak is largely dependent on small-scale wind stresses over the southern North Sea (Rodhe, 1996).

Coastal areas around the North Sea are mostly highly populated, especially in the southern North Sea. Approximately 80 Mio people inhabit a 150 km wide highly industrialised stretch along the coastlines, which have led to modifications of the coastal environment during times of human settlement in these areas.

2.1.1 Helgoland mud area

The Helgoland mud area, covering an area of approximately 500 km^2, plays a special role in the generally high-energetic North Sea. Besides the Skagerrak in the NE as the most prominent example for the deposition of finer sediments, the Helgoland mud area is the only deposition centre for finer sediments in the southern North Sea with up to 30 m of Holocene sediments in its centre (ignoring the estuaries and intertidal flats, in which a significant amount of sediment is trapped; Figge 1981).The Helgoland mud area is located in the south-eastern North Sea in the German Bight, ~ 25 km north of the mainland of Germany.

Despite generally low water depths of ~ 30 m in the west and ~ 15 m in the east (Fig. 2.2), the sediments in the Helgoland mud area are mainly undisturbed (Hebbeln et al., 2003) and, thus, can be used for paleoenvironmental studies (e.g. Hebbeln et a., 2003; Scheurle et al., 2005; Hebbeln et al., 2006).

The evolution of the Helgoland mud area is controversially discussed. However, this thesis follows the evolutional theory outlined by Hertweck (1983), von Haugwitz et al. (1988), and Mayer (1995). Initially two halotectonic depressions were found south and south-east of Helgoland. The eastern depression, the Helgoland mud area, was filled up with up to 30 m of rather fine-grained Holocene sediments, whereas the western depression, the Helgoland Hole, still exists as a halotectonic depression. Subsequent to the sea level rise ~ 8000 BP to ~ 40 m below the modern sea level, the Elbe-Weser estuary was located at the present-day Helgoland mud area location. The estuary formed a bight that was dammed to the north by the Steingrund Ridge, the connection between the Eiderstedt Peninsula and the island of Helgoland (Fig. 2.2). Pleistocene North Sea sediments, which account for the largest part of the relict Helgoland mud area, were deposited in this bight. The ongoing sea level rise and the erosive wave action in the southern North Sea resulted in the disconnection of the Eiderstedt Peninsula and the island of Helgoland between 1,500 years (von Haugwitz et al. 1988) and 2,000 – 3,000 years ago (Irion et al. 1987). This event marks the establishment of the modern circulation in the south-eastern North Sea with longshore eastwards currents in the southern and northward currents in the eastern German Bight. This is also assumed to be the main trigger for the onset of the still ongoing deposition of suspended particulate matter in the Helgoland mud area (Reineck et al., 1967).

Today, the continuous deposition of mainly muddy sediments, is attributed to a cyclonic, small-scale, anti-clockwise eddy that is driven by the interactions of longshore coastal currents, the discharge from the Elbe and Weser rivers, and tidal dynamics (Hertweck, 1983). This eddy is subdivided into five small-scale eddies with one of them being the main driver for the deposition of fine sediments in the Helgoland mud area (Mayer, 1995). The existence of vertical eddies with the rising side situated above the Helgoland mud area, which appears to be consistent at nearly every wind direction, leads to a net-accumulation of fine suspended particulate matter (SPM) in the Helgoland mud area (Mayer, 1995). Due to the low horizontal velocities, the fine particles, once caught in the vertical eddies, cannot be transported away and start to accumulate at the seabed.

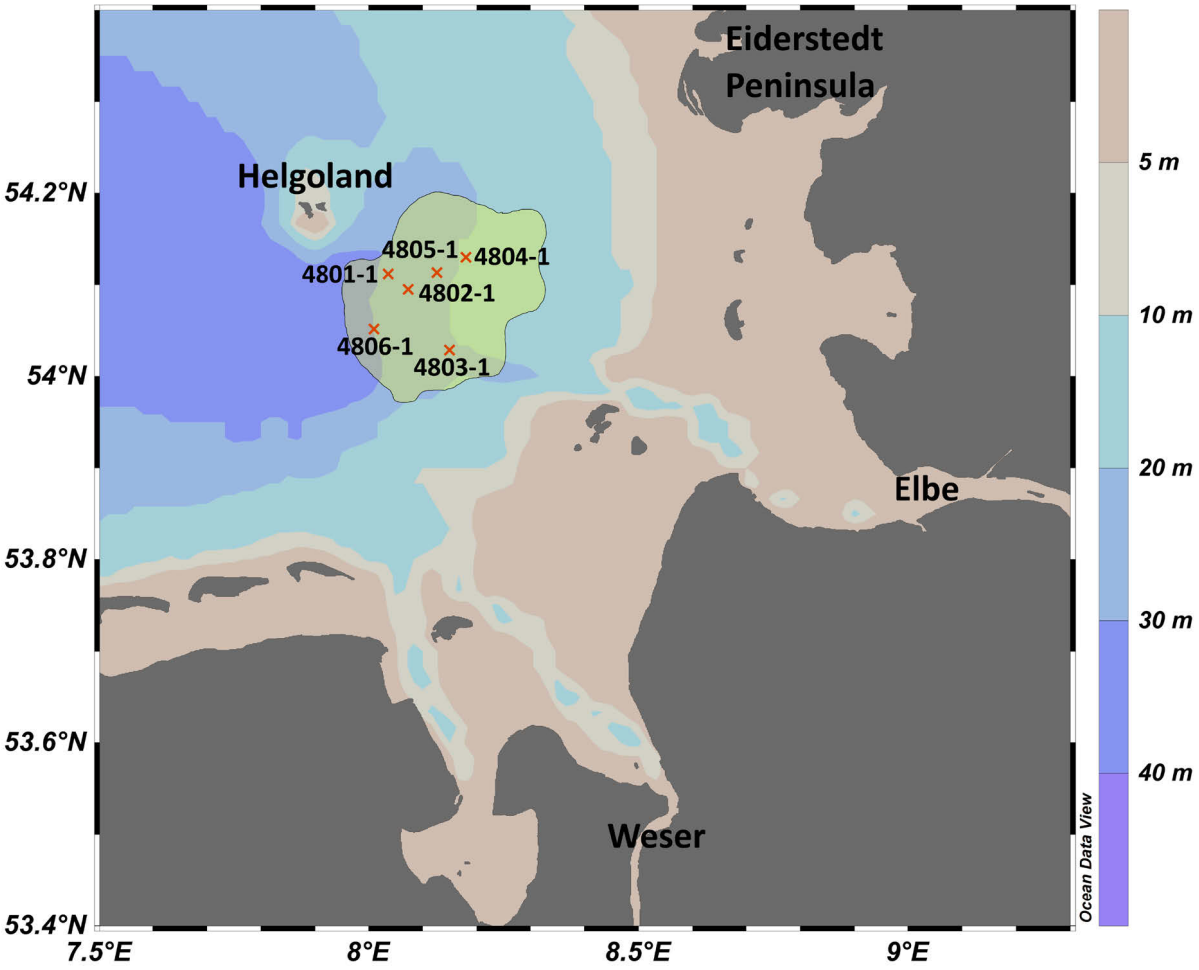

Fig. 2.2 *Bathymetric map of the German Bight in the south-eastern North Sea. The extension of the Helgoland mud area is marked by the yellow-shaded area southeast of the island of Helgoland (after von Haugwitz et al., 1988). Red crosses mark the locations of the six studied sediment cores.*

However, the origin of the accumulated sediments in the Helgoland mud area was controversially discussed in the past. According to Irion et al. (1987), the fine sediment has not been supplied by German rivers (Elbe, Weser and Ems). Under normal condition fine fluviatile sediments are either trapped in the estuaries of the rivers (Milliman and Eade, 1983; Irion et al., 1987) or transported further north and deposited in the Skagerrak (Wirth and Wiesner, 1988). A more recent study by Dellwig et al. (2000) indicated that most of the fine material accumulated in the Helgoland mud area is derived from the back-barrier system of the East Frisian Islands. However, more recent studies clearly showed that at least parts of sediments in the Helgoland mud area are transported to the Helgoland mud area by the Elbe and Weser (Pache et al., 2008), indicated by the close genetic relationship between the sediments in the Helgoland mud area and those of the Elbe River derived from similar K/Rb ratios. Furthermore, Hebbeln et al. (2003) linked the increasing Zn contents in recent sediments to mining activities in the Harz and the Erzgebirge, transported by Weser and Elbe to the Helgoland mud area.

2.1.2 Skagerrak

The Skagerrak as part of the Norwegian Trench, forms the north-eastern extension of the North Sea (Fig. 2.3). With a maximum water depth of ~ 700 m, the Skagerrak is a unique feature of the North Sea, combining both shelf and slope morphology (van Weering et al., 1993a) and serves as a natural sediment trap (Rodhe, 1987). The irregular shape of the Skagerrak is characterised by a steep northern slope and more gentle southern and eastern slopes.

Currents in the Skagerrak are largely controlled by direct inflows from the North Atlantic with important contributions from the South- and North Jutland Current and from less saline Baltic Sea outflows via the Kattegat (e.g. Longva and Thorsnes, 1997) (Fig. 2.3). These currents mix in the Skagerrak, forming an anti-clockwise circulation leading to a considerable decrease of surface current speeds. The reduced current speeds allows far-transported fine-grained sediments in suspension to get deposited - partly with high sedimentation rates - in the southern, central, and eastern Skagerrak (van Weering, 1982; Rodhe and Holt, 1996) making it the most important sediment depocenter in the entire North Sea. The Skagerrak as a natural topographic sediment trap receives inputs from the entire northwest European drainage system and the North Sea coast. The largest amount of these water masses contribute to the

Norwegian Coastal Current (NCC) that leaves the Skagerrak westward. Bottom currents in the Skagerrak generally follow the same patterns as the surface current. However, the velocities are significantly weaker (e.g. Qvale and van Weering, 1985).

The North Atlantic Oscillation (NAO) plays an important role in the circulation of the North Sea and the Skagerrak, because the NAO mainly controls the wind direction and strength towards Scandinavia (Hurrell, 1995; Marshall et al., 2001) and the atmospheric forcing plays an important role in the hydrodynamics of the Skagerrak and the North Sea (Rodhe, 1987; Svendsen et al., 1996; Rodhe, 1996; Longva and Thorsnes, 1997). The high sedimentation rates in combination with the coupling of oceanic and atmospheric circulations (van Weering et al, 1993) make the Skagerrak an ideal place for paleoenvironmental studies (e.g. Nordberg, 1991, Haas, 1993; Heier-Nielsen et al., 1995; Knudsen et al., 1996; Hebbeln et al., 2006).

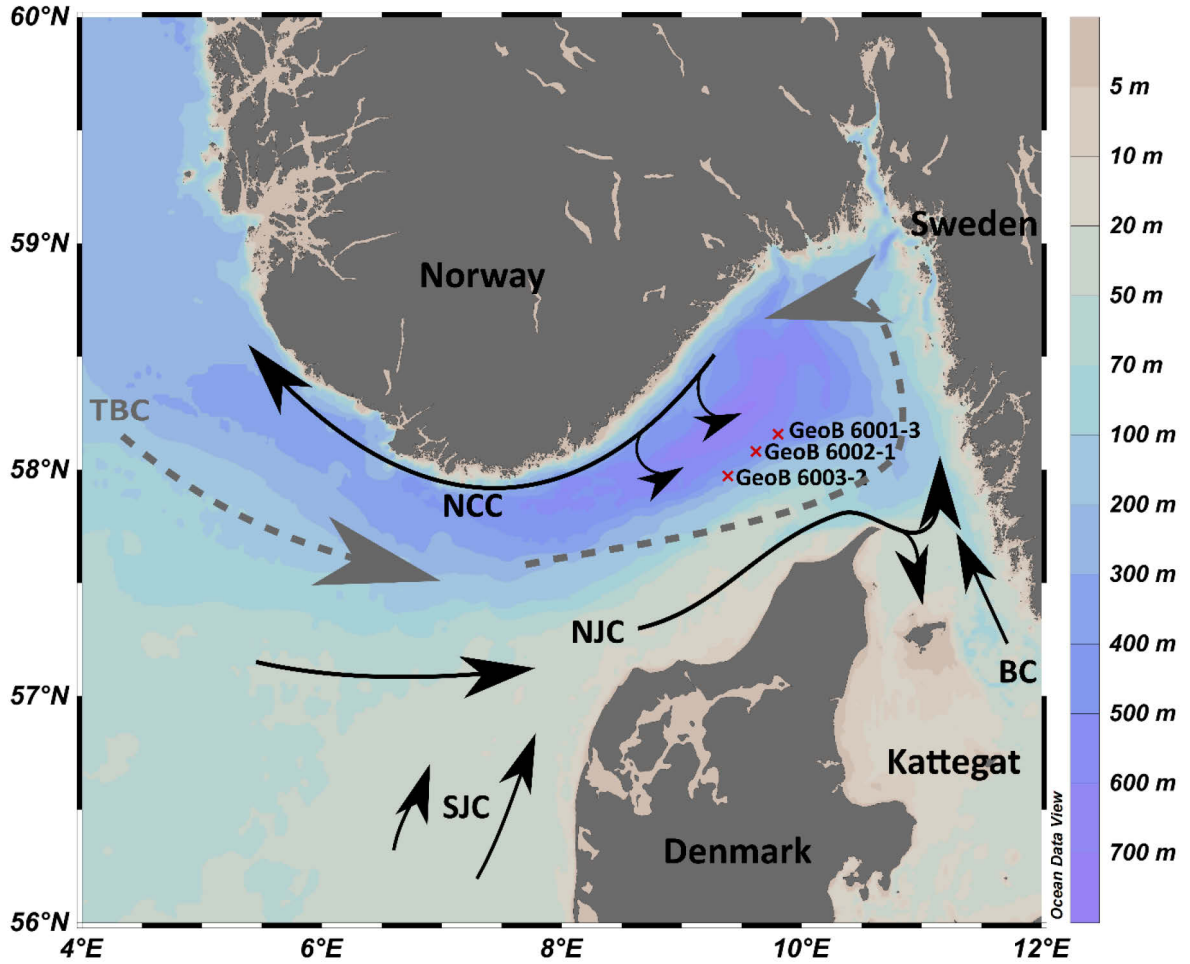

Fig. 2.3 *Bathymetric map of the Skagerrak and the northern Kattegat with the locations of the three studied sediment cores (red crosses) and the prevailing surface currents. Direct inflows of North Atlantic waters are indicated by grey-stippled arrows, modified North Atlantic and Baltic Sea waters are shown by black arrows. Abbreviations: SJC, South Jutland Current; NJC, North Jutland Current; BC, Baltic Current; NCC, Norwegian Coastal Current; TBC, Tampen Bank Current. Modified from Danielssen et al. (1991) and Nordberg (1991).*

Sediments that are accumulated in the Skagerrak mainly derive from the southern North Sea and its major rivers (e.g. Rhine and Elbe) transported to this depocenter by the Jutland Current along the Danish coast (Fig. 2.3). The SPM from Swedish and Norwegian rivers is predominantly trapped in the Scandinavian fjords with only small amounts reaching the Skagerrak through spring meltwater pulses (Svansson, 1975; van Weering, 1981, Eisma, 1981; Kuijpers et al., 1993a; Zöllmer and Irion, 1993). However, the influence of SPM derived from the southern North Sea decrease from the western to the eastern Skagerrak (Nolting and Eisma, 1981). 50-70% of the SPM of the entire North Sea is estimated to be accumulated in the Skagerrak-Kattegat-Norwegian Channel and ~ 50% of the SPM transported annually through the North Sea is assumed to originate from sources in the southern North Sea (van Weering et al., 1993a).

2.2 Hauraki Gulf

The Hauraki Gulf is a partially open coastal embayment on the northeast coast of the North Island of New Zealand (Fig. 2.4). Bounded to the east by the Coromandel Peninsula and to the south and the west by the mainland, the ~ 400,000 km^2 large Gulf is largely protected towards the Pacific Ocean by Great Barrier Island and Little Barrier Island. Water depths in the Gulf vary between < 40m in the inner Gulf south of Tiritiri Matangi Island, <40-50 m in the central Gulf Between Tiritiri Matangi Island and Cape Rodney, and 50-100 m in the outer Gulf between Cape Rodney and the Hen and Chicken Islands (Manighetti and Carter, 1999) (Fig. 2.4). The continental shelf along the north-eastern North Island is typically narrow with < 20 km, but widens to ~ 80 km in the Hauraki Gulf region (Manighetti and Carter, 1999).The central Gulf is relatively flat (slopes 1:1200) but steepens in the outer Gulf reaching gradients of 1:400 towards the shelf break at ~ 150 m water depth. The Firth of Thames marks the southern limit of the Gulf and shoals gradually from 35 m to swampy, estuarine mudflats with a gradient of 1:1500 (Manighetti and Carter, 1999).

The Hauraki Gulf is bordering the largest population centre in New Zealand (Auckland) and, hence, is important for both commercial and recreational activities. It has been subject to a broad range of studies including amongst others sediment distribution (e.g. Carter and Eade, 1980; Eade, 1974; Greig, 1982; Manighetti and Carter, 1999), water circulation in the Gulf (e.g. Greig and Proctor, 1988; Proctor and Greig, 1989; Greig, 1990; Black et al., 2000; Zeldis et al.

2004), geophysical observations of sub-seabed structures (e.g. Hochstein and Nixon, 1979; Thrasher, 1986), organic matter distribution (e.g. Uhle et al., 2007; Sikes et al., 2009), and paleoenvironmental studies (e.g. Greig, 1982; Pocknall et al., 1989).

The water exchange between the open Pacific Ocean and the Hauraki Gulf takes place through three major Channels: Jellicoe Channel, Cradock Channel and Colville Channel (Fig. 2.4). In general, water circulation and currents in the Gulf are driven by the interaction of tidal flows, which concentrate flows through the main Channels, the seafloor topography, and by winds, which create pressure gradients within the Gulf varying in strength with wind direction and magnitude (Black et al., 2000).

Oceanic waters, which enter the Gulf via Cradock, usually leave directly through Colville Channel before entering the central and inner Gulf. Waters entering the Gulf through Jellicoe Channel flows anti-clockwise across the central and inner Gulf, leaving the Gulf through Colville Channel (Greig, 1990) (Fig. 2.4). The net circulation in the Hauraki Gulf is from north to south along its western side, driven by residual currents (Greig and Proctor, 1988; Proctor and Greig, 1989; Sharples, 1997; Black et al., 2000; Zeldis et al., 2004) and in opposite direction on the eastern side of the Gulf. The tidal vertical range in the Gulf varies between ~ 1.35 in the southern Firth of Thames and ~ 0.85 m in the outer Gulf with the tendency of greater values on the eastern side of the inner Gulf and the Channels (e.g. Greig and Proctor, 1988; Black et al., 2000). Tidal currents are generally strongest in the three Channels (Greig and Proctor, 1988). Under common weather conditions, the circulation within the Gulf is dominated by tidal flows. Under meteorological forcing, however, the non-tidal circulation is dominant, mainly driven by the wind direction.

The Hauraki Gulf occupies the northern zone of the active continental Hauraki Rift, which consists of a series of fault-angle basins bounded by active faults striking ~ 340° (Hochstein et al., 1986). These basins are up to 2-3 km deep and have been infilled with inferred Pliocene volcanics, and younger Pleistocene and Holocene sediments. The Pleistocene sediments reach a depth of at least 700 m in the deeper basins (Hochstein et al, 1986; Thrasher, 1986). The uppermost Holocene post transgressive sediment thickness, forming since the flooding of the rift during the last marine transgression, has been estimated by Manighetti and Carter (1999) to be up to 12 m within relatively confined depocenters overlying the fault-angle basins.

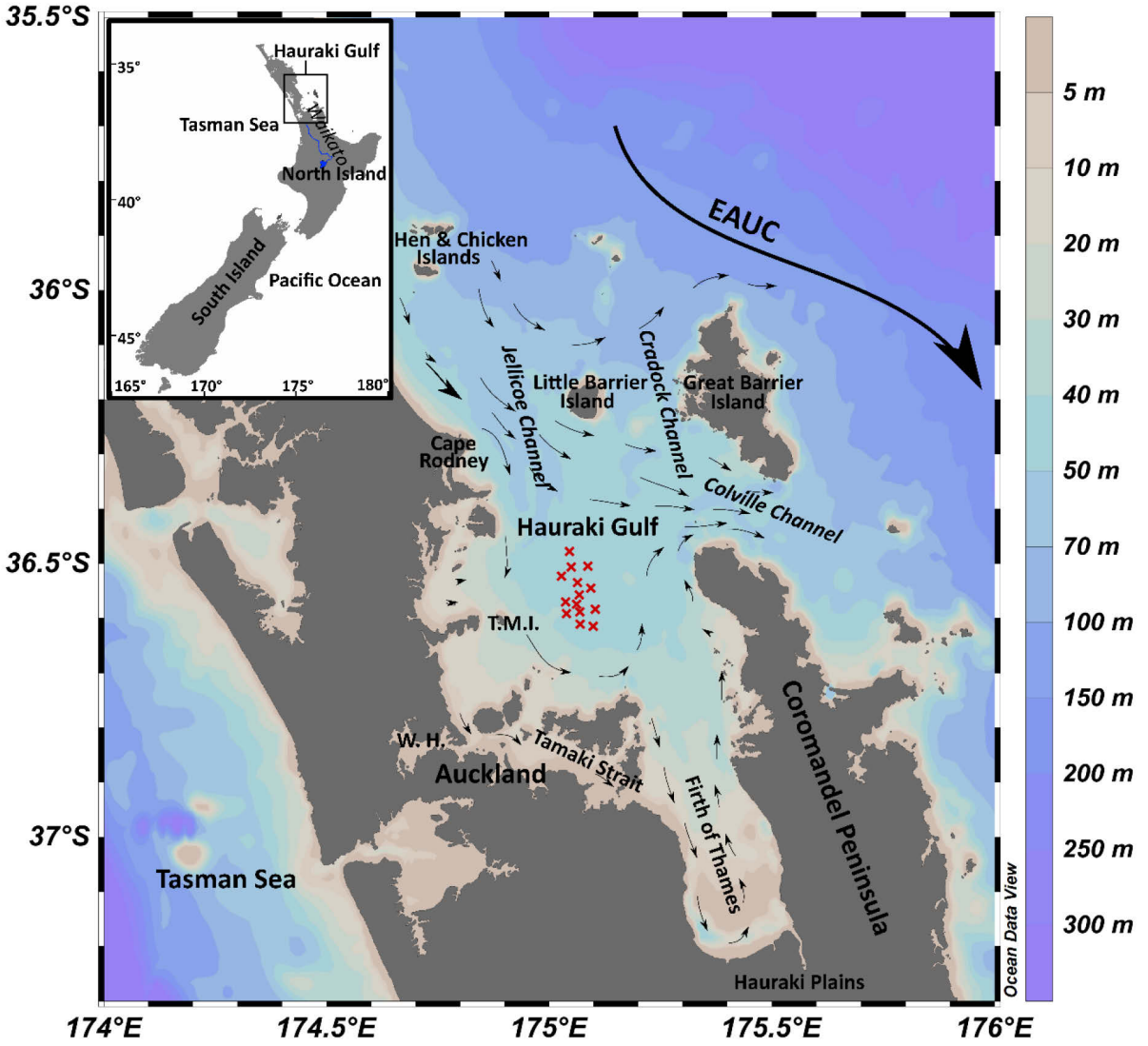

Fig. 2.4 *Bathymetric map of the Hauraki Gulf and the surrounding Pacific Ocean in the E and the Tasman Sea in the W on the northern North Island of New Zealand. Red crosses mark the locations of the studied sediment cores (see chapters 3.1 and 7 for further information on the coring locations). The prevailing surface currents in the Hauraki Gulf according to Black et al. (2000) are indicated by black arrows (W.H., Waitemata Harbour; T.M.I. – Tiritiri Matangi Island; EAUC – East Auckland Current).*

Surficial sediments in the Gulf vary from sandy and calcareous mud in the sheltered Firth of Thames to sandy mud and muddy sand in the northern parts of the Gulf (Eade, 1974; Carter and Eade, 1980; Greig, 1982). The grain-size distribution in the Gulf is mainly controlled by the distribution of waves and currents rather than by depth (Sikes et al., 2009), as indicated by finer sediments in the sheltered areas. Sedimentation rates in the southern and central Gulf were inferred to be higher and with a higher proportion of fine particles than in the more energetic outer Gulf, due to the divergence and weakening of the currents in southern direction (Sikes et al., 2009). Today the terrigenous sediment input is rather low, consists

mainly of mud and fine sands, and is supplied by several small rivers (Manighetti and Carter, 1999). However, the bulk of the supplied terrigenous sediments gets trapped within estuaries and sheltered embayments as e.g. the Firth of Thames (Carter and Eade, 1980; Greig, 1982).

The main factor for the redistribution of the sediments in the Gulf are near-bottom currents, which are affected by tides, winds and oceanic incursions of the East Auckland Current (Manighetti and Carter, 1999) (Fig. 2.4). Meteorological forcing may produce larger storm-waves with the potential to stir the seafloor down to 100 m water depth and, hence, the potential to sediment reworking (Manighetti and Carter, 1999).

The catchment area of the Hauraki Gulf is comprised of industrialised urban areas (Auckland), agricultural areas (e.g. Hauraki Plains), and natural areas (Coromandel Peninsula). The river catchment of the Hauraki Plains make the largest contribution to the catchment of the Hauraki Gulf. Situated at the southern end of the Firth of Thames, these catchments comprise ~47% of the total river catchment area of the Hauraki Gulf (Hauraki Gulf Forum, 2011). The second largest catchment area is the eastern side of the Coromandel Peninsula contributing 18% of the total river-catchment area. The remaining third of the total catchment area is made up of the western Coromandel Peninsula, the Tamaki Strait, and the western Gulf north of Waitemata Harbour, which each contribute around 8 % to the total area, and the Waitemata catchment, which contributes 5 % to the total area and the western Firth of Thames and Barrier Islands, which each contribute around 3 % to the total area (Hauraki Gulf Forum, 2011).

The Waikato River, New Zealand's longest river with a total length of ~ 425 km, is draining the central volcanic region of New Zealand`s North Island and has been the major supplier of sediments in the Hauraki Gulf in the past. However, approximately 22.5 ka ago, the river changed its course from flowing into the glacial alluvial plain of the modern Hauraki Gulf to flowing into the Tasman Sea (Manville and Wilson, 2004)and, thus, is not delivering sediments to the Gulf in recent times. The central Hauraki Gulf with water depths of ~ 45 m was flooded by the marine transgression between 12 ka and 9.5 ka B.P. (Smith, 1992).

3. Material and Methods

3.1 Material

In this study, a total of 23 sediment cores have been investigated: Six gravity cores from the Helgoland mud area, three gravity cores from the central Skagerrak, and 14 Rumohr cores from the Hauraki Gulf (Table. 3.1).

The six gravity cores from the Helgoland mud area were collected during the RV Meteor cruise M40/0 in 1997 in water depths ranging from 21 to 29 m. Core lengths vary between 6.87 m (GeoB 4804-1) and 11.41 m (GeoB 4801-1) (Table 3.1). The sediments generally consist of olive-green to brown to grey-black coloured clayey silts with varying amount of fine sands.

The sediment cores obtained in the central Skagerrak were taken in 1999 with a gravity corer during RV Meteor cruise M45/5 in water depths between 312 and 466 m. The core lengths range from 3.83 m to 10.92 m (Table 3.1). In general, the sediments the sediment consist of clay and silt with small proportions of sand.

The set of 14 sediment cores from the central Hauraki Gulf were taken in 2015 from aboard the MV Macy Gray. Different to the sediment cores from the Helgoland mud area and the Skagerrak, the sediment cores from the Hauraki Gulf were taken with a Rumohr type gravity corer. The Rumohr Corer is especially designed to take short, undisturbed sediment cores from the seafloor surface with an undisturbed sediment/water boundary. In contrast to a common gravity core used to retrieve the sediment cores in the Helgoland mud area and the Skagerrak and usually is operated from large research vessels, the Rumohr corer can be operated from smaller vessels in shallow near-coastal areas.

With a total weight of ~80 kg, the corer consisted of a 1m long plastic tube fitted with metallic weights and a lid on the top opening. The corer was released with a speed of 0.5 m/s to the seafloor. As soon as the corer hit the seafloor, the tube sunk into the sediments solely by gravity and the mechanism keeping the lid open was disengaged. By pulling up the corer, the lid sealed the top opening causing a suction that prevents the sediment from sliding out of the tube. As soon as the corer is on deck, the bottom of the tube is sealed with a rubber plug. The relatively short cores with lengths between 0.13 m and 0.57 m were retrieved in water depths between 44.5 and 47.7 m (Table 3.1). The sediments generally consist of olive green fine sands with varying amounts of finer and coarser particles. Several sediment layers with a great proportion of shell debris were found in the cores.

Table 3.1 Site information of the sediment cores used in this study.

	Core identification	Latitude	Longitude	Water depth (m)	Core length (m)
Helgoland mud area	**GeoB 4801-1**	054° 06.7' N	008 02.2' E	25	11.41
	GeoB 4802-1	054° 05.7' N	008 04.4' E	25	8.01
	GeoB 4803-1	054° 01.7' N	008 09.0' E	22	7.25
	GeoB 4804-1	054° 07.8' N	008 10.8' E	20	6.87
	GeoB 4805-1	054° 06.8' N	008 07.6' E	21	7.34
	GeoB 4806-1	054° 03.1' N	008 00.6' E	29	7.40
Skagerrak	**GeoB 6001-3**	058° 09.4' N	009° 48.3' E	466	3.83
	GeoB 6002-1	058° 04.8' N	009° 37.2' E	430	4.88
	GeoB 6003-2	057° 58.3' N	009° 23.2' E	312	10.92
Hauraki Gulf	**NZ-IC- 1**	036° 36.795' S	175° 4.107' E	44.5	0.57
	NZ-IC- 2	036° 36.897' S	175° 5.963' E	45.8	0.42
	NZ-IC- 3	036° 35.019' S	175° 6.256' E	47.1	0.40
	NZ-IC- 4	036° 35.308' S	175° 4.131' E	44.1	0.31
	NZ-IC- 5	036° 35.514' s	175° 02.321' E	45.3	0.57
	NZ-IC- 6	036° 34.490' s	175° 3.724' E	44.9	0.34
	NZ-IC- 7	036° 34.225` S	175° 02.237' E	45.6	0.30
	NZ-IC- 8	036° 33.444' S	175° 04.054' E	45.1	0.42
	NZ-IC- 9	036° 32.719' S	175° 05.646' E	46.5	0.34
	NZ-IC- 10	036° 32.097' S	175° 03.689' E	45.5	0.32
	NZ-IC- 11	036° 31. 397' S	175° 01.767' E	46.2	0.20
	NZ-IC- 12	036° 30.308' S	175° 05.244' E	45.5	0.13
	NZ-IC- 13	036° 30.374' S	175° 02.969' E	46.9	0.23
	NZ-IC- 14	036° 28.697' S	175° 02.744' E	47.7	0.20

3.2 Methods

3.2.1 X-Ray Fluorescence Analysis

The X-Ray Fluorescence (XRF) Analysis is a widely used tool for the determination of elemental contents in many different disciplines. For the determination of heavy metal compositions in the sediments in the study areas described in chapters 2.1 and 2.2, three different types of XRF analyses were used, providing different types of data: semi-quantitative data (energy dispersive XRF core scanner analysis and energy dispersive Handheld XRF analysis) and quantitative data (wavelength dispersive XRF analysis).

The principle of the XRF analysis is based on the excitation of electrons by incident X-radiation (Weltje and Tjallingii, 2008). An electron is ejected from an inner shell of an atom under the influences of incoming X-radiation. The ejections of electrons create vacancies in the inner shells, which are filled by electrons falling back from an outer shell (Wejtje and Tjallingii, 2008) and the energy difference between both shells, the surplus energy, is emitted as a pulse of secondary X-radiation (Weltje and Tjallingii, 2008) (Fig. 3.1). The emitted fluorescence energy as well as the wavelength spectra characteristic for atoms of a specific element are detected, allowing for the estimation of their relative abundances.

3.2.1.1 X-Ray Fluorescence Core Scanner (energy-dispersive)

The analysis of elemental compositions of whole sediment cores is an essential tool for the reconstruction of past environmental and climate changes over time. Elemental composition and ratios can be used as proxies to reconstruct temperature, rainfall, vegetation cover (e.g. Croudace and Rothwell 2015), aeolian dust input (e.g. Arz et al., 2001, 2003; Bozzano et al., 2002; Andres et al., 2003; Hanebuth and Lantzsch, 2008; Hanebuth and Henrich, 2009) precipitation and river runoff (e.g. Haug et al., 2001; Jahn et al., 2005; Itambi et al., 2009; Holzwarth et al., 2010; Kissel et al. 2010), anthropogenic pollution (e.g. Guyard et al., 2007; Miller et al., 2014) and several others.

XRF Core Scanning is a modern, commonly used tool for the rapid determination of elemental compositions in high-resolution. XRF core scanners provide the capability to rapidly and non-destructively determine semi-quantitative elemental composition of major and minor elements and proxy variations in very small scales. The determination of element intensities

directly at the surface of split sediment cores is the major advantage over conventional geochemical analysis of discrete samples.

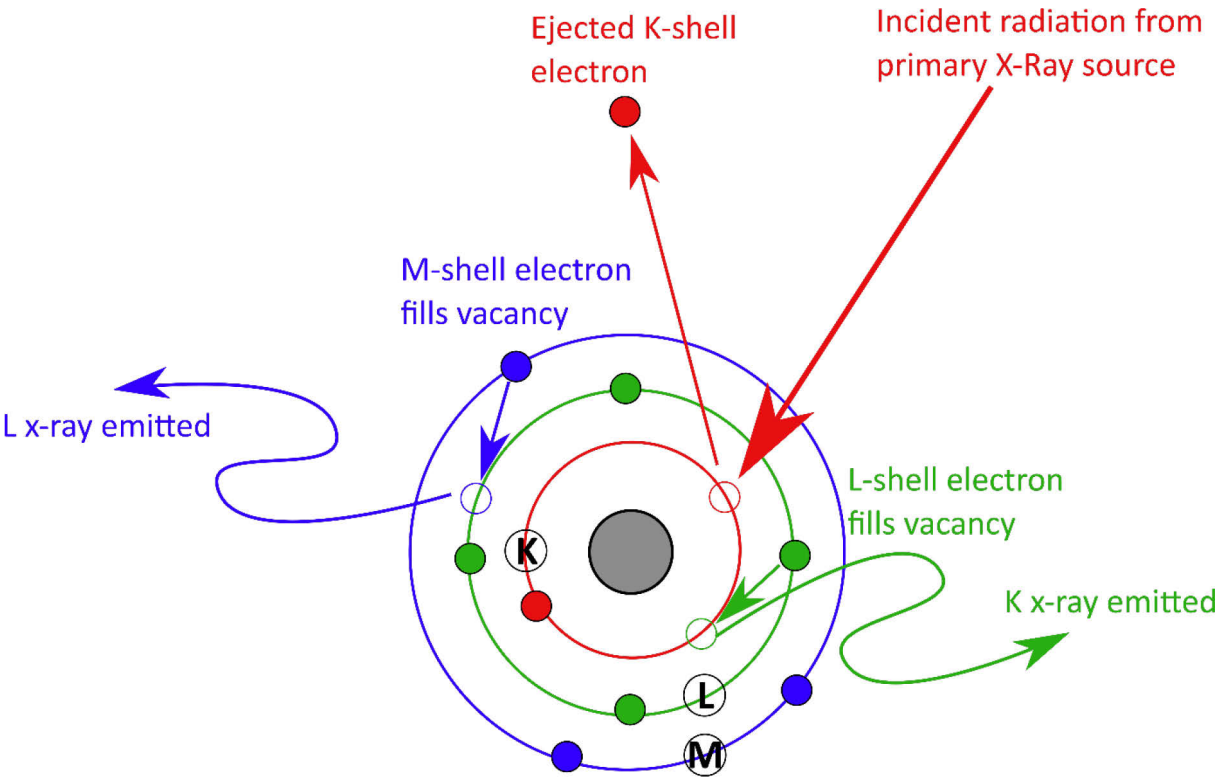

Fig. 3.1 *Principle approach of the XRF analysis. Incident X-radiation leads to the ejection of electrons from an inner shell of an atom (modified after Jansen, 2003).*

The XRF core scanning of the sediment cores from the Helgoland mud area (see chapter 5) was carried out at MARUM, the Centre for Marine Environmental Sciences of the University of Bremen, using an AVAATECH (Serial No. 12) XRF core scanner. Prior to the scanning, the sediment cores were split into two halves, the working half and the archive half. The archive half was covered with a 4 µm thin SPEXCerti Prep Ultralene 1 foil to avoid contamination of the XRF measurement unit and desiccation of the sediment. The measurements were performed over a 1 cm^2 area with a down-core split size of 10mm using generator settings of 30 kV, a current of 1.0 mA, and a sampling time of 20 seconds directly at the split core surface. A Canberra Digital Spectrum Analyzer DAS 1000 and an Oxford Instruments 100W Neptune X-ray tube with Rhodium (Rh) target material was used for the acquisition of the data. Raw data were processed by the Iterative Least square software (WIN AXIL) package from Canberra Eurysis. The measurement interval was 1 cm for the Helgoland mud area sediment cores and the Skagerrak sediment cores, but was increased to 2cm intervals in the lower sections of the

mud area cores. The resulting data is reported in counts per 20 seconds (cp20s) giving semi-quantitative elements amount.

3.2.1.2 X-Ray Fluorescence Spectrometer (wavelength-dispersive)

As the XRF core scanning method only provides semi-quantitative elemental contents, it is necessary to calibrate the data when element concentration are needed/wanted. In contrast to the XRF core scanner analysis, the quantitative determination of element concentrations via wavelength-dispersive XRF-spectrometer (WD-XRF) is destructive (Beckhoff et al., 2006). In general, WD-XRF analysis uses the same method as the XRF core scanner with the detection of the emitted fluorescence energy as a consequence of the excitation of electrons by incoming X-radiation. However, WD-XRF analysis uses an analysing crystal to disperse the different energies. The crystal diffracts all the X-rays with different energies (wavelengths) in different directions allowing for the determination of the intensities of each wavelength (Beckhoff et al., 2006). These intensities are used to estimate the quantitative amount of elements in a sample.

For the calibration of the semi-quantitative XRF core scanning data of the sediments from the Helgoland mud area, 66 discrete specimens of 10 cm^3 at positions corresponding to the XRF core scanner measurements were taken, freeze dried and grounded using a mortar and a pestle (see chapter 5). Prior to the analysis, the samples were weighted into a ceramic crucible (700 ± 0.6 mg) and mixed with 4200 ± 1 mg of a di-lithium tetraborate fusion flux (Spectromelt® A10, Merck) and with about 1000 mg of ammonium nitrate. Subsequent to the pre-annealing for ~ 1 hour at 500° C, the specimens were fused and transformed into glass beads and measured via wavelength dispersive XRF-spectrometry (WD_XRF) at the ICBM, Institut für Chemie und Biologie des Meeres, at the University of Oldenburg. International reference material (GSR_6) and in-house standards (Peru-1, Loess 1.6) were used for the determination of accuracy and precision of the method.

3.2.1.3 X-Ray Fluorescence Handheld Analyser (energy-dispersive)

Elemental concentrations of sediments in the Hauraki Gulf, New Zealand, were determined using the energy-dispersive Olympus Innov-X Delta 50 keV Handheld XRF Analyser gun (Olympus Innov-X 50KV DP4050CX) (see chapter 7). The emitted fluorescence energy is detected and allows for the determination of major and minor elements. The generated data is reported in ppm, but has to be regarded as semi-quantitative, due to the missing calibration.

Approximately 1 mg of each sample was grounded and homogenized using mortar and pestle. In the next step, the sample was filled into a sample cup and covered with a thin Mylar film. Prior to the measurements, the Handheld XRF Analyser gun was set to “soil mode” and mounted in a benchtop stand. The content of major and trace elements were recorded by the Innov-X Delta Advanced PC software. The following elements were analysed: P, S, Cl, K, Ca, Ti, V, Cr, Mn, Fe, Co, Ni, Cu, Zn, As, Se, Rb, Sr, Y, Zr, Nb, Mo, Ag, Cd, Sn, Sb, Te, W , Au, Hg, Pb, Bi, Th, U. Except for P, the limits of detection for these elements are all in the ppm range. Scanning time was approximately 90 seconds per sample. An international reference material (Green River Shale, SGR-1), measured after every 10^{th} sample, has been used to determine accuracy and precision of the method.

3.2.2 Age determination

An essential tool for reconstructing the long-term development of heavy metal enrichments in the marine realm is the determination of absolute ages. Radiometric dating methods suitable for the Holocene chronology of sediments are numerous (Fig. 3.2). In order to establish robust age-depth relationships of the sediment cores, the most common radionuclide dating methods for the Holocene chronology, the Accelerator Mass Spectrometry (AMS) ^{14}C (radiocarbon) , was used.

3.2.2.1 Radiocarbon dating

The AMS ^{14}C dating is a widely used tool for the age determination of organic samples younger than 45 ka (e.g., Lowe and Walker, 2014). With a half-life of ~5,730 years (Godwin, 1962), AMS ^{14}C dating is the most common tool in reconstructing Holocene environments.

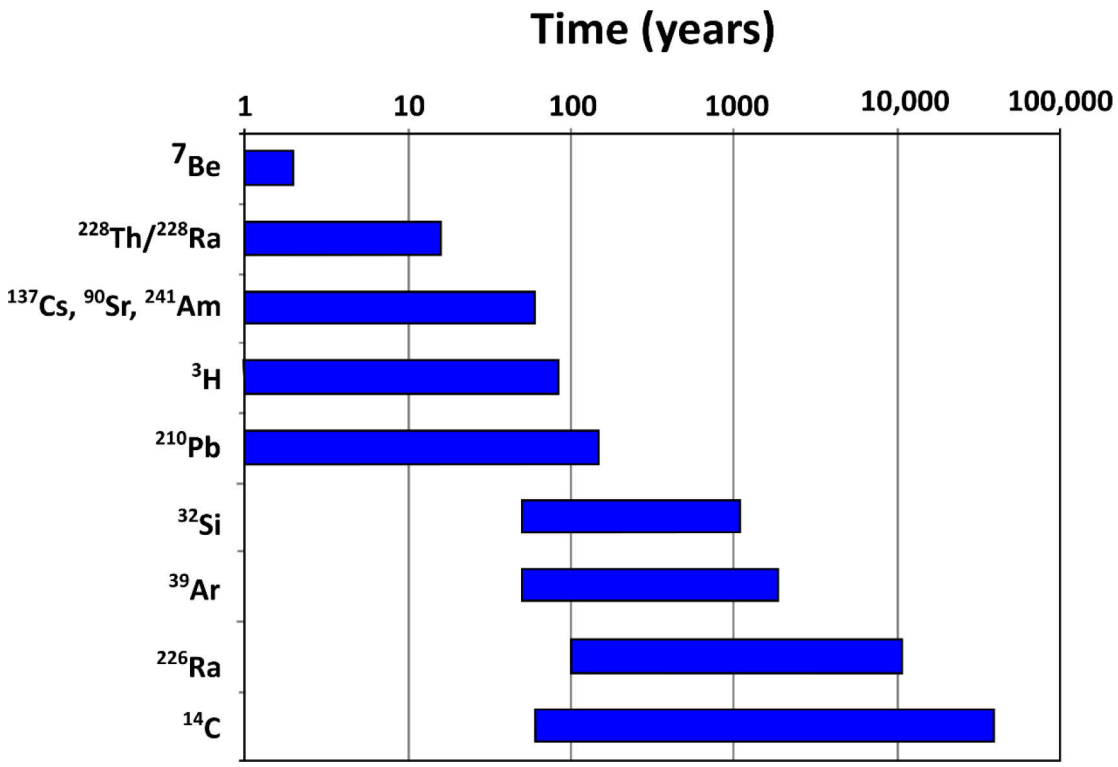

Fig. 3.2 *Timescale of radiometric dating methods suitable for the Holocene chronology of sediments with approximate age ranges (modified after Pittauerová, 2013).*

The radiocarbon dating method is based on the radioactivity of ^{14}C, one of three carbon isotopes naturally occurring on Earth. The radioactive ^{14}C isotope is constantly formed in the upper atmosphere due to the effects of cosmic rays on ^{14}N atoms (Bowman, 1990). ^{14}C in the atmosphere is rapidly oxidised to $^{14}CO_2$. By means of photosynthesis, $^{14}CO_2$ is absorbed from the air by plants, enters the food chain, and, hence, gets absorbed by all kinds of animals (Geyh and Schleicher, 2012). After death, ^{14}C in organisms is not replenished anymore and continues decaying, whereas ^{12}C remains constant in the organisms (Fig. 3.3). The comparison of the $^{14}C/^{12}C$ ratio in the dead organic matter with that ratio in the atmosphere enables the determination of the radiocarbon age, the time between the measurement and the death of the organism (Bowman, 1990). This assumes that the initial concentration of ^{14}C in the atmosphere was the same as today. In the past, it was assumed that the concentration of ^{14}C remains constant in living organisms due to the constant assimilation of ^{14}C from the atmosphere. However, the atmospheric ^{14}C concentration in the atmosphere in the last 50 ka has varied significantly. Therefore, different correction methods have to be applied to account for the effects of isotopic fractionation, past variations of atmospheric ^{14}C and reservoir effects (Stuiver and Polach, 1977).

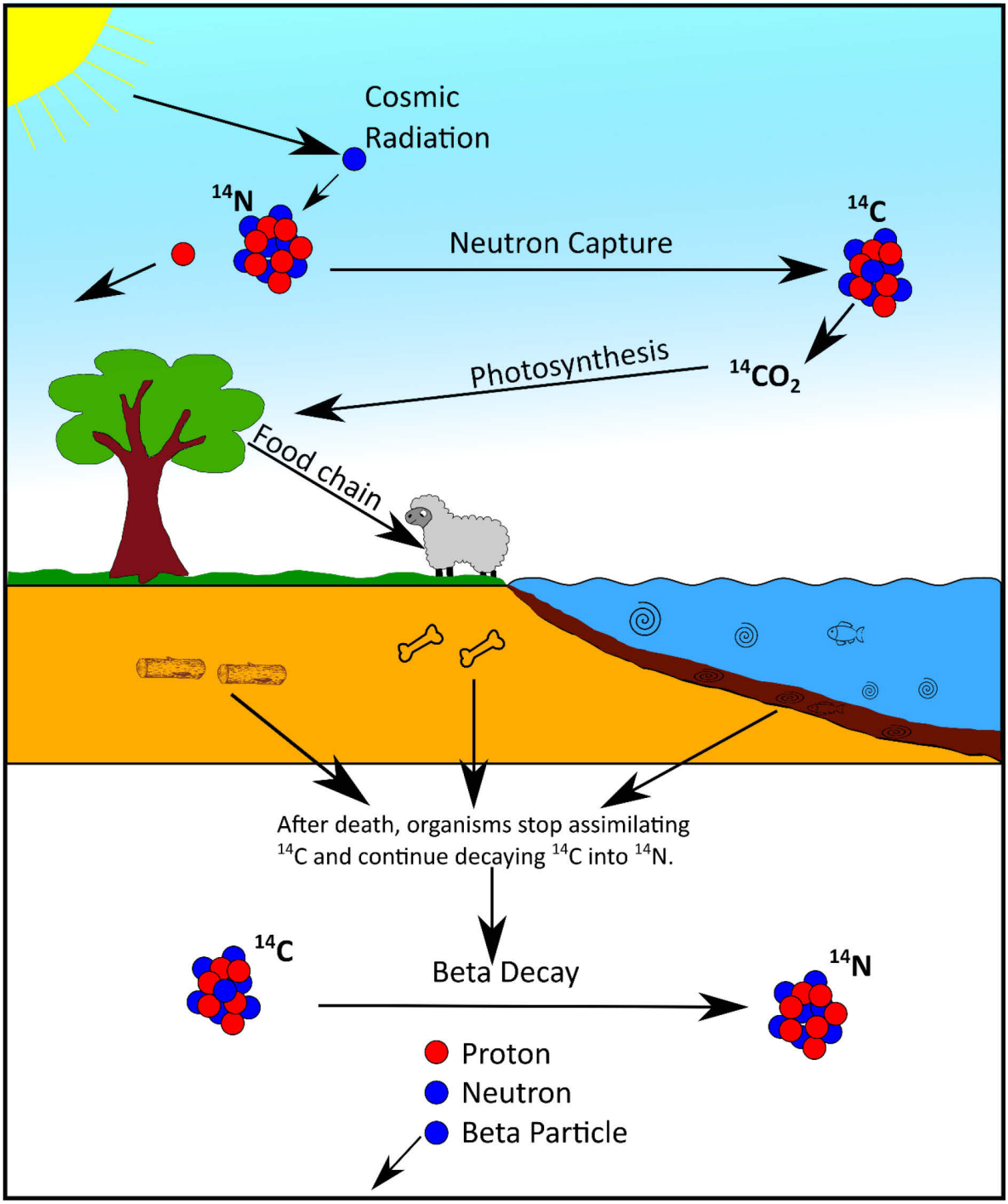

Fig. 3.3 *Principles of radiocarbon dating. Cosmic rays in the atmosphere collide with atoms and produce secondary cosmic rays in the form of a neutron. When the neutron collides with ^{14}N, it converts into ^{14}C. ^{14}C, together with ^{12}C and ^{13}C, is constantly absorbed by living plants for the purpose of photosynthesis and to other organisms via the food chain. After death, organisms stop absorbing ^{14}C and start to decay ^{14}C to ^{14}N, whereas ^{12}C remains constant. The $^{14}C/^{12}C$ ratio in the dead organic matters enables the time between the measurement and the death of the organism.*

Isotopic fractionation takes into account the different carbon isotope ratios in organisms, which differ from the ratios in the atmosphere. ^{14}C concentration in the atmosphere changed over time (Bowman, 1990). This has been shown by comparing tree rings with known calendar

ages to radiocarbon measurements. Calibration curves based on the calendar ages of tree rings enable to calibrate radiocarbon ages to calendar ages. Furthermore, the reservoir effect of radiocarbon has to be taken into account. Organisms that receive carbon from other sources than the atmosphere (e.g. from ocean water) usually indicate lower $^{14}C/^{12}C$-ratios, known as the reservoir effect. The measured radiocarbon age in marine sediments is, therefore, commonly too old and has to be corrected for the reservoir effect. Typical reservoir ages in the marine realm range between 300 and 800 years but can also be substantially higher in upwelling regions (Reimer and Reimer, 2001).

The radiocarbon method was applied to sediment samples from all three study regions. The method was applied to either mixed benthic foraminifera or macroscopic bivalve and gastropod shells. For the radiocarbon dating of foraminifera, samples were wet-sieved over 500, 150, and 63 µm mesh size sieves and oven dried for 24 hours. Benthic foraminifera were picked from the fraction 150-500 µm and approximately 10 mg of it were sent either to Beta Analytics Radiocarbon lab in London, United Kingdom or to Poznań Radiocarbon Laboratory in Poznań, Poland. Measured conventional radiocarbon ages were converted into calendar years using the Calib 7.1 software (Stuiver et al., 2017) and the Marine13 calibration curve (Reimer at al., 2013). The global mean reservoir age of 400 years (Bard, 1998) was confirmed for Danish waters (Heier-Nielsen et al., 1995) and for East coast marine waters, NZ (Higham and Hogg, 1995) and, thus, also used for the samples from the Helgoland mud area and the Hauraki Gulf.

Well established age models were used for cores GeoB 4801-1 (Scheurle et al., 2005) from the Helgoland mud area and GeoB 6003-2 (Hebbeln et al., 2006) from the Skagerrak.

3.2.3 Particle Size Analysis

The analysis of particle size distributions is a useful tool allowing for the identification of transport mechanisms and hydrodynamics affecting the sediment composition. In this thesis two different types of grainsize analyses were used for the different studies: wet sieving of the sediments from the Helgoland mud area (see chapter 5) and Laser Diffraction Particle Size Analysis of sediments from the Hauraki Gulf (see chapter 7).

3.2.3.1 Laser Diffraction Particle Size Analysis

The laser diffraction method is a widely used tool for the determination of particle size distributions in sediments with particle sizes ranging from 0.002 µm to 2000 µm. It is based on the Fraunhofer diffraction theory assuming that particle size is directly proportional to the intensity of light that is scattered by the particle, and on the Mie theory of light scattering, which requires knowledge of the optical properties of the sample and the dispersant (de Boer et al., 1987) (Fig. 4.5). Laser Diffraction Particle Size Analyser measure the angular variation in the intensity of light that is scattered when a laser beam passes through a dispersed particulate sample (Syvitski, 1991). Small particles scatter the light at large angles relative to the laser beam, whereas larger particles scatter the light in small angles. The device analyses the angular scattering intensity to calculate the size of the particle causing the scattering pattern (Syvitski, 1991).

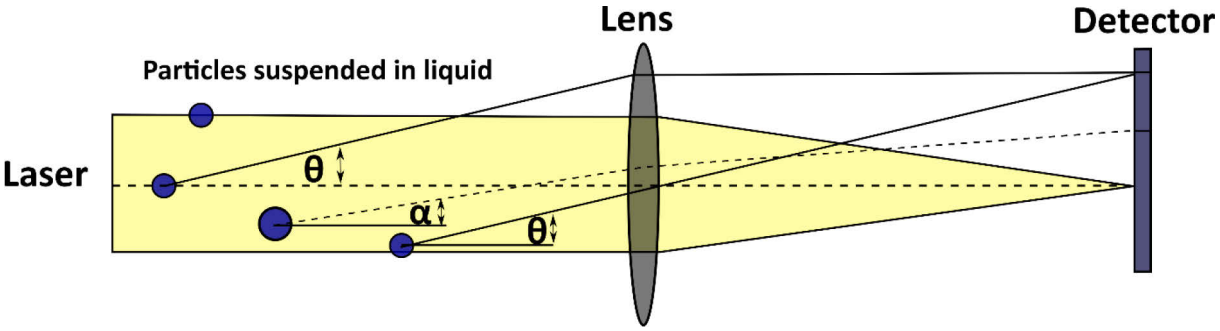

Fig. 3.4 *Schematic figure of laser diffraction particle size analysis (modified after McCave et al., 1986). Particles passing through a laser beam scatter light at an angle that is related to their size.*

Particle size analyses of sediments from the Hauraki Gulf were performed in the Particle-Size Laboratory of the University of Waikato using a Malvern Mastersizer 2000a Laser Diffraction Particle Size Analyser. To isolate the terrigenous sediment fraction from the organic and calcium carbonate components, the samples were treated with hydrogen peroxide (H_2O_2) and hydrochloric acid (HCl). 10 ml of 10% H_2O_2 was frequently added to the samples until the reaction stopped. Samples were heated up gently to speed up the reaction. Samples were diluted with filtered, demineralised water to a pH-value of ~ 7 after every preparation step. Carbonate material was removed by adding 1 ml of 25% HCl solution until all carbonate material was removed. Prior to the measurement, the samples were dispersed with 1 ml of calgon and stirred. Particle size distributions are given in 100 size classes ranging from 0.05 to 2000 µm.

3.2.3.2 Wet Sieving

Wet-sieving of sediments is a simple method to separate different particle size fractions. Sediment samples from the Helgoland mud area were washed over sieves with different mesh sizes: 63 µm, 150µm, and 500 µm (see chapter 5). The weight percentage of the fractions were calculated by weighing the dry sediment before and after sieving. The wet-sieving was performed at the MARUM, Centre for Marine Environmental Sciences, University of Bremen, and at the Senckenberg Institute, Department of Marine Science, Wilhelmshaven.

3.2.4 SWAN (Simulating WAves Nearshore) simulation

SWAN is a useful tool to compute random, short-crested wind-generated waves in coastal regions and inland on the base of given wind, seabed, and current conditions.

A regional nonstationary SWAN model was setup (Zijlema et al. 2010) to evaluate the potential role of wind-generated waves in the distribution of terrigenous and marine sediments in the Hauraki Gulf (Fig. 3.5) (see chapter 7). The SWAN simulates the wave parameters for the Hauraki Gulf and adjacent areas over the period 1989 - 2009. The unstructured grid comprises 27673 cells with varying grid cell sizes between 50 km^2 (offshore, in water depths > 1000 m) and 0.5 km^2 in the vicinity of the Hauraki Gulf (water depths < 100 m). The regional SWAN model is embedded into the global WaveWatch III (WW3) Ocean Wave hindcast model (National Oceanic and Atmospheric Administration, NOAA) similar to the approach by Blossier et al. (2016). Hourly 0.5° spatial resolution winds (Climate Forecast System Reanalysis Reforecast (CFSRR), provided by the NCEP (National Centers for Environmental Prediction) drive the global model and are included in the local nested model. Spectral wave conditions are extracted from the nearest WW3 output locations (seven points) and applied to the model boundaries. The bathymetry for the simulated region was supplied by NIWA, the National Institute for Water and Atmospheric Research, for New Zealand (Mitchell et al., 2012) and the Hauraki Gulf (Mackay et al., 2012). Validation of the model was based on wave buoy data from nearby Motiti Island, maintained by the Bay of Plenty Regional Council. Reasonable model validation were found for significant wave height Hs (R^2 = 0.85 and RMSE = 0.2) and mean period Tm (R^2 = 0.75 and RMSE = 0.9), whereas validation for wave direction was slightly worse (R^2 = 0.60), but values increased to 0.75 for significant wave heights > 0.7 m.

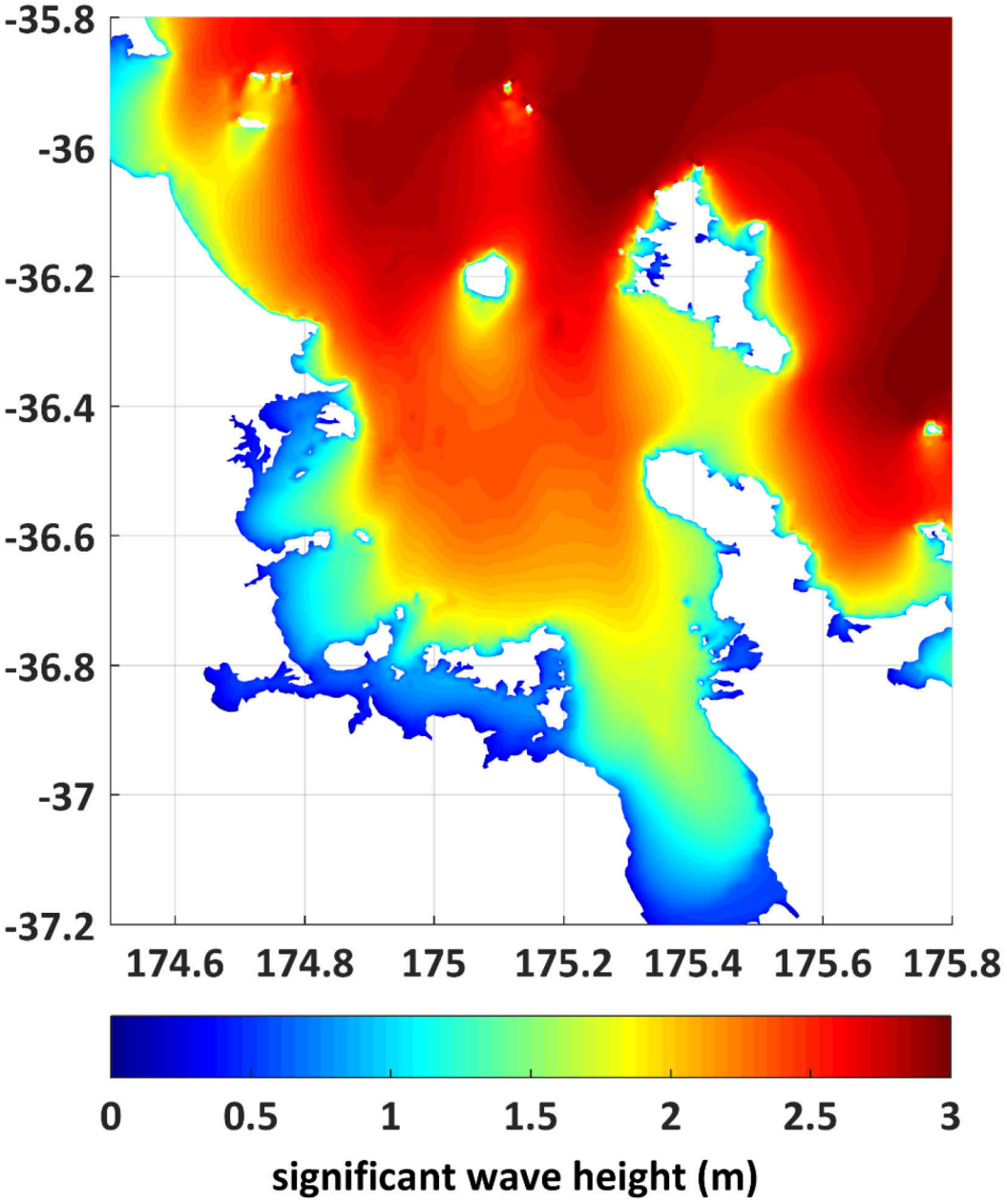

Fig. 3.5 *SWAN simulation map of the Hauraki Gulf indicating the significant wave heights (m) on the 29th of January 2011.*

4. Overview of own research

The scientific questions and hypotheses that are in the focus of this thesis are discussed in three individual studies presented in chapters 5 to 7. The main findings of these studies as well as the contributions of all co-authors are summarised in the following.

The initial objective for the individual studies was to decipher the historical, anthropogenic induced, heavy metal enrichments in the study areas and a final comparison between the human impacts on the different marine environments (see chapter 1.2). Literature review indicated the central Hauraki Gulf to be a modern sediment depocenter with up to 12 m of Holocene sediments (Manighetti and Carter, 1999) and, thus, to be a suitable site for studying the timing of the anthropogenic induced heavy metal inputs.

However, the new findings reveal a generally low modern-day sediment input in the study area and a strong reworking of the sediments (see chapter 7). Therefore, an anthropogenic induced heavy metal contamination of the sediments cannot be shown and resulted in a change of the research objectives in this study. The study now identifies and discusses the patterns of deposition and reworking of surficial sediments in the central Hauraki Gulf. Consequently, a final comparison between the human impacts on the marine ecosystems focuses on the Helgoland mud area and the Skagerrak.

The first manuscript (Chapter 5)

Historical anthropogenic heavy metal input to the south-eastern North Sea

F. Boxberg, S. Asendorf, A. Bartholomä, B. Schnetger, W. P. de Lange, D. Hebbeln

to be submitted to Continental Shelf Research

By using six high-resolution sediment cores from the Helgoland mud area, the temporal and spatial development of anthropogenic induced heavy metal inputs to the Helgoland mud area is reconstructed. The elevated Zn and Pb levels in the topmost sediments are dated back to an early onset at ~ AD 750 and reveal a time-transgressive pattern from SE to NW. Oldest Zn and Pb enrichments are assumed to reflect mining and smelting activities in the Harz Mountains and the Erzgebirge, that are directly linked to the Helgoland mud area by the Elbe

and Weser rivers. Since the onset of anthropogenic heavy metal input, approximately 12,000 tons of Zn and 4,000 tons of Pb have been accumulated in the Helgoland mud area.

Contribution: The study was designed by D. Hebbeln and S. Asendorf. S Asendorf generated the XRF core scanner data, quantitative XRF data and a first set of radiocarbon data. F. Boxberg picked assemblages of benthic foraminifera for further radiocarbon analyses and conducted the grainsize analysis of core GeoB 4803-1. Grainsize analysis of cores GeoB 4801-1 and GeoB 4806-1 were carried out by A. Bartholomä. All interpretations were developed and formulated by F. Boxberg, and discussed with the Co-authors of the manuscript. Text, tables and figures are the work of F. Boxberg with refinements made after discussions with the co-authors.

The second manuscript (Chapter 6)

Anthropogenic input of heavy metals to the Skagerrak in historical times

F. Boxberg, D. Hebbeln

in preparation

By using XRF core scanner data of three high resolution sediment cores from the southern flank of the Skagerrak, the historical heavy metal input into the sediments is reconstructed and discussed. Early Cu and Pb enrichments starting at ~ AD 1230 are assumed to reflect medieval mining and smelting activities in the Falun copper mining area in central Sweden. The heavy metals were most likely transported to the study sites via direct atmospheric transport as well as via fluvial and marine transport. The elevated Zn levels in the sediments starting ~ AD 1660 might partly be attributed to the elevated Zn levels in the Helgoland mud area sediments, transported to the study area via the South- and North Jutland Current.

Contribution: The study was designed by F. Boxberg and D. Hebbeln. The age model of Hebbeln et al. (2006) was used for the manuscript, and XRF core scanner analysis was carried out by C. Scheurle. All interpretations were developed by F. Boxberg, who wrote the manuscript and made the graphics and tables with refinements made after the discussion with D. Hebbeln.

The third manuscript (Chapter 7)

Sediment deposition in the central Hauraki Gulf, New Zealand

F. Boxberg, B. Blossier, W. P. de Lange, B. Fox, D. Hebbeln

to be submitted to Geo-Marine Letters

This manuscript identifies and discusses the effects of the interaction of wind-generated waves and currents with regards to deposition and reworking of surficial sediments in the central Hauraki Gulf. The central Hauraki Gulf is dominated by palimpsest sediments, a consequence of low overall sediment input to the region and continuous reworking of the sediments under strong wind and wave forcing. A steep N-S gradient in wave energy affecting the study area results in a latitudinal N-S trend in sediment texture and composition.

Contribution: The study was designed, by F. Boxberg, D. Hebbeln, and W.P. de Lange. The fieldwork in the Hauraki Gulf was performed by F. Boxberg, D. Immenga, W.P. de Lange, Vicky Moon, and crew members from Western Work Boats. All laboratory analyses were performed by F. Boxberg. The SWAN simulation of the wave patterns in the Hauraki Gulf was conducted by B. Blossier. F. Boxberg wrote the manuscript, made the tables and figures and developed and formulated the interpretations of the manuscript. The co-authors contributed with fruitful discussion and guidance during the analyses and the writing process.

5. Historical anthropogenic heavy metal input to the south-eastern North Sea

Florian Boxberg[1], Sanja Asendorf[1], Alexander Bartholomä[2], Bernhard Schnetger[3], Willem P. de Lange[4], Dierk Hebbeln[1]

[1]MARUM - Centre for Marine Environmental Sciences, University of Bremen, Bremen, Germany

[2]Senckenberg am Meer, Marine Sedimentology Research Department, Wilhelmshaven, Germany

[3]Institut für Chemie und Biologie des Meeres (ICBM), Carl von Ossietzky Universität, Oldenburg, Germany

[4]School of Science, University of Waikato, Hamilton, New Zealand

5.1 Abstract

The Helgoland mud area in the German Bight, covering an area of approximately 500 km^2, is one of a few depocenters for finer sediments in the North Sea. Radiocarbon and ^{210}Pb analyses revealed continuous sedimentation over the last several centuries. Zinc and other heavy metals in the sediments were determined for 6 sediment cores via XRF core scanning and quantitative analysis. A distinct increase in the zinc and lead contents towards the core tops is related to silver and zinc mining in the Harz Mountains and the Erzgebirge, well-known mining areas since the Bronze Age. Both regions are directly linked to the Helgoland mud area by the Elbe and Weser rivers. The thickness of the heavy metal enriched sediments differs between 15 and 103 cm among the sediment cores. Radiocarbon dating, used to date the onset of increasing zinc and lead contents, reveals a regional, time-transgressive pattern. The heavy metal enriched sediments were first deposited in the south-eastern mud area around AD 760. Subsequently with increasing delivery of these metals, the zone of enrichment slowly progressing north-westward. This time-transgressive pattern is most likely due to hydrodynamic conditions in the Helgoland mud area. Quantitative assessments of the Zn and

Pb content in the sediments suggests that since the onset of enhanced Zn and Pb deposition, the anthropic Zn and Pb input in the Helgoland mud area amounts to ~ 12,000 t and ~4,000 t respectively.

Key Words: North Sea; Helgoland mud area; heavy metals; zinc; lead

5.2 Introduction

The southern North Sea with its' high tidal- and wave-energy levels is generally characterised by sediment redistribution as the dominating sedimentological process. Only a few depocenters for the deposition of finer sediments exist in the North Sea (Lohse et al., 1995). One is the Helgoland Mud Area (HMA) in the German Bight in the SE North Sea (Fig. 5.1). In its center, up to 30 m of sediments of Holocene age have accumulated (von Haugwitz et al., 1988). Despite generally low water depths of ~30 m in the west and ~15 m in the east (Fig. 5.1), a spatially coherent sedimentation pattern (Irion et al., 1987; Hebbeln et al., 2003) as well as the presence of undisturbed paleo-records (e.g. Scheurle et al., 2005) demonstrate the long-term depositional nature of the HMA. This also holds true for the most recent times, when human activities contributed substantially to sediment redistribution in the German Bight (Rijnsdorp et al., 1998; OSPAR Commission, 2000), as high-resolution paleo-records from the HMA can be well correlated to the 120 year long instrumental Helgoland Roads time series (Scheurle and Hebbeln, 2003).

Förstner and Reineck (1974) were the first to describe a (sub)-recent increase in the content of heavy metals in the uppermost decimetres of the sediments of the HMA. Based on ^{210}Pb and ^{137}Cs dating, Dominik et al. (1978) estimated that the increased input of these heavy metals (including Zn and Pb) started in the second half of the 19th century; with a second marked increase between AD 1930 and 1950. Analysing a set of 21 sediment cores, Irion et al. (1987) showed the presence of a distinct spatial pattern within this depocenter, marked by increasing thicknesses of Zn-enriched layers from a few centimetres in the west to >300 cm in the east. Without having any detailed stratigraphic data, Irion et al. (1987) assumed that the increased Zn input only began in post-war times due to the dumping of contaminated harbour muds. However, their interpretation yielded sedimentation rates for the uppermost sediments of the HMA of 30 to 60 mm y^{-1}, which are much higher than estimates of 2 mm y^{-1}

based on sedimentological observations (Reineck, 1963), 7.7 mm y^{-1} based on ^{210}Pb and ^{137}Cs dating (Dominik et al., 1978), 5.2 mm y^{-1} based on ^{210}Pb and radiocarbon dating (Serna et al. 2010), or inferred from seismic data (von Haugwitz et al., 1988). Hence, with values being significantly higher than other estimates, the analysis of Irion et al (1987) and the assumed west-to-east increase in sedimentation rates across the HMA requires critical evaluation.

Based on the analysis of sediment core GeoB 4801-1 from the HMA, Hebbeln et al. (2003) showed an onset of the Zn increase as early as AD 1750. Such an early onset was linked to silver and zinc mining activities in the Harz Mountains and the Erzgebirge. Both are well-known mining areas located along the tributaries of the Elbe and Weser rivers that both drain into the German Bight. Near these mining areas and along the rivers, silver and zinc mining left traces in the environment since medieval times (e.g., Bartels, 1996; Matschullat et al., 1997; Ortlam et al., 1989).

Heavy metal enrichment (pollution) can cause severe problems. A mobilization of heavy metals, such as Zn and Pb, from the sediments in marine environments could endanger marine organisms and consequently negatively influence the marine food chain (Förstner and Müller 1973). And indeed, Rotstigen (2009) showed that both the absolute abundance and the diversity of benthic foraminifera in the HMA has decreased dramatically since the beginning of the 1800s, coinciding with an increase in abnormal foraminifera morphologies.

Knowledge about the natural, pre-industrial background concentrations of heavy metal is essential when studying anthropogenic heavy metal enrichments (pollution). However, the assignment of natural and anthropogenic heavy metal contributions on the enrichment necessitates a careful interpretation due to the considerably variable background concentrations (Hinrichs et al., 2002). Although the available data draw a coherent picture of increased contents of Zn and Pb (and other heavy metals) in near-surface sediments of the HMA, the spatial pattern of the thickness of the Zn- and Pb-enriched layers as well as the temporal development of anthropogenic induced Zn and Pb input are uncertain. Furthermore, the few reported sedimentation rates from the HMA show a rather wide spread, suggesting that temporal changes in spatial pattern of Zn deposition reflected in the thickness of the Zn-enriched layers may be different from the current spatial distribution of contaminated sediments. Therefore, based on a set of five new dated sediment cores combined with published data (see above), this study aims to analyse the spatio-temporal development of

anthropic Zn and Pb input to the HMA, to identify possible sources and to understand the transport and deposition of heavy metals (and sediments).

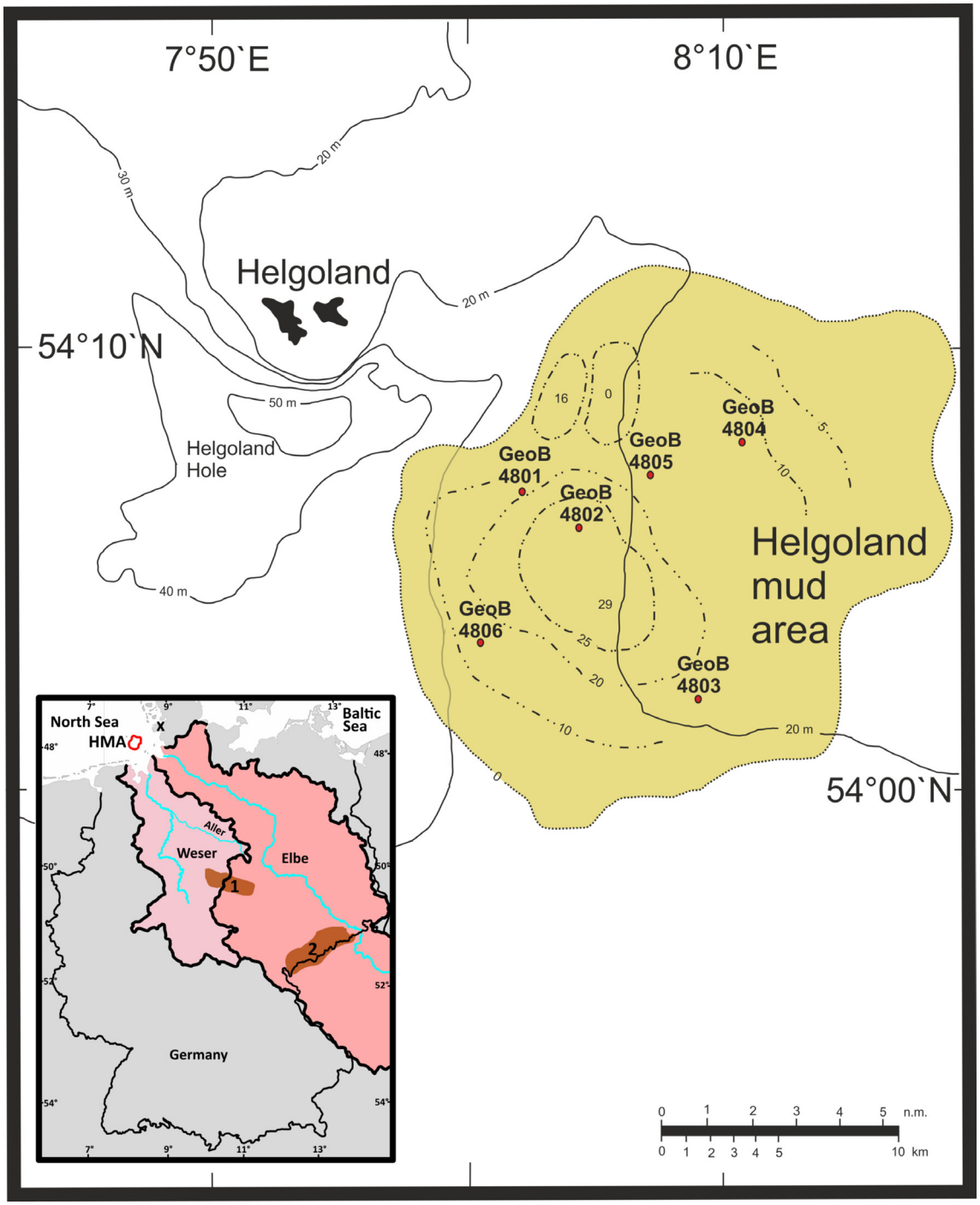

Fig. 5. 1 *Location, extent and thickness (m) of the HMA (shaded area and bold dashed lines; (after von Haugwitz et al. 1988) to the southeast of the Island of Helgoland in the German Bight, SE North Sea (see inset map). The red dots mark the locations of the investigated sediment cores. Modified from Hebbeln et al. (2003). Inset map shows the location of the HMA and the catchments of the Elbe and Weser. X marks the location of the Eiderstedt Peninsula, 1 and 2 mark the Harz Mountains and the Erzgebirge.*

5.2.1 Regional setting

The sediment transport mechanisms in the southern North Sea are dominated by the bedload transport of mobile sands and by the suspended load of fine particles supplied by several rivers, however, with the latter being largely exported from the region due to relatively high hydrodynamic energy levels (e.g. Puls et al., 1997; Zeiler et al., 2000). The HMA is the only significant depocenter for fine sediments in the southern North Sea, except for some intertidal flats and some estuaries (Figge, 1981). However, its' evolution is still under discussion. The following theory for the evolution of the HMA based on the studies of Hertweck (1983), von Haugwitz et al. (1988), and Mayer (1995) is followed in this study. When sea level rise and erosive wave action resulted in the disconnection between Eiderstedt Peninsula and the island of Helgoland between 1,500 years (von Haugwitz et al., 1988) and 2,000 – 3,000 years ago (Irion et al. 1987), the modern-day circulation in the SE North Sea with longshore currents from W to E and from S to N was established. This has been assumed to be the main trigger for the onset of the deposition of suspended particulate matter (SPM) in the HMA (Reineck et al., 1967).

The continuous deposition of finer sediments in the HMA is attributed to a small-scale, anti-clockwise eddy that is driven by the interactions of longshore coastal currents, the discharge from the Elbe and Weser rivers, and tidal dynamics (Hertweck, 1983). This eddy can be subdivided into five small-scale eddies, one of them being the main driver for the deposition of fine sediments in the Helgoland mud area (Mayer, 1995). A 3-dimensional, numerical model for the transport of SPM revealed the existence of vertical eddies with the rising side situated above the HMA that appear to be consistent at nearly every wind direction (Mayer, 1995). This leads to a net-accumulation of the fine suspended matter as the sinking fine particles cannot be transported out of the eddy due to the low horizontal velocities (Mayer, 1995).

Presently, the HMA covers an area of approximately 500 km^2 with a mean water depth of ~ 20 m (Fig. 5.1). The sea bottom rises from W to E with the western part mainly being composed of muddy sediments with an increasing amount of sand in the sediments towards the eastern part (Hertweck 1983).

5.3 Methods

A set of six gravity cores with lengths between 6.87 m and 11.41 m was collected from the HMA during the RV Meteor cruise M 40/0 in 1997 (Table 5.1) in close proximity to each other (Fig. 5.1). The sediment cores were split lengthwise into two halves. One half was analysed for the chemical composition of the sediments using an XRF Core Scanner III (AVAATECH Serial No. 12) at MARUM, University of Bremen. This instrument allowed for a non-destructive, semi-quantitative determination of major and minor elements (e.g. heavy metals). In this study only Zn and Pb contents will be discussed. The other half was used to take discrete samples for the quantitative analysis of Zn and Pb contents and to determine the age of the sediment at selected intervals.

Table 5.1 Site information for six sediment cores from the HMA taken by the German RV Meteor during cruise M40/0 in 1997.

Core no.	Latitude	Longitude	Water depth (m)	Core length (m)
GeoB 4801-1	54 06.7 N	008 02.2 E	25	11.41
GeoB 4802-1	54 05.7 N	008 04.4 E	25	8.01
GeoB 4803-1	54 01.7 N	008 09.0 E	22	7.25
GeoB 4804-1	54 07.8 N	008 10.8 E	20	6.87
GeoB 4805-1	54 06.8 N	008 07.6 E	21	7.34
GeoB 4806-1	54 03.1 N	008 00.6 E	29	7.40

For XRF scanning the split core surface was covered with a 4 µm thin SPEXCerti Prep Ultralene 1 foil to avoid contamination of the XRF measurement unit and desiccation of the sediment. Net intensities of Zn and Pb were measured at 1 cm intervals for the upper two core sections for each core. Further downcore the scanning interval was increased to 2 cm. Measurements were conducted over a 1 cm^2 area with a down-core split size of 10 mm using generator settings of 30 kV, a current of 1.0 mA, and a sampling time of 20 seconds directly at the split core surface. Data were acquired using a Canberra Digital Spectrum Analyzer DAS 1000 and an Oxford Instruments 100W Neptune X-ray tube with Rhodium (Rh) target material. The raw data spectra were processed by the analysis of X-ray spectra by applying the Iterative Least

Square software (WIN AXIL) package from Canberra Eurisys. The resulting data were provided for every measured element in counts per 20 seconds (cp20s).

To calibrate the XRF scanner data for Zn and Pb, 66 discrete samples of 10 cm^3, taken at positions corresponding to the core-scanner measurements, were taken, freeze dried and grounded using a mortar and pestle. 700 ± 0.6 mg of each sample were weighed into a ceramic crucible and mixed with 4200 ± 1 mg of a di-lithium tetraborate fusion flux (Spectromelt® A10, Merck) and about 1000 mg of ammonium nitrate. After one hour of pre-annealing at 500°C, the samples were fused and transformed into glass beads and measured for the Zn and Pb contents via wavelength dispersive XRF-spectrometry (WD-XRF) at ICBM, University of Oldenburg. To determine the accuracy and precision of the method, an international reference material (GSR_6) and in-house standards (Peru-1, Loess 1.6) were used. The results for the three different reference materials used as standards matched the contents given in the literature.

The normalised XRF core scanner net intensities (i.e. the net intensities for Zn and Pb in cp20s obtained from the XRF core scanner analysis were divided by the sum of all measured net intensities to minimize errors due to variable water content, grain size variations and others) were converted to element contents using linear regressions between XRF scanner-derived intensities and element contents measured on the corresponding discrete samples (e.g. Jansen et al., 1998; Kido et al., 2006; Tjallingii et al., 2007). All normalised net intensities for Zn and Pb gathered from the XRF Core Scanner-analysis were then calibrated using the 66 quantitatively measured samples based on the following linear equation:

$$W_{ij} = a_j I_{ij} + b_j$$

in which W_{ij} represents the weight proportion (content) of element j in sample i. I_{ij} represents the normalised net intensity of the raw spectrum gathered from the XRF Core Scanner – analysis. Coefficients a_j and b_j are empirical constants specific to the data set and element under consideration derived from the linear correlation.

To put the historic development of Zn and Pb contents in the HMA in a stratigraphic framework, discrete samples from different depths were taken for accelerator mass spectrometer radiocarbon (AMS ^{14}C) dating. Samples were wet-sieved over 500, 150 and 63 µm mesh size sieves and oven dried at 50°C for 24 hours for further analysis. For 17 samples approximately 10 mg of mixed benthic foraminifera were picked from the fraction 500 - 150

µm and sent to the Beta Analytics Limited radiocarbon lab in London and to the Poznan Radiocarbon Laboratory. Radiocarbon measurements were performed on cores GeoB 4802-1, 4803-1, 4805-1 and 4806-1. For core GeoB 4801-1 the age model of Scheurle et al. (2005) was used. All AMS ^{14}C ages were corrected for isotopic fractionation using $\delta^{13}C$ values. Resulting conventional radiocarbon ages were converted into calendar years using the Calib 7.1 software (Stuiver et al. 2017) with the Marine 13 calibration curve (Reimer et al. 2013) considering the global mean reservoir age of 400 years (Bard, 1998), which has been confirmed for nearby Danish marine waters (Heier-Nielsen et al., 1995). Results are given as the median probability calendar ages accompanied by the 1σ- (68.3 % probability) and 2σ-ranges (95.4 % probability) (Table 5.3).

Particle-size measurements of sediments of cores GeoB 4801-1 and 4806-1 were performed at the Senckenberg Institute, Department of Marine Science, Wilhelmshaven. Samples taken every 5 cm were desalted in semi-permeable hoses over 24 hours. The desalted samples were washed through a 63 µm mesh size sieve to separate the mud fraction (< 63 µm) from the sand fraction (>63 µm). In addition, at the MARUM, University of Bremen, 17 samples of core GeoB 4803-1 were washed through a 63 µm mesh size sieve to separate the mud fraction (<63 µm) from the remaining sediment. The weight % of the mud (<63 µm) and the sand fractions (>63 µm) calculated by weighing the dry sediment before and after sieving.

5.4 Results

XRF scanner data

The Zn and Pb intensities reveal similar background values in the lower parts of all cores, with Zn values between 600 and 650 cp20s.and Pb values between 270 and 290 cp20s(Fig. 5.2). A significant increase of the Zn and Pb intensities towards the top of the cores reaching Zn values of >1000 cp20s and Pb values of >400 cp20s can be observed for all the cores, except for GeoB 4804-1. The uppermost 8 cm of core GeoB 4804-1 was crushed and squeezed during retrieval, and, therefore, could not be analysed via XRF Core Scanner. The enriched sediments differed in both intensity and thickness, with GeoB 4803-1 showing both the thickest enriched sediment layer (103 cm) as well as the generally highest Zn (1600 cp20s) and Pb (900 cp20s) intensities, followed by core GeoB 4802-1 (43 cm, 1100 cp20s, 500 cp20s, respectively). Both these cores are also characterised by a decreasing trend in the Zn and Pb intensities in the

uppermost sediments. In cores GeoB 4801-1, 4805-1 and 4806-1 the pattern of the Zn and Pb intensities is very similar with the significant increase occurring at similar core depths of 15-25 cm, with Zn values reaching 1000 to 1200 cp20s and Pb values 400 to 600 cp20s.

The quantitative XRF-measurement of the 66 samples used for the calibration of the semi-quantitative XRF core scanner data yielded Zn contents up to 300 ppm and Pb concentrations up to 100 ppm. These quantitative XRF data show similar downcore patterns as the XRF core scanner results.

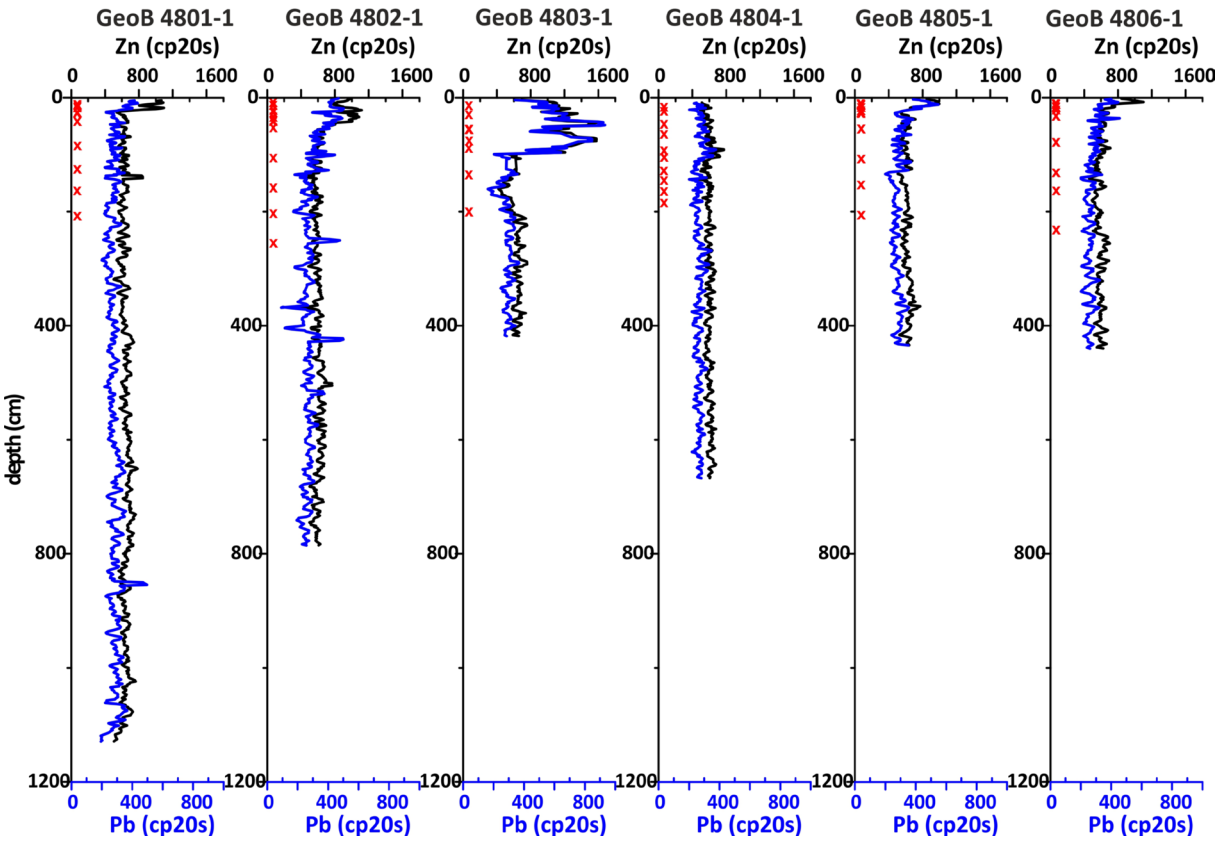

Fig. 5.2 *XRF core scanner-based Zn and Pb intensities in counts per 20 seconds (cp20s) for the six sediment cores. The curves display 3-point running averages. The red crosses mark the position of 66 samples used for quantitative Zn and Pb measurements forming the base for the calibration of the semi-quantitative core scanner results.*

Calibration of Zn and Pb scanner data

Cross-plots between the quantitatively measured Zn and Pb contents and the corresponding normalised (i.e. element counts vs total counts) semi-quantitative scanner data show coefficients of determination (R^2) of 0.65 for Zn and 0.72 for Pb (Fig. 5.3). For the Zn data, the cross-plot reveals one outlier (Fig. 5.3a) that, however, does not strongly influence the calibration. Thus, the equations used to calibrate the Zn and Pb XRF scanner data (see Fig. 5.3) include all 66 quantitatively measured samples

Calculated Zn and Pb contents

For the lowermost core sections the calibrated XRF Core Scanner net intensities reveal background Zn contents of ~ 40-46 ppm (Fig. 5.4). After the increase in the upper core sections, the maximum zinc contents vary between ~100 ppm (GeoB 4805-1) and ~200 ppm (GeoB 4802-1 and GeoB 4803-1; Table 5.2). The maximum contents of ~200 ppm in cores GeoB 4802-1 and GeoB 4803-1 correspond to almost 5 times the natural background. However, on average the zinc contents of the upper polluted sediment layers are between 2.0 and 2.9 times higher than the natural background content (Table 5.2).

Fig. 5.3 *Cross plots showing the correlation of Zn (a) and Pb (b) XRF core scanner normalised net intensities and quantitatively measured Zn and Pb contents (ppm). The red dot in 3a marks the outlier mentioned in the text.*

The Pb contents show a very similar pattern to the Zn contents, however, with lower values. The Pb background contents in the lower parts of the cores range between 17 and 20 ppm (Fig. 5.4, Table 5.2), whereas average contents in the enriched layers are 28 to 55 ppm (Table 5.2). Thus, the Pb contents within the enriched layers are on average 1.5 to 2.7 times higher than the natural background contents (Table 5.2). These enrichment factors are somewhat lower than the Zn enrichment factors, which range from 2.0 to 2.9 times higher than the background (Table 5.2).

Table 5.2 *Overview over the average Zn and Pb contents in the sediments of the HMA (*indicates the respective mean values for all GeoB cores; **considers also the data provided by Irion et al. 1987). The boxes marked in dark grey indicate the numbers used to estimate the entire anthropogenic Zn and Pb inputs to HMA covering 500 km².The value for the dry bulk density is based on the average dry bulk density of core GeoB 4801 (unpubl. data).*

	Core no.	GeoB 4801	GeoB 4802	GeoB 4803	GeoB 4805	GeoB 4806	GeoB cores*	all cores**
Zinc (Zn)	max. content (ppm)	148	200	193	108	115	-/-	-/-
	aver. content enriched sediments (ppm)	102	104	132	89	79	101	-/-
	background content (ppm)	41	41	46	41	42	42	-/-
	excess content in enriched sediments	60	64	87	48	43	59	-/-
	aver. enrichment fatcor	2.5	2.6	2.9	2.2	2.0	2.4	-/-
	depth of increasing content (cm)	24	43	103	15	17	41	48
Lead (Pb)	max. content (ppm)	42	61	83	45	37	-/-	-/-
	aver. content enriched sediments (ppm)	31	36	55	39	29	38	-/-
	background content (ppm)	17	19	20	19	19	19	-/-
	excess content in enriched sediments	14	18	35	20	9	19	-/-
	aver. enrichment fatcor	1.8	2.0	2.7	2.1	1.5	2,0	-/-
	depth of increasing content (cm)	24	43	103	15	17	41	48
Zn-Pb ratio	background sediments	2.4	2.2	2.3	2.1	2.3	2.3	-/-
	enriched sediments	3.3	2.9	2.4	2.3	2.7	2.7	-/-
	dry bulk density (g cm^{-3})	0.86	-/-	-/-	-/-	-/-	-/-	-/-

The Zn-Pb ratios in the background sediments range between 2.13 (GeoB 4805-1) and 2.41 (GeoB 4801-1). In the upper sediment layers enriched in Zn and Pb, this ratio changes in each core to higher values ranging from 2.26 (GeoB 4805-1) and 3.33 (GeoB 4801-1), thereby demonstrating a relatively larger increase in the Zn content compared to the Pb content.

Particle size results

The particle size distribution in core GeoB 4801-1 and 4806-1 indicate similar patterns, with the sediment being dominated by mud (<63 µm) with average contents of 87 wt% and 76 wt%, respectively (Fig. 5.5). In contrast, the sediments of core GeoB 4803-1 are generally coarser and show larger variations, with an average mud content of 49 wt% (Fig. 5.5). Whereas there are hardly any differences in the particle size distribution between the heavy enriched and the "normal" sediments in cores GeoB 4801-1 and 4806-1, in core GeoB 4903-1 the "normal" sediments appear to be somewhat coarser than the enriched sediments.

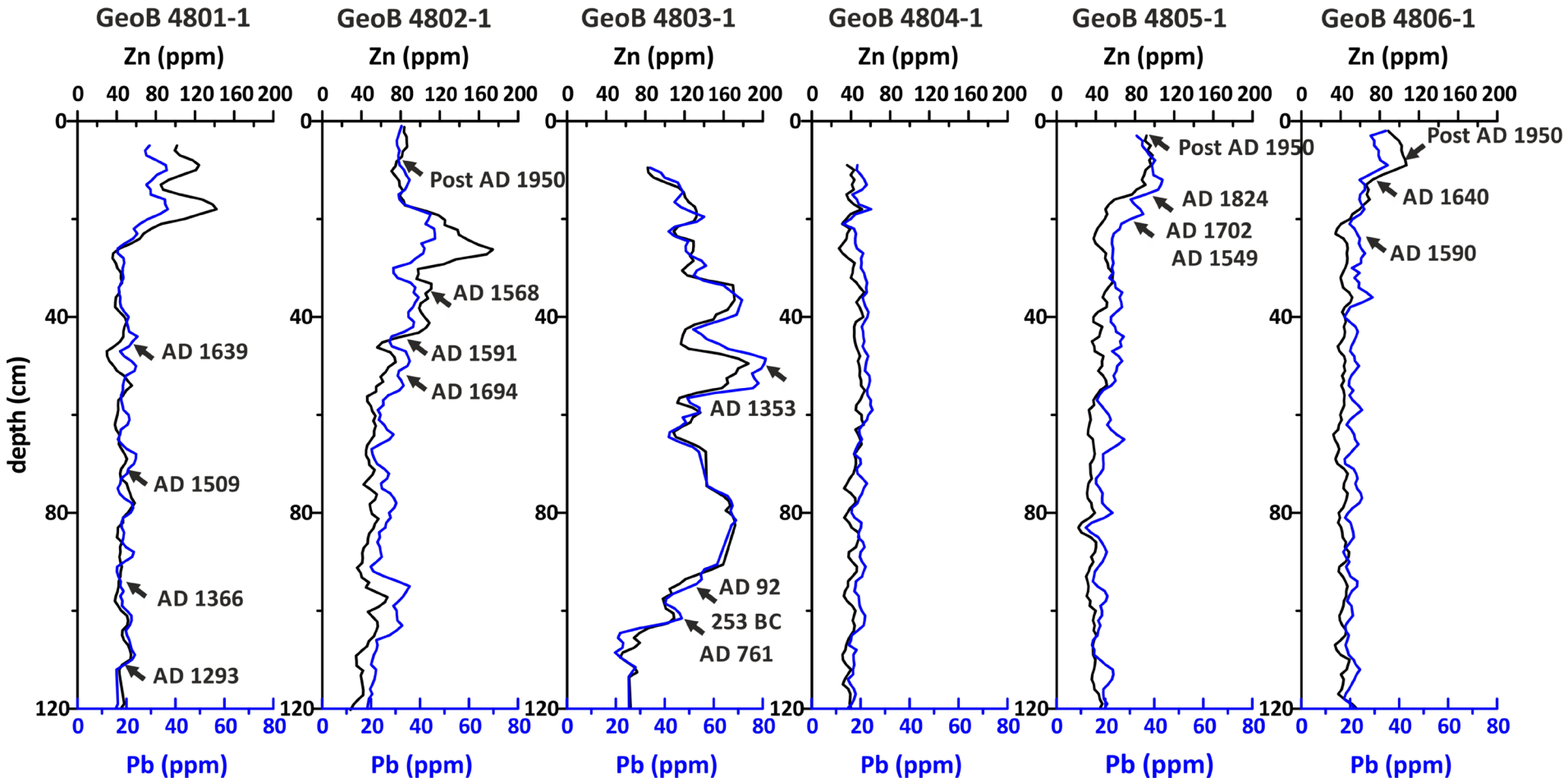

Fig. 5.4 *Calibrated Zn and Pb contents (ppm) of the sediment cores from the HMA. All curves display 3-point running averages. In addition, the results of the AMS radiocarbon dating are indicated.*

Radiocarbon ages

The AMS-^{14}C radiocarbon dates based on mixed benthic foraminifera reveal ages going back as far as 253 BC, thus the dated sections of the cores span roughly the last 2300 years (Table 5.3). Although some age reversals occur indicating the possibility of some re-sedimentation and/or bioturbation, for all four investigated cores average sedimentation rates across the dated core sections oriented along the youngest dates (i.e. not re-sedimented) or along overlapping sigma ranges, respectively (Fig. 5.6), result in rather consistent values. For the past centuries these range between 0.5 and 1.2 mm y^{-1}, close to the value of 1.4 mm y^{-1} since AD 1600 for core GeoB 4801-1 taken from a detailed age model (Scheurle et al., 2005), with highest rates of >1 mm y^{-1} being confined to the central and north-western HMA.

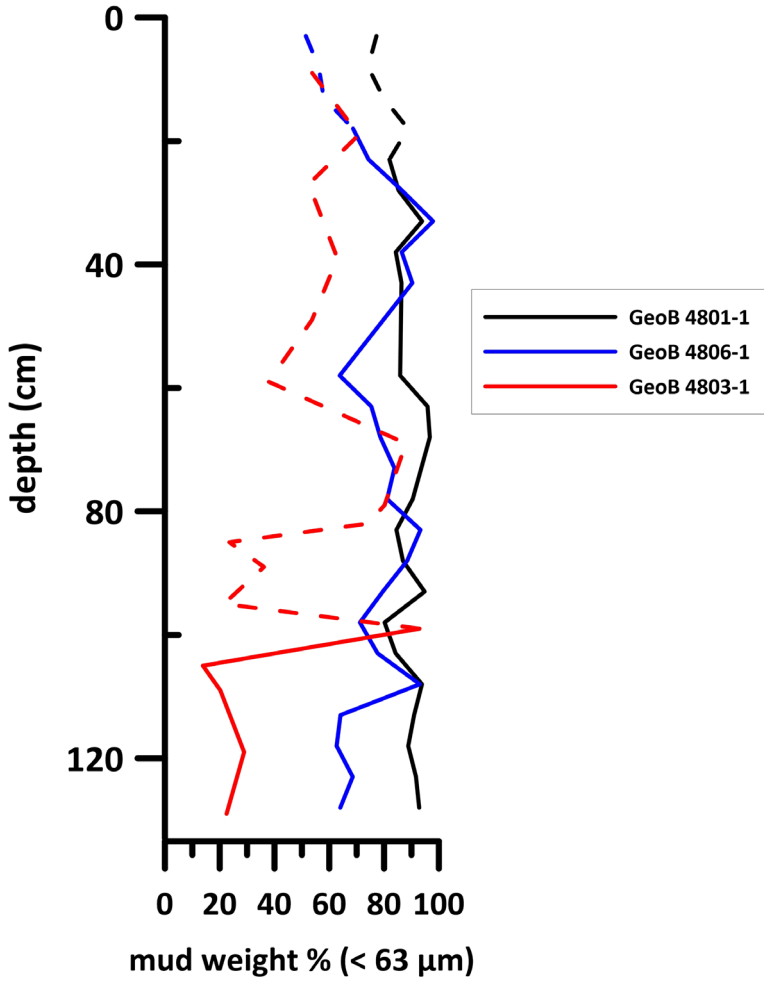

Fig. 5.5 *Mud contents < 63 µm wt,-% for GeoB 4801-1, 4806-1 and GeoB 4803-1 of the sediment cores from the HMA. For all three cores, data for the background sediments are marked by continuous lines, whereas data for the Zn and Pb enriched sediments are given in dashed lines according to the indicated colour code.*

Table 5.3 Overview of the AMS-14C dates in the sediments based on the analysis of mixed benthic foraminifera.

Core no. GeoB	Depth (cm)	Lab. Ident.	Conventional radiocarbon age (BP)	1σ range of calender age	2σ range of calender age	Median probability calender age
4802-1	**9**	Poz-65886	modern	modern	modern	**Post 1950**
4802-1	**37**	Beta - 361007	690 ± 30	AD 1518 to 1626	AD 1480 to 1660	**AD 1568**
4802-1	**45**	Beta - 361008	660 ± 30	AD 1544 to 1636	AD 1498 to 1676	**AD 1591**
4802-1	**51**	Poz-65913	560 ± 30	AD 1645 to 1728	AD 1568 to 1827	**AD 1694**
4803-1	**49**	Beta - 361009	970 ± 30	AD 1314 to 1393	AD 1286 to 1427	**AD 1353**
4803-1	**93**	Poz-66014	2200 ± 50	AD 14 to 165	BC 55 to AD 252	**AD 92**
4803-1	**93**	Poz-75174	2475 ± 30	BC 324 to BC 195	BC 365 to BC 127	**BC 253**
4803-1	**102**	Beta - 361010	1570 ± 30	AD 702 to 805	AD 676 to 879	**AD 761**
4805-1	**4**	Poz-65914	55 ± 30	modern	modern	**Post 1950**
4805-1	**15**	Beta - 361011	450 ± 30	AD 1724 to 1744; 1751 to 1790;1800 to 1892; 1944 to 1950	AD 1712 to 1950	**AD 1824**
4805-1	**21**	Poz-65916	555 ± 35	AD 1650 to 1762	AD 1566 to 1847	**AD 1702**
4805-1	**21**	Poz-75173	710 ± 30	AD 1491 to 1594	AD 1467 to 1649	**AD 1549**
4806-1	**5.5**	Poz-75172	315 ± 30	modern	modern	**Post 1950**
4806-1	**12**	Beta-361012	650 ± 40	AD 1540 to 1670	AD 1500 to 1690	**AD 1640**
4806-1	**25**	Poz-65918	660 ± 40	AD 1539 to 1649	AD 1489 to 1683	**AD 1590**

5.5 Discussion

The spatial pattern of enhanced Zn and Pb contents in the Helgoland mud area

In a first spatial assessment, Irion et al. (1987) reported enhanced Zn contents in the sediments, measured from the fraction < 2 µm, in 21 sediment cores distributed all over the HMA (Fig. 5.7) and even beyond its limits as defined by von Haugwitz et al. (1988). The trend towards thicker Zn-enriched deposits in the eastern HMA reported by Irion et al. (1987) is also reflected in the new data presented here, based on the Zn content in the total sediment (Fig. 5.7). Due to the different references (<2 µm fraction vs. the entire sediment) the determined Zn contents cannot be quantitatively compared directly. However, both data sets also reveal that those sites characterised by thicker Zn-enriched sediment layers also show higher Zn contents compared to the other sites in the respective studies. Despite several age reversals in the stratigraphic record of the cores presented here, this coherent spatial pattern of thicknesses of the Zn-enriched layers and their (relative) Zn contents is a clear indicator for continuous, essentially undisturbed sedimentation in the HMA, as also reflected in the coherent pattern of sedimentation rates. The pattern provided by the Zn-contents in the GeoB cores studied here is almost completely mirrored in the Pb contents (Fig. 5.4).

The temporal pattern of increasing Zn and Pb inputs to the Helgoland mud area

The most intriguing result of combining the new Zn and Pb measurements with the new age determinations is the time transgressive onset of the anthropic input of Zn and Pb to the HMA. Whereas the strongly varying thickness of the heavy metal enriched sediment layers was previously explained by strongly varying sedimentation rates (Irion et al., 1987), the new data reveal the onset of contaminated sediment deposition occurred much earlier in the south-eastern HMA compared to its north-western part. The first enrichments of Zn and Pb occurred in core GeoB 4803-1 in the southeast as early as ~AD 750 (Fig. 5.4). From this south-easternmost part of the HMA, the enhanced input of Zn and Pb progressed northwest-ward to reach site GeoB 4806-1 in the southernmost and site GeoB 4802-1 in the central HMA by ~AD 1600. Progressing further to the northwest, sites GeoB 4805-1 and GeoB 4801-1 were reached at ~AD 1700 and ~AD 1850, respectively.

The latter date for core GeoB 4801-1 is approximately 100 years later than a previously published age for the onset of enhanced Zn input to this site (~ AD 1750 in Hebbeln et al., 2003). This offset results from the new XRF-scanning results revealing that the earlier increase

in the Zn-content reported in 2003 was an artefact. Interestingly, the spatial pattern of the onset of enhanced Zn and Pb input appears to be entirely unrelated to the spatial pattern of sedimentation rates, which over the recent centuries is marked by higher sedimentation rates in the north-western (GeoB 4801-1) and central HMA (GeoB 4802-1) compared to the other sites. The elevated sedimentation rates in these cores correlate well with increased thickness of the mud deposits at those locations as reported by von Haugwitz et al. (1988).

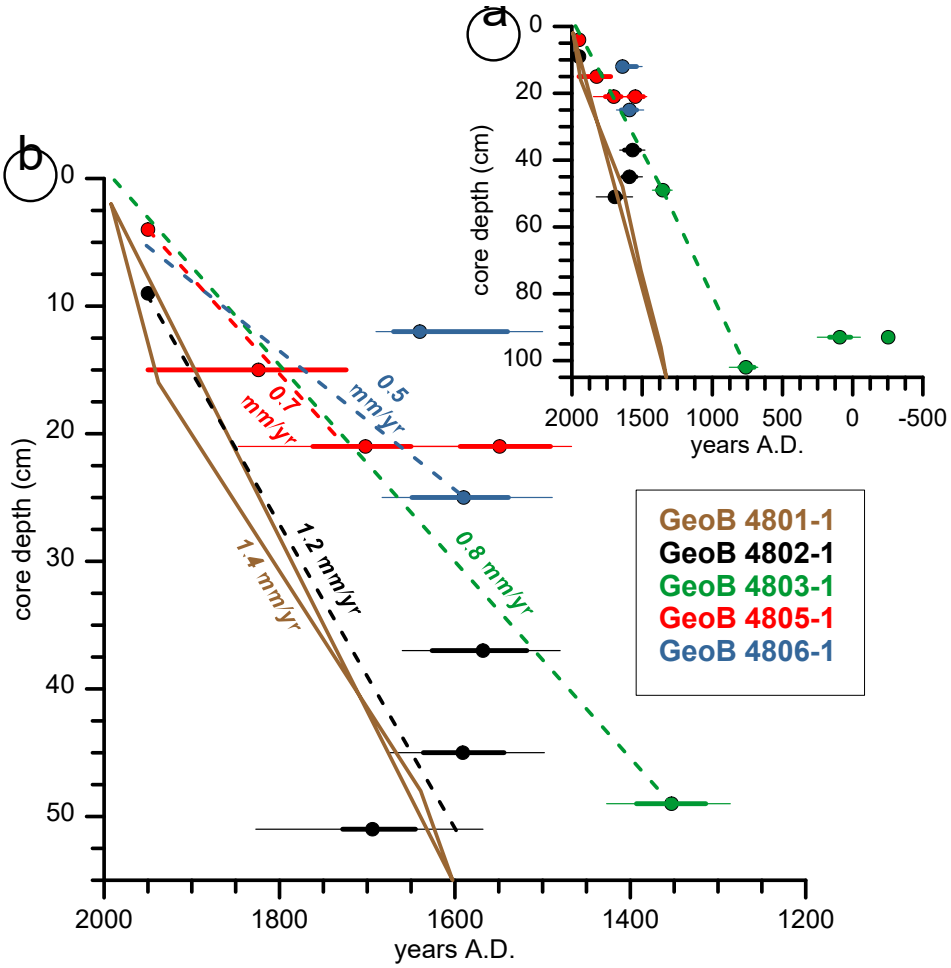

Fig. 5.6 *Age vs. depth plots for five sediment cores from the HMA showing an overview of calibrated AMS radiocarbon ages (a) and an enlarged view of results from the upper 54 cm of the cores. 1-sigma (bold error bars) and 2-sigma (thin error bars) ranges are added to the individual data points. Average sedimentation rates are indicated for each core. Data for core GeoB 4801-1 are taken from Scheurle et al. (2005).*

The sedimentation rates reported here are significantly lower than sedimentation rates for the HMA reported in the literature, e.g, Dominik et al. (1978) and Serna et al. (2010) that determined average sedimentation rates of 7.7 mm y^{-1} and 5.2 mm y^{-1}, respectively. While no information exists about the location of the core mentioned by Dominik et al. (1978), core HE215/4-2 (Serna et al., 2010) has been taken from the very center of the HMA where

sediment thicknesses are >29 m (Fig. 5.1, von Haugwitz et al., 1988). Given the correlation between sedimentation rates and thickness of the mud deposits mentioned above, the very high sedimentation rates reported by Dominik et al. (1978) and Serna et al. (2010), would be consistent with time transgression pattern proposed by this study. However, the even higher sedimentation rate estimates of 30 to 60 mm y^{-1}, especially those determined for the eastern HMA by Irion et al. (1987), based on the assumption of only a post-war deposition of enhanced Zn inputs, cannot be supported.

Source of the enhanced Zn and Pb input

The constant low background values in the Zn and Pb contents as well as their parallel significant increase in historical times indicates that the enhanced heavy metal inputs are due to anthropogenic activities. This is further corroborated by the Zn-Pb ratios, which show a distinct increase from 2.25 in the background sediments to 2.72 in the polluted sediments. This shift indicates a change in the source area, with the source(s) for the enhanced Zn and Pb inputs most likely differing from those producing the older and deeper sediments.

Earlier studies attributed enhanced Zn and Pb contamination to a variety of anthropic sources, including: since the 1850s due to fossil fuel burning and sewage effluent (Dominik et al., 1978), and since the 1950s to dumping of acidic iron waste from titanium dioxide production (Dominik et al., 1978); enhanced availability of SPM due to dredging activities in the estuaries that would not naturally contribute to deposition in the HMA (Irion et al., 1987); or to direct dumping of dredged harbour muds close to the HMA (von Haugwitz et al., 1988). However, these proposed anthropic sources are inconsistent with the new data in this study, which clearly demonstrate a much earlier onset of heavy metal enrichment (Fig. 5.4).

However, the new data do support the interpretation by Hebbeln et al. (2003), which related the anthropogenic signal to early mining activities in the Harz Mountains and in the Erzgebirge, both of which are well-known, long established mining areas along the tributaries of the Elbe and Weser Rivers. Although the new data indicate a much earlier onset (~AD 760 AD) than the before AD 1750 estimated by Hebbeln et al. (2003), evidence for mining activities, especially in the Harz Mountains extends back to ~3500 years BP (Monna et al., 2000). Further, findings of enhanced Zn contents in medieval sediments from the western foothills of the Harz Mountains (Matschullat et al., 1997) and in Weser sediments (Ortlam et al., 1989), and isotope studies on Weser sediments proving early smelting and mining activities in the Harz Mountains (Monna et al., 2000), clearly support potential fluvial transport of heavy metals from the

mining locations to the German Bight to the HMA. In particular, a fluvial link to the Harz Mountains is also indicated by increasing heavy metal contents in Weser sediments downstream of the confluence with the Aller River, a Weser tributary draining parts of the Harz Mountains (Pache et al., 2008). Earlier mining activities in the Harz Mountains, dating back to 3,500 years BP (Monna et al., 2000), may have been conducted at a smaller scale than more recent mining, without contributing a detectable level of Zn and Pb to the HMA. Thus, the timing of the onset of enhanced Zn and Pb deposition in the HMA at ~AD 760 probably is a function of mining intensity/methodology and on the velocity of the signal propagation from the source areas through the rivers to the southern North Sea.

Interestingly, on the nearby island of Helgoland itself copper was mined and smelted, probably from the early Bronze Age to medieval times (Schulz, 1981). However, average Zn-Pb ratios of 0.27 in copper slices found near Helgoland (Schulz, 1981) are significantly different from those found in our cores (2.25 to 2.72). In contrast, Zn/Pb ratios of heavy metal enriched Weser overbank sediments analysed by e.g. Ortlam (1989) and Monna et al. (2000) indicate significantly higher Zn/Pb ratios of >2 that have been attributed to the influence of early mining activities in the Harz Mountains. In addition, there is no indication of enhanced copper contents in our cores mimicking the pattern of the Zn and Pb enrichments. Therefore, copper mining on Helgoland most likely had no influence on the Zn and Pb enrichments found in the HMA sediment cores.

The time-transgressive pattern of enhanced Zn and Pb input

The time transgressive pattern of enhanced Zn and Pb input reflected by an early onset of contamination in the south-eastern HMA, followed by contamination progressing northwest-ward, is most likely a consequence of the specific hydrodynamic conditions in the SE North Sea. The thicker Zn and Pb enriched sediments in the shallower south-eastern HMA are coarser and marked by lower sedimentation rates and, thus, are most likely controlled by slightly higher wave and tidal energy levels as the finer and faster accumulating sediments in the north-western HMA. Hence, the following scenario appears to be a possible explanation for the time-transgressive pattern of enhanced Zn and Pb inputs: enhanced deposition of Zn and Pb began in the south-eastern HMA that is closest to the mouths of the Elbe and Weser rivers that most likely delivered this material from the source areas further upstream. The documented initial deposition of Zn and Pb in this area (Fig. 5.4) was probably facilitated by an eddy overlying this part of the HMA (Mayer, 1995). Varying energy levels, triggered by

winds and tides, with most likely highest levels in this shallowest part of the HMA, may have resulted in the partial resuspension of small amounts of fine material. Then, tidal currents possibly allowed for its transport north-westward where re-deposition took place in slightly more quite, deeper settings as e.g., in the north-western HMA. Assuming this to be a slow, but regular and continuous, on geological time scales synsedimentary process, the resulting sediments would still appear as continuous, undisturbed record. And indeed, within the temporal resolution achievable, core GeoB4801-1 provides an excellent, undisturbed paleo record with partly decadal resolution (Scheurle et al., 2005) that even can be linked to instrumental records of the last century (Scheurle et al., 2003). Such a synsedimentary redistribution of finer particles would slowly and continuously transport finer material from the shallower north-eastern HMA, where most of the Zn and Pb is initially deposited, to its deeper parts in the north-west, thereby also most likely redistributing Zn and Pb. Such a scenario also would explain the observed differences in sedimentation rates and sediment grain sizes, with resuspension causing lower (higher) sedimentation rates and coarser (finer) sediments in the south-eastern (north-western) HMA. However, other scenarios invoking changes in the paleogeography and/or sea level also might be generally feasible, but appear less likely on the time scales considered here.

Total anthropogenic Zn and Pb input to the mud area

Using average values for the thickness of uppermost sediment layer characterised by elevated Zn and Pb contents, this layer's average Zn and Pb contents above the natural background and the sediment's dry bulk density of ~0.86 g/cm3 (see Table 5.2), the total anthropogenic Zn and Pb input to the whole HMA was estimated. Applying these values to an overall extent of the HMA of 500 km^2, a total volume of 245,000,000 m^3 or 0.245 km^3 of enriched sediments can be assumed. This volume in combination with the average Zn and Pb contents above the natural background of 59 ppm for Zn and of 19 ppm for Pb and the average bulk density of 0.86 cm^3 add up to rough estimate of anthropogenic induced inputs of ~12,000 t of Zn and ~4,000 t of Pb to the HMA. Although the density obtained from only one core might vary within the HMA, such variability would not affect the order of magnitude of the estimated anthropogenic Zn and Pb input.

At first glance, these numbers seem to be rather large. However, the loads of the suspended heavy metals in the Elbe showed peak values of 4,400 t of Zn and 350 t of Pb per year at the station Magdeburg in 1986 (FGG Elbe, 2010) putting the numbers from the HMA into a

broader perspective. Furthermore, in only one year, in 2014, a total of 4.5 Mm^3 of sediments were dredged from the port of Hamburg. At the Tonne E3 dumping site located ~15 km south of Helgoland, and close to the HMA, ~440,000 t of this dredged material were dumped containing ~14.87 t of Pb and ~104 t of Zn (Hamburg Port Authority, 2015). These amounts are just a fraction of the total amount of material from Hamburg Harbour that has been dredged and dumped at various sites in 2014, and which in total contained ~ 180 t of Pb and ~ 1600 t of Zn (Hamburg Port Authority, 2015). Thus, the heavy metals deposited in the HMA obviously only reflect a fraction of the heavy metals that are present in the marine system of the German Bight. Most likely, other depocenters like the estuaries of the Elbe and Weser rivers, and the Skagerrak, which is the most prominent fine sediment depocenter in the North Sea, also serve as sinks for anthropogenic heavy metal inputs to the German Bight.

Interestingly, the high amounts of Zn and Pb in the dredged material dumped close to the HMA in recent years/decades seem to not have caused an increase in contamination within the cores analysed here. Instead they show a decline in the Pb and Zn contents in the youngest sediments. Therefore, it seems that these dumped sediments somehow do not enter the eddy-controlled depositional system of the HMA, maybe due to the particle dynamics linked to the dumping process that might release only a fraction of the dumped material into a sustained suspension. Alternatively, the declining Zn and Pb contents in the youngest HMA sediments may reflect reduced river sourced SPM loads due to the construction of various dams along the Weser and Elbe rivers.

5.6 Conclusion

The heavy metal enrichment history in the Helgoland mud area in the SE North Sea is more complex than previously reported. Zn and Pb enrichment in the HMA sediments follows a regional, time-transgressive pattern. Enhanced Zn and Pb inputs first reached the south-eastern HMA around AD 760, probably as a consequence of increased mining activities in the Harz Mountains and the Erzgebirge within the upper catchments of the Weser and Elbe rivers that drain into the German Bight close to the HMA. In the Bight, the deposition of Zn- and Pb-contaminated SPM was influenced by a local eddy that focused deposition within the south-

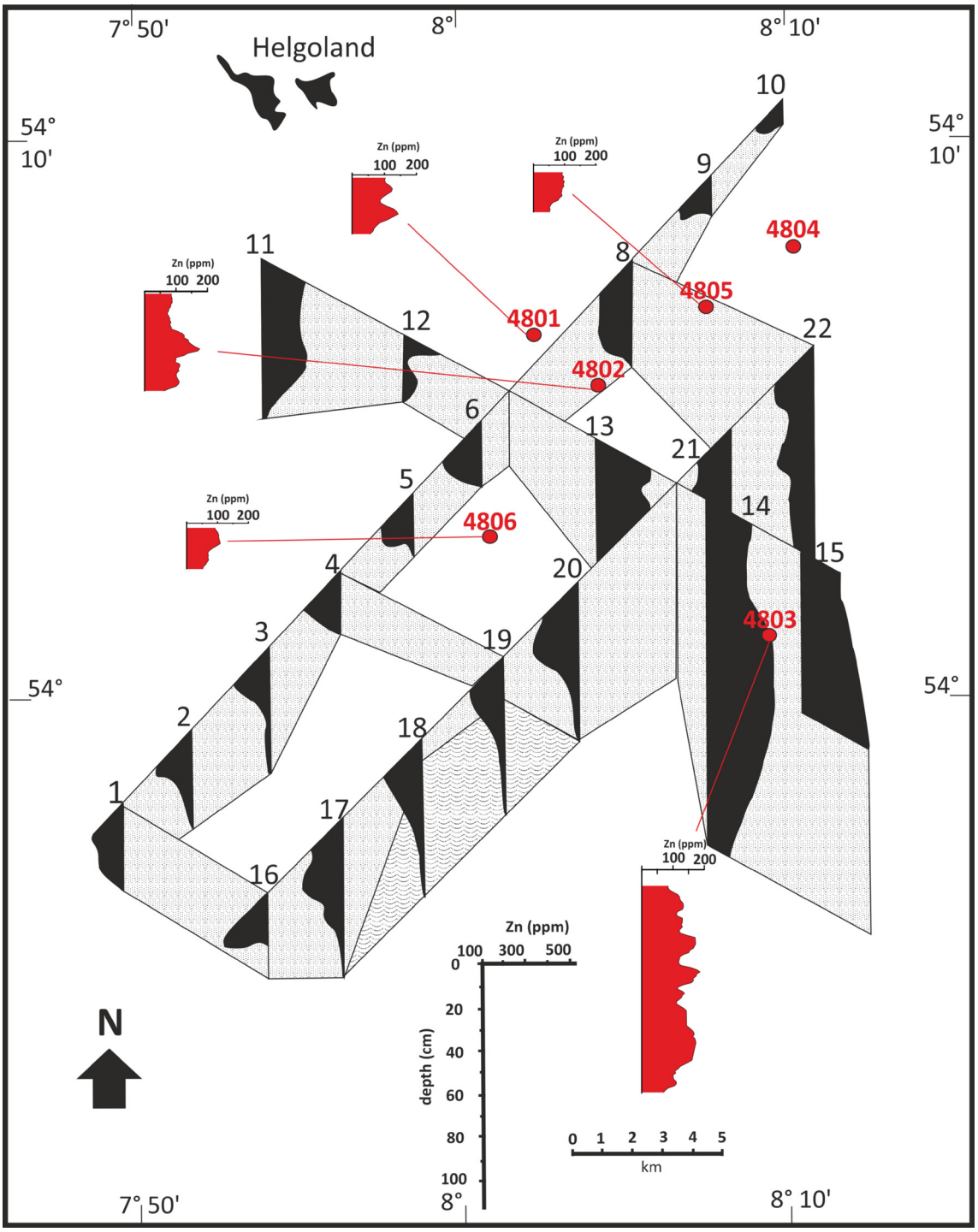

Fig. 5.7 *Zn distribution map (modified after Irion et al. 1987) showing the total Zn contents (ppm) in the upper Zn-enriched sediments of the six sediment cores investigated here (marked in red) and the Zn content above the natural background in the particle size fraction < 2 µm of the sediment cores studied by Irion et al. (1987) (marked in black). In core GeoB 4804-1 from the north-eastern HMA, where the enriched layers are the thinnest, and no enriched layer could be found due to lacking data from the uppermost 8 cm that probably contained the contaminant signal.*

eastern HMA, which is most proximal to the river mouths. Over time the regional extent of contaminated sediment deposition expanded northwest wards, reaching the north-western

part of the HMA by AD 1850. The mechanism by which this occurred is assumed to be related to the hydrodynamic processes of the German Bight, but is not well understood at present. The anthropic Zn and Pb inputs to the 500 km^2 large HMA since AD 760 AD are estimated to comprise a total mass of 12,000 t of Zn and 4,000 t of Pb.

Acknowledgements

This research was funded by the German Research Foundation (DFG) through the International Research Training Group INTERCOAST – 'Integrated Coastal Zone and Shelf-Sea Research' (project no. GRK 1598). Further support was provided through the DFG-Research Center / Cluster of Excellence „The Ocean in the Earth System" in Bremen. Sample material has been provided by the GeoB Core Repository at the MARUM. The data reported in this paper will be archived in Pangaea (www.pangaea.de).

6. Anthropogenic input of heavy metals to the Skagerrak in historical times

Florian Boxberg[1], Dierk Hebbeln[1]

[1]MARUM - Centre for Marine Environmental Sciences, University of Bremen, Bremen, Germany

6.1 Abstract

Three high resolution sediment cores from the southern flank of the Skagerrak, the most important depocenter in the entire North Sea, were analysed by means of XRF core scanning to provide new insights into the temporal development of anthropogenic heavy metal inputs to the Skagerrak. Early Cu and Pb enrichments in the sediments date back to an onset at ~ AD 1230 and are estimated to reflect medieval mining and smelting activities in the Falun mining area in central Sweden, which was of great importance during its 1,000 year lasting history of mining and smelting. A later additional input of Zn and Pb to the Skagerrak sediments, dated back to an onset at ~ AD 1660, is likely derived from the highly polluted southern North Sea, which is directly linked to the Skagerrak by the general circulation in the North Sea. The onset of Zn and Pb inputs from the southern North Sea is assumed to be a result of small-scale oceanographic changes that resulted in a change of predominant SPM and heavy metal supply to the study sites.

Key Words: North Sea; Skagerrak; heavy metals; zinc; lead; copper

6.2 Introduction

Anthropogenic induced heavy metal pollution, as it is recorded in environmental archives such as lake sediments and peat deposits, is known to have started in historical times reaching back ~4000 years (e.g. Hong et al., 1996; Renberg et al., 2001). A major source for such "old" heavy metal inputs are thought to be early mining and smelting activities, which are also known from around the North Sea as, e.g., the medieval silver and zinc mining in the Harz Mountains in northern Germany (e.g., Bartels, 1996; Matschullat et al., 1997; Ortlam et al., 1989) and the medieval copper mining in the Falun mining district in central Sweden (Ek and Renberg, 2001). Atmospheric transport of emissions from such activities can explain the wide spreading of the heavy metals, which are even detectable in Greenland ice cores back to approximately 2,500 years ago (e.g. Hong et al., 1994; Hong et al., 1996) However, also fluvial transport of heavy metals from such mining areas can be traced back in time for several millennia (e.g. Monna et al., 2000), eventually leaving distinct traces of such riverine transport in marine sediments (e.g., Hebbeln et al., 2003; Boxberg et al., in prep.). After transport to the ocean by atmospheric or riverine transport and deposition at the sea floor, the mobilisation of heavy metals such as Zn and Pb could harm marine organisms and consequently negatively influence the marine food chain (Förstner and Müller, 1973).

Heavy metals in surface sediments of the Skagerrak have been subject to several studies (e.g. Olausson, 1975; Kuijpers et al., 1993b). The surface sediments are generally enriched in heavy metals compared to natural background values with different studies indicating different enrichment factors for example, ranging from 1.5 to 3.3 for copper (Cu), from 1.6 to 3.0 for zinc (Zn), and from to 2.0 to 5.2 for lead (Pb) (Zöllmer and Irion, 1993; Madsen and Larsen, 1986; Kuijpers et al., 1993b). The enrichment factors generally decrease from SW in eastern and northern directions due to the advancing sedimentation of heavy the heavy metal enriched sediments originating from the comparatively highly polluted southern North Sea and transported north-eastward with the South- and North Jutland Currents (Kuijpers et al., 1993b). Additionally, relatively high enrichment factors for Cu, Pb, and Zn of up to 4.8 in the north-eastern Kattegat are explained by heavy metal enriched materials discharged to the Kattegat from industrial sites in Sweden that result in high heavy metal concentrations in sediments close to the point sources and decreasing concentrations with increasing distance from these (Kuijpers et al., 1993b).

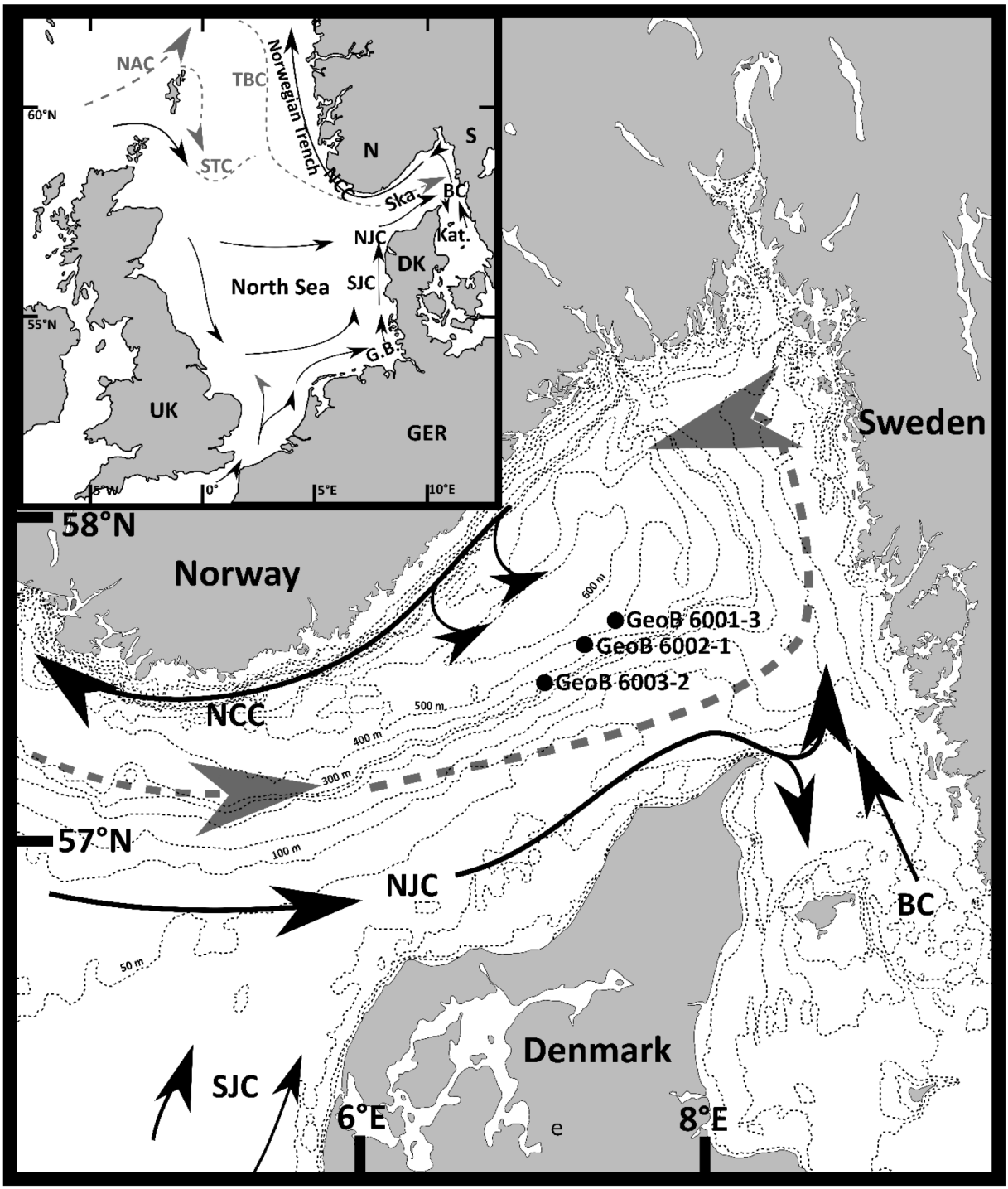

Fig. 6.1 *Bathymetric map of the Skagerrak region showing the locations of the three studied cores and the prevailing surface currents. North Atlantic water masses directly flowing into the Skagerrak are indicated by grey-stippled arrows, modified North Atlantic water masses are shown by black arrows. Abbreviations: SJJ, South Jutland Current; NJC, North Jutland Current; BC, Baltic Current; NCC, Norwegian Coastal Current; STC, Southern Trench Current; TBC, Tampen Bank Current; NAC, North Atlantic Current; G.B., German Bight; Ska., Skagerrak; Kat., Kattegat.. Inlet map shows the prevailing surface currents in the North Sea. Modified from Danielssen et al. (1991) and Nordberg (1991).*

Even though a lot is known about the recent heavy metal inputs to surficial sediments in the Skagerrak (e.g., Olauson, 1975; Madsen and Larsen, 1986; Kuijpers et al., 1993b), the

knowledge about the temporal development of anthropogenic heavy metal inputs in historical times is sparse. Former studies mainly focused on anthropogenic heavy metal inputs to estuarine environments in highly industrialised areas as, e.g., the Oslo Harbor (Lepland et al., 2010) and the Göta River estuary in the northern Kattegat (Brack and Stevens, 2002), in industrial times, and, hence, these studies only span the last 100-150 years. However, anthropogenic heavy metal emissions in Scandinavia are known to have started 4,000 years ago, as indicated by the presence of elevated Pb levels in peat and lake sediments in Sweden (Brännvall et al., 1997). This early evidences of anthropogenic Pb pollution is followed by further episodes of increasing heavy metal emission during the Greek and Roman period (500 BC – AD 400), the Late Middle Ages (AD 900 – AD 1400), the period between AD 1400 and AD 1800, and the modern industrial period (Brännvall et al., 2001). These elevated lead levels were assumed to reflect mining and smelting activities from all over Europe, whose emission are even visible in Greenland ice cores (Hong et al., 1994; Hong et al., 1996). Consequently, the long-range transport of Pb and other heavy metals is very likely to have resulted in elevated heavy metal concentrations in the Skagerrak, the most prominent depocenter in the entire North Sea, in historical times.

Based on the analysis of three high-resolution sediment cores from the southern flank of the Skagerrak, this study aims to analyse the historical anthropogenic heavy metal inputs to the Skagerrak and to identify possible source areas.

6.2.1 Regional setting

The Skagerrak is the deepest part of the Norwegian trench and of the entire North Sea. With a mean water depth of ~210 m and a maximum water depth of ~700 m, the Skagerrak acts as a natural sediment trap (Rodhe, 1987). The irregular shape of the Skagerrak is characterised by a steep northern slope and more gentle southern and eastern slopes (Fig. 6.1) reflecting that the main sediment input is entering the Skagerrak from the south (Svansson, 1975; van Weering, 1981, Eisma, 1981; Kuijpers et al., 1993a; Zöllmer and Irion, 1993), and underlining the suitability of these sediments for generating temporally highly resolved paleo records allowing detailed investigations of sediments deposited over the last millennia. Consequently, Skagerrak sediment records have been widely used for paleoenvironmental studies (e.g. Nordberg, 1991, Haas, 1993; Heier-Nielsen, 1995; Knudsen et al., 1996; Hebbeln et al., 2006),

however, without to our knowledge any analyses on the long-term development of heavy metal inputs.

Hydrodynamic conditions and sediment supply

The general surface water circulation in the Skagerrak is anti-clockwise and forms a part of the anti-clockwise circulation of the North Sea (Fig. 6.1). The South and the North Jutland Currents, coming from the southern North Sea, and the Tampen Bank Current and the Southern Trench Current, coming as direct inflow from the North Atlantic, enter the southern and central Skagerrak from the east (Fig. 6.1). These waters partly recirculate to the west close to the Swedish coast, where relatively fresh Baltic Sea waters enter the Skagerrak via the Kattegat. All these waters form the Norwegian Coastal Current flowing parallel to the Norwegian coast and leave the Skagerrak in north-westerly direction (e.g. Qvale and van Weering, 1985; Rodhe, 1987) (Fig. 6.1).

The main modern sediment supply to the Skagerrak system is provided by the South and North Jutland Currents transporting sediments from the southern North Sea along the eastern Danish coast to the Skagerrak (Fig. 6.1) (Svansson, 1975; van Weering, 1981, Eisma, 1981; Kuijpers et al., 1993a; Zöllmer and Irion, 1993). Kuijpers et al. (1993b) estimated that a large proportion of the fine material deposited in the Skagerrak and the adjacent Kattegat is originally riverine suspension load from (central) western European rivers (e.g. Rhine and Elbe). The strongest influence of suspended particulate matter (SPM) derived from the southern North Sea has been found in the western Skagerrak with a decreasing trend in eastern direction (Nolting and Eisma, 1988). About 50-70% of the SPM of the entire North Sea is estimated to be deposited in the Skagerrak-Kattegat-Norwegian Channel system (Eisma and Kalf, 1987). Approximately 50 % of the SPM transported annually through the entire North Sea is estimated to originate from sources in the southern North Sea (van Weering et al., 1993b). SPM concentrations in the Skagerrak generally decrease in northern direction from the Danish coast to the central Skagerrak (Eisma and Kalf, 1987). Estimated sedimentation rates in the Skagerrak differ between ~0.1 mm/yr in the central Skagerrak, ~ 0.2 mm/yr in the southern and northern Skagerrak, and up to 4.4 mm/yr in the eastern Skagerrak (van Weering et al., 1987) The major reason for the deposition of the SPM in the Skagerrak is the presence of vortexes (eddies) preventing the SPM from being exported from the Skagerrak (Fig. 6.1). For example, in the low-velocity area in the central Skagerrak SPM can sink down to deeper layers, where it eventually escapes the influence of the dynamic surface currents (Eisma and

Kalf, 1987) and, hence, starts accumulating at the seabed. This vortex tends to be absent in winter times due to the common easterly winds (in winter) pushing the water out of the Skagerrak. Most of the suspended material supplied by Norwegian and Swedish rivers in the northern Skagerrak is trapped close to the outlets and in the adjacent fjord basins (Pederstad et al., 1993). However, especially during large-scale meltwater pulses in early springtime large rivers in the eastern Skagerrak as, e.g., the Göta River have the potential to transport huge amounts of SPM into the Skagerrak and the northern Kattegat (Kuijpers et al., 1993b). Surface sediments in the deeper Skagerrak consist mainly of moderately sorted silty clay (e.g. van Weering, 1981; van Weering and Qvale, 1983).

6.3 Methods

The sediment cores GeoB 6001-3, GeoB 6002-1 and GeoB 6003-2 were taken in 1999 during RV Meteor cruise M45-5 along the southern flank of the Skagerrak with a gravity corer in water depths ranging from 312 m to 466 m (Table 6.1). The sediment cores were split lengthwise into two halves. One half of each core was analysed for its chemical composition using the Bremen X-Ray Fluorescence (XRF) Core Scanner at MARUM, University of Bremen. This instrument allows for the determination of relative variability in the elemental composition by scanning split sediment-cores in a non-destructive way (Jansen et al., 1998; Röhl et al., 2000). Elemental net intensities were measured in 1 cm-resolution over the entire core lengths. The obtained net intensities, given in counts per seconds, were divided by the sum of all measured net intensities to minimize errors due to variable water content, grainsize variations, and others. The resulting normalised net intensities provided here, thus, can be read as the relative contents of the respective elements in relation to all measured elements. In this study only the normalised net intensities of Cu, Pb, and Zn as well as their respective ratios are discussed.

Table 6.1 *Site information of the investigated sediment cores in the Skagerrak.*

Core no.	Latitude [N]	Longitude [W]	Water depth (m)	Core length [m]
GeoB 6001-3	58° 09.4`	09° 48.3`	466	3.83
GeoB 6002-1	58° 04.8`	09° 37.2`	430	4.88
GeoB 6003-2	57° 58.3`	09° 23.2`	312	10.92

6.4 Results

The net intensities for Zn, Pb, and Cu obtained from the XRF core scanner analysis are given in counts per second. The net intensities were divided by the sum of all measured net intensities to minimise errors due to variable water contents, grain size variations, and others. Thus, the normalised net intensities provided here can be read as the relative contents of the respective elements in relation to all measured elements.

Table 6.2 *Overview over the average normalised Zn, Pb, and Cu intensities in the sediment cores from the Skagerrak.*

	Core no.	GeoB 6001-3	GeoB 6002-1	GeoB 6003-2
Copper (Cu)	max. normalised intensity	0.0096	0.0088	0.0092
	aver. normalised intensity in the enriched sediments	0.0045	0.0048	0.0043
	aver. background normalised intensity	0.0032	0.0034	0.0034
	aver. enrichment fatcor	1.41	1.41	1.27
	depth of increasing normalised intensity (cm)	113	106	92
Lead (Pb)	max. normalised intensity	0.011	0.0035	0.0033
	aver. normalised intensity in the enriched sediments	0.0013	0.0015	0.0014
	aver. background normalised intensity	0.0009	0.0010	0.0010
	aver. enrichment fatcor	1.38	1.48	1.43
	depth of increasing normalised intensity (cm)	113	113	88
Zinc (Zn)	max. normalised intensity	0.0077	0.0058	0.0070
	aver. normalised intensity in the enriched sediments	_	0.0030	0.0033
	aver. background normalised intensity	0.0025	0.0024	0.0026
	aver. enrichment fatcor	-	1.27	1.27
	depth of increasing normalised intensity (cm)	_	46	40

The normalised net intensities generally show the highest values in the Cu contents with mean values of 0.0037 (GeoB 6001-3), 0.0038 (GeoB 6002-1), and 0.0036 (GeoB 6003-2). Mean values for Zn normalised net intensities range from 0.0025 (GeoB 6001-3 & GeoB 6002-1) to 0.0027 (GeoB 6003-2), whereas average Pb normalised net intensities are 0.0011 in all three cores. In general, the normalised net intensities indicate noisy signals for Cu, Pb, and Zn with generally low, but noisy background signals and an increase towards the tops of the cores.

Copper

The shifts from background to enriched Cu normalised net intensities occur in core depths of 113 cm (GeoB 6001-3), 106 cm (GeoB 6002-1), and 92 cm (GeoB 6003-2) (Table 6.2; Fig. 6.2). Average background normalised net Cu intensities in the sediments range between 0.0032 (GeoB 6001-3), and 0.0034 (GeoB 6002-1 & GeoB 6003-2). Average Cu normalised net intensities in the upper, Cu-enriched sediments range from 0.0043 (GeoB 6003-2) and 0.0056 (GeoB 6001-3). Enrichments factors of Cu enriched sediments to background sediments vary between 1.41 (GeoB 6001-3 & GeoB 6002-1) and 1.27 (GeoB 6003-2) indicating the lowest enrichment in the north-western core GeoB 6003-2 (Table 6.2).

Lead

The Pb normalised net intensities indicate a pattern similar as found for Cu with low noisy background values and an increase towards the top of the cores, occurring at core depths between 88 cm (GeoB 6003-2) and 113 cm (GeoB 6001-3 & 6002-1) (Table 6.2; Fig. 6.3). The average background normalised Pb net intensities are in the range of 0.0009 to 0.0010 for all three cores. The Pb enrichment factor is lowest in core GeoB 6001-2 (1.37), followed by cores GeoB 6003-1 (1.43) and GeoB 6002-1 (1.48) and (Table 6.2).

Zinc

In general, the normalised Zn net intensities indicate a pattern similar to the Cu and Pb patterns with low and noisy background intensities and an increase in the intensities towards the top of the cores. However, the increase occurs higher up in the cores GeoB 6002-1 (46 cm) and GeoB 6003-2 (40 cm), and is absent (hardly visible) in core GeoB 6001-3 (Table 6.2; Fig. 6.4). Furthermore, the enrichment factors in the cores are rather low with values of 1.27 for GeoB 6002-1 and GeoB 6003-2. Average background normalised net intensities range from 0.0024 (GeoB 6002-1) to 0.0026 (GeoB 6003-2).

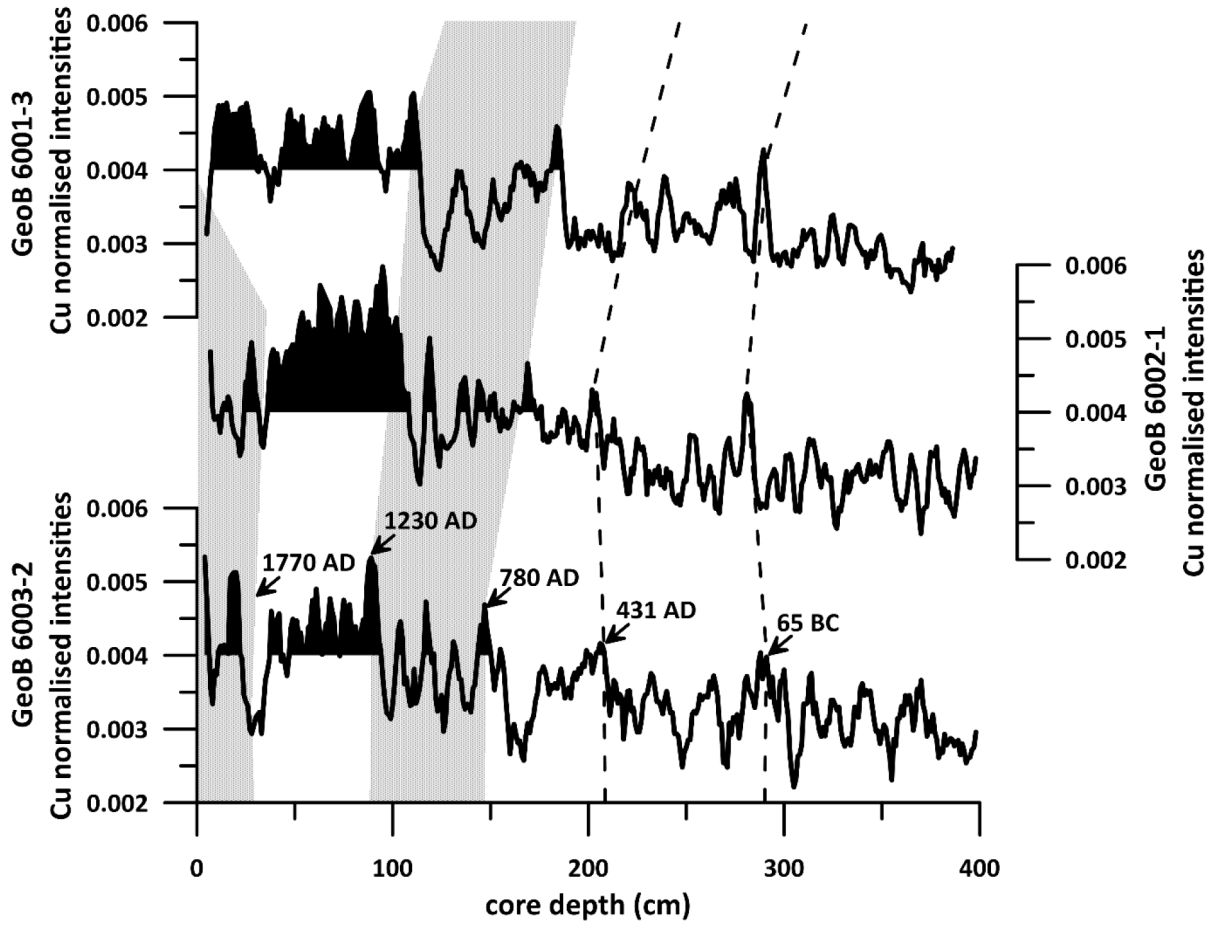

Fig. 6.2 *5-point running averages of normalised copper (Cu) net intensities in the upper 400 cm of cores GeoB 6001-3, GeoB 6002-1, and GeoB 6003-2. Grey shaded areas and black dashed lines indicate core sections and depth levels that are tentatively correlated stratigraphically. Age information is based on the age model for core GeoB 6003-2 provided by Hebbeln et al. (2006). Black shading of the curves display normalised Cu net intensities above 0.004.*

Interestingly, the increase of normalised Cu and Pb net intensities occur in rather similar core depths within the individual cores, but also within the set of all three cores (Cu: 92 to 113 cm; Pb: 88 to 113 cm; see Table 6.2; Fig. 6.2 and Fig. 6.3). In contrast, the Zn contents increase higher up in the cores GeoB 6002-1 and GeoB 6003-2, but is absent in the south-eastern core GeoB 6001-3. Furthermore, the increase of the Zn net intensities goes along with a decrease in the Cu net intensities and rather constant elevated Pb net intensities (Fig. 6.2, 6.3, and 6.4). Following the initial Zn increase, the uppermost sediment layers of GeoB 6002-1 and GeoB 6003-2 are generally marked by high and noisy Cu and Zn net intensities with partly opposing trends (Fig. 6.2 and 6.4).

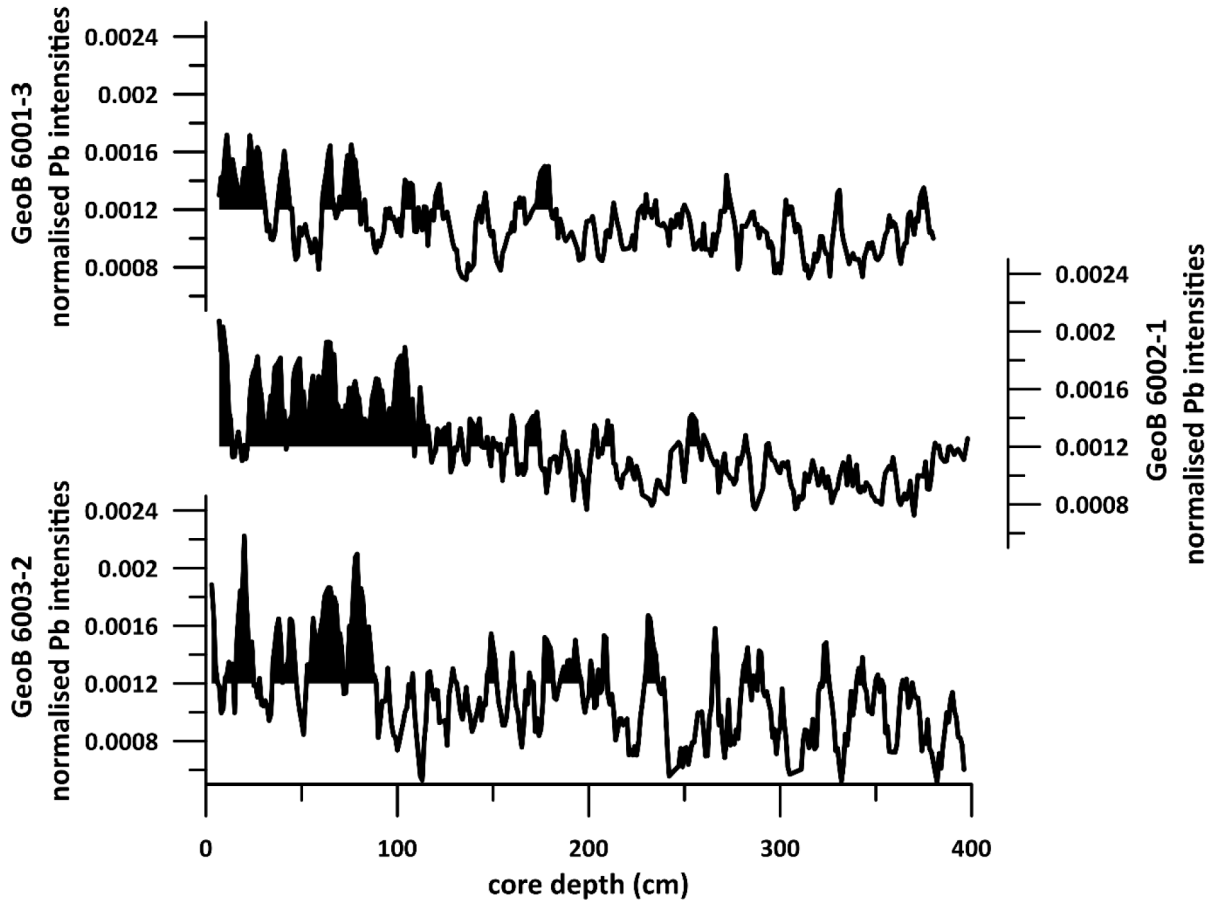

Fig. 6.3 *5-point running averages of normalised lead (Pb) net intensities in the upper 400 cm of core GeoB 6001-3, GeoB 6002-1, and GeoB 6003-2. Black shading of the curves display normalised Pb net intensities above 0.0012.*

Correlation and stratigraphy of the cores

The smoothed 5-point running averages of the Cu, Pb, and Zn normalised net intensities allow – in parts – a good correlation of the three sediment cores. The Cu record displays some significant changes in the pattern with the most pronounced being the major increase towards the top of the cores, which appears to be easy to correlate in all three cores (Fig. 6.2). Since the Pb net intensities increase in the same depth as the Cu net intensities, it is a clear indication for the overall good correlation of the cores. However, in the uppermost parts of the cores, the correlation gets more difficult. The obvious increase in Zn net intensities seen in cores GeoB 6003-2 and GeoB 6002-1 is missing in core GeoB 6001-3 (Fig. 6.4). In addition, also decreasing Cu values close to the core top observed in cores GeoB 6003-2 and GeoB 6002-1 are not displayed in the core GeoB 6001-3 record (Fig. 6.2). Thus, it seems that core GeoB 6001-3 lacks the youngest sediments (post ~AD 1660) that are preserved in the other two cores.

Based on such a correlation, the cores can be interpreted stratigraphically based on the published age model for core GeoB 6003-2, which in turn is based on four AMS ^{14}C dates and ^{210}Pb data in combination with grain size data (Hebbeln et al. 2006). According to this correlation, the increase in Cu and Pb normalized net intensities can be dated to ~AD 1230, while the onset in the Zn normalized net intensities occurred later at ~AD 1660 (Fig. 6.2 and 6.4). As this study focuses on the heavy metal enrichment in the sediments and the timing of the initial heavy metal enrichments, it is sufficient to only date/correlate the onset of the heavy metal enrichments.

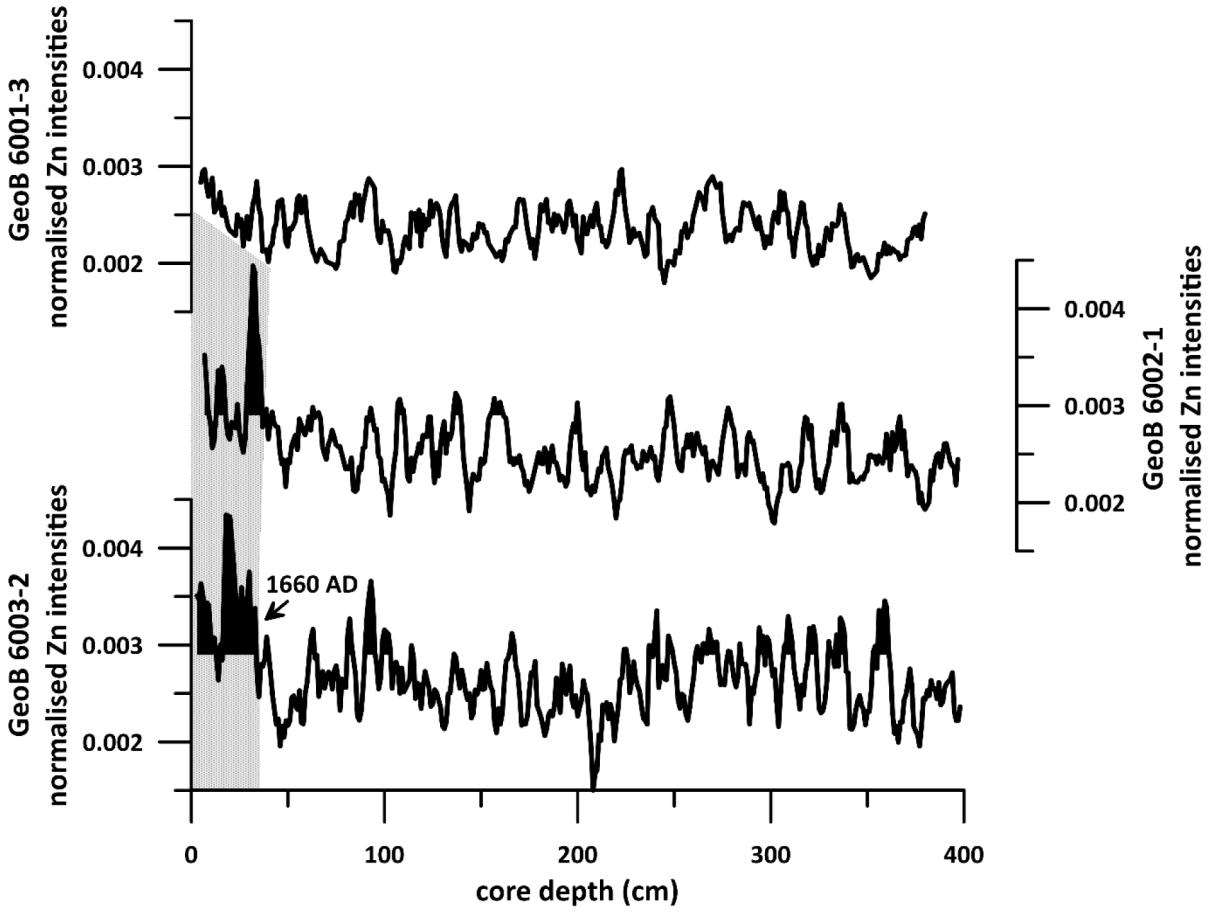

Fig. 6.4 *5-point running averages of normalised Zinc (Zn) net intensities in the upper 400 cm of core GeoB 6001-3, GeoB 6002-1, and GeoB 6003-2.* Grey shaded areas and black dashed lines indicate core sections and depth levels that are tentatively correlated stratigraphically. Age information is based on the age model for core GeoB 6003-2 provided by Hebbeln et al. (2006). *Black shading of the curves display normalised Zn net intensities above 0.0029.*

6.5 Discussion

Sedimentation rates

Sedimentation rates based on the timing of the onset of the Cu contents, dated to AD 1230 in core GeoB 6003-2, range between 1.20 mm/yr (GeoB 6003-2), 1.38 mm/yr (GeoB 6002-1), and 1.47 mm/yr (GeoB 6001-3), indicating increasing sedimentation rates from SW to NE. However, considering the obvious lack of the youngest sediments in core GeoB 6001-3 and assigning the preserved core top an age of AD 1660, the sedimentation rate for GeoB 6001-3 increases to 2.6 mm/yr. These sedimentation rates are in good agreement with the spatial distribution of sedimentation rates given in the literature (e.g. van Weering et al., 1987). Generally, the highest recent sedimentation rates in the Skagerrak have been found on the upper slopes of the southern and eastern Skagerrak with maximum values of up to 4.4 mm/yr (van Weering et al., 1987).

Temporal development of heavy metal inputs to the Skagerrak

The most obvious change in the heavy metal data of the investigated sediment cores is the significant increase of the normalised Cu net intensities in core depths of 113 cm (GeoB 6001-3), 106 cm (GeoB 6002-1), and 92 cm (GeoB 6003-2) (Table 6.2; Fig. 6.2). This increase has been used to stratigraphically correlate the cores and to provide an estimated age for the onset of increasing Cu and Pb contents at ~AD 1230 (Fig. 6.2) based on the published stratigraphic interpretation of core GeoB 6003-2 (Hebbeln et al., 2006). While the Pb contents increase parallel to Cu, interestingly, two of the three sediment cores show a later onset of enhanced Zn input estimated to approximately AD 1660 corresponding to core depths of 40 cm (GeoB 6003-2) and 46 cm (GeoB 6002-1). In core GeoB 6001-3 an increase in the Zn content is hardly detectable, which might be an indication for the absence of the youngest sediments in this core (Fig. 6.4), possibly lost during coring operations. Nevertheless, comparison of all the records of the three elements reveals that the increase in Zn input only began >400 years after the onset of increased Cu and Pb inputs.

These obvious increases in the normalised heavy metal net intensities in historical times following periods marked by comparably low but varying values ranging around rather constant means (i.e., natural background values) most likely reflect an anthropogenic impact on the heavy metal input to the Skagerrak. However, the different timing of enhanced Cu and Pb inputs on the one hand and Zn input on the other hand points to different sources and/or

processes linked to these specific elements (see below). This is further supported by the Zn/Cu ratios indicating a distinct offset at ~ AD 1230 with the onset of increasing Cu and Pb intensities (Fig. 6.5). With the increase of the Zn intensities and the simultaneous decrease in the Cu intensities at ~ AD 1660, Zn/Cu ratios increase again to values slightly above the background values. The respective ages for the onsets, ~AD 1230 and ~AD 1660, clearly demonstrate that these increases pre-date the industrialisation that in Europe only began at the end of the 18th century.

Potential sources of enhanced Cu and Pb inputs

In general, sediments in the Skagerrak derive from the entire North Sea and adjacent areas. Based on a provenance analysis of heavy minerals in the Skagerrak and the northern Kattegat, it was concluded that the major source for the deposited heavy minerals is the sediment transport along the Danish west coast from the southern North Sea, glacial deposits eroded from the Scandinavian mainland, and point sources on the Scandinavian mainland (Bengtsson and Stevens, 1996). Similar to the heavy minerals, heavy metals in the Skagerrak are assumed to be predominantly derived from the comparatively highly polluted south-eastern North Sea, to which heavy metals are discharged by major rivers such as the Rhine, Weser, and Elbe, transported towards the Skagerrak by the South and North Jutland Currents (Fig. 6.1; Kuijpers et al., 1993b; Zöllmer and Irion, 1993). Sediment cores from the Helgoland mud area, the only centre of continuous sediment deposition in the south-eastern North Sea, indicate elevated inputs of Zn and Pb dating back to ~AD 750, which have been related to early mining activities in the Harz Mountains and the Ore Mountains in northern and eastern Germany (Boxberg et al., in prep.). The Helgoland mud area and the Skagerrak are directly linked by the general circulation in the North Sea (Fig. 6.1) facilitating northward suspended matter and heavy metal transport (Svansson, 1975; van Weering, 1981, Eisma, 1981; Kuijpers et al., 1993a; Zöllmer and Irion, 1993).

However, as in contrast to our Skagerrak data, increased Zn and Pb inputs to the south-eastern North Sea are not accompanied by enhanced Cu inputs, any exclusive heavy metal supply from the south-eastern North Sea to the Skagerrak can be excluded. This is supported by the provenance analysis by Bengtsson and Stevens (1996), which indicates that heavy minerals around our core sites are derived from different sources and not predominantly from the south-eastern North Sea. This becomes even more obvious considering the temporal offset of enhanced Zn and Pb inputs to the Skagerrak, which both go in parallel in the Helgoland mud

area (Boxberg et al., in prep.). As there have never been any significant mining activities in Denmark (Bak et al., 1997) any suddenly increasing lateral Cu input along the Danish coast in the path of the South and North Jutland Currents also can be excluded.

Another potential source for the early anthropogenic induced Cu and Pb inputs to the Skagerrak is the generally increasing atmospheric heavy metal pollution in historical times as a consequence of the general advancement of mining and smelting activities. Such Cu and Pb emissions were transported over long distances and are even visible in Greenland ice cores (Hong et al., 1994; 1996). Pb concentration in the Greenland ice first started to increase ~2,500 BP (500 BC) and remained high until ~1,700 years BP (AD 300), reflecting smelting and mining activities of the Greco-Roman civilizations in major mining centres in Spain, Central Europe, Britain, and Greece (Hong et al., 1994). A period of lower Pb concentrations in the Greenland ice cores lasting from ~1,700 BP to ~1,500 BP is followed by continuously increasing concentrations from 1,500 BP (AD 500) to 500 BP (AD 1500) that is attributed to medieval mining and smelting activities (Hong et al., 1994). This temporal development of historic atmospheric Pb emissions were also found in peat deposits and lake sediments in Sweden, indicating the most significant increase at ~ AD 1000 (e.g. Renberg et al., 1994; Brännvall, 1997; Brännvall et al., 2000; Renberg et al., 2001). Also documented in Greenland ice cores is the onset of atmospheric Cu pollution at ~2,500 BP (500 BC) that also was interpreted to be a result of different phases of smelting activities in Europe long before the industrial revolution (Hong et al., 1996). Medieval times with high Cu concentrations in the Greenland ice cores were mainly linked to mining and smelting activities in Germany beginning in the ninth century and with mining and smelting of Swedish ores in the 13th century (Hong et al., 1996).

As traces of advancing mining and smelting activities in Europe in the last ~ 2,500 years can even be found in Greenland ice cores, the direct atmospheric transport of these emissions consequently might have contributed to the heavy metal inputs to the Skagerrak. However, as the onset of strong anthropogenic Cu and Pb inputs in the Skagerrak cores is dated back to ~AD 1230 and, thus, several hundred years later than early evidences of Cu and Pb pollution observed in Greenland ice cores and in Swedish peat deposits and lake sediments, these early heavy emissions seemingly did not contribute significantly to the heavy metal signal in our sediment cores. However, minor increases in this heavy metal load starting around BC 65 (Fig. 6.2, 6.3, and 6.4) might be attributed to this effect.

An alternative potential point source for anthropogenic Cu and Pb inputs reaching back for almost a millennium is the Falun copper mining district in central Sweden, approximately 400 km NE of our core sites (Fig. 6.6). Copper ores were mined and smelted in the Falun mining area for at least 1,000 years until mining finally came to an end in 1993 (Lundqvist, 1963; Qvarfort, 1984; Eriksson & Qvarfort, 1996; Ek and Renberg, 2001). In the historic context, the Falun mine was of great importance and in the 17th century the mine supplied approximately 2/3 of the world's Cu production (Ek and Renberg, 2001). Elevated Cu, Pb, and Zn contents in lake sediments from near the mine and adjacent smelting sites related to the mining activities even date back to the 13th century (Ek and Renberg, 2001), which is in very good alignment with an onset of enhanced Cu and Pb input to the central Skagerrak at ~AD 1230, as revealed by our sediment cores. For instance, Nilsson (1998) and Cooke and Bindler (2015) indicated heavy metal pollution in sediments of Lake Runn, located directly south of the former Falun mine, to have started as early as AD 1230 - AD 1245, demonstrated by rapidly increasing Cu, Pb, and Zn concentrations in the lake sediments. With increasing distance from the Falun mine and the major smelting sites, the Cu contents decrease more severely than the corresponding Pb contents (Ek and Renberg, 2001). This was explained by the emission of predominantly larger Cu particles > 1 µm compared to predominantly smaller Pb particles < 1 µm, as described by Kelley et al. (1995) and Jaffe et al. (1995) for heavy metal emissions on the Kola Peninsula. These observations could explain a comparatively further transport of Pb particles through the atmosphere. However, atmospherically transported Cu particles observed in Greenland ice cores clearly indicate the general potential of Cu emission to get transported over long distances (Hong et al., 1996).

The general consistency in the temporal development of heavy metal enrichments in lake sediments around the Falun mine with the timing of Cu and Pb inputs to the Skagerrak, clearly point to the Falun mine as the primary source for the almost parallel increase of Cu and Pb in our sediment cores (Fig. 6.2 and 6.3; Table 6.2). Assuming the Falun mine to be an important source for the enhanced Cu and Pb inputs to the Skagerrak requires a suitable transport pathway. The comparatively short distance (< 450 km) between the Falun mining district and the Skagerrak core sites, as compared to the major mining centres in southern and central Europe during the Greco-Roman period (Hong et al., 1994), suggests the direct atmospheric transport of Cu and Pb emissions from the Falun district to be a suitable transport pathway. In addition to a direct atmospheric input of Cu and Pb, the following scenario also describes a

plausible transport mechanism: heavy metal emissions might have been transported towards Lake Vänern, the third largest European lake, which is only 200 km away from the Falun mine, with its catchment reaching even closer (Fig. 6.6). Any local to regional atmospheric transport of smelting emissions towards the catchment and the lake during easterly winds possibly resulted in the enrichment of heavy metals derived from the Falun mine in the lake's SPM. From Lake Vänern heavy metal enriched SPM could have been transported further through the Göta River to the northern Kattegat. From there, it might have been transported by the Baltic Current and the Norwegian Coastal Current towards the central Skagerrak and might have been caught in the low-current-velocity area (Eisma and Kalf, 1987), where it possibly sunk through the water column and finally accumulated at the seafloor.

The rather large distance as well as the huge area of the Skagerrak sediment depocenter might explain the low enrichment factors in the Cu and Pb contents in the sediment cores in relation to background values (Table 6.2) in comparison to,e.g., sediments in the Helgoland mud area (Boxberg et al., in prep.), which have been retrieved from a well-defined small depocenter close to the fluvial point sources of the Elbe and Weser Rivers (Boxberg et al., in prep.). Heavy metal emissions from the Falun mining district might have been diluted with non-polluted air and non-polluted SPM, respectively, on the way through the atmosphere and through the fluvial and marine realm to the study sites on the southern flank of the Skagerrak.

Surprisingly, the Zn contents in the Skagerrak sediment cores do not show any enrichments in the same depths and, hence, at the same time, even though the Zn concentrations in the vicinity of the Falun mine mainly show a similar temporal pattern as the Cu and Pb concentrations with decreasing concentrations with increasing distance from the source. We assume that Zn emissions, similar to the observations for Cu particles by Kelley et al. (1995) and Jaffe et al. (1995), generally do not get transported to a huge amount over longer distances and, hence, the Zn emissions did not reach the Skagerrak through direct atmospheric transport to a detectable amount and left no significant traces along the fluvial and marine transport pathway to the Skagerrak. In contrast to the large-scale atmospheric transport of Cu and Pb (Hong et al., 1994; Hong et al., 1996), atmospheric emissions of Zn first became visible in the Greenland in the course of the industrial revolution (Hong et al., 1997). This might be another hint pointing to generally weaker long-range transports of Zn particles in comparison to Cu and Pb particles.

Additional input of Zn and Pb since ~AD 1660

Interestingly, the ~430 years delay of increasing Zn enrichments with respect to the onset of increased Cu and Pb levels in the Skagerrak sediments and the spatial pattern of increasing Zn enrichments and decreasing Cu enrichments in SW direction (Fig. 6.2, 6.3, and 6.4; Table 6.2), both point to different source for the increased Zn input. This is further corroborated by opposite trends in Zn and Cu net intensities after the Zn contents began to increase at AD 1660 (Fig. 6.2 and 6.4) and by distinct offsets in the Zn/Cu ratios in the sediment cores through core depth and, thus, through time (Fig. 6.5). Actually, the enhanced Zn levels in combination with high Pb levels and decreasing Cu contents suggest a parallel input of Zn and Pb from this additional source.

Several indicators point to the southern North Sea as the additional source for the enhanced Zn and Pb inputs after AD 1660. Elevated Zn and Pb levels in the Helgoland mud area, dated back to an onset at ~AD 750 and attributed to medieval mining and smelting activities in eastern and northern Germany (Boxberg et al., in prep.), indicate the potential of SE North Sea as a source for anthropogenic heavy metal inputs to the Skagerrak. Furthermore, Zöllmer and Irion (1993) showed decreasing heavy metal concentrations in surface sediments along the Danish west coast indicating a northward transport of anthropogenic heavy metals with the Jutland Current (Zöllmer and Irion, 1993). This is also supported by Kuijpers et al. (1993b), who found out that the deposition of fine-grained material transported from the southern North Sea by the Jutland Current is the main mechanism determining the recent regional accumulation of Pb in the Skagerrak. The highest Zn/Cu ratios found in the uppermost 50 cm of the southernmost core GeoB 6003-2 likewise indicate the Zn (and additional Pb) source to be located in the south and most likely delivered by the Jutland Current (Fig. 6.6).

The most plausible explanation for the shift in the source for the heavy metals deposited at our core sites in the southern Skagerrak at AD 1660 is a small northward shift of the vortex that is assumed to have supplied Cu and Pb enriched SPM derived from the northern Skagerrak. Whereas before AD 1660 Cu and Pb inputs were most likely delivered by the Norwegian Coastal Current, trapped and finally deposited within this low-current velocity vortex (Eisma and Kalf, 1987), a slight northward shift of this vortex might have prevented the advection of such “northerly sourced” heavy metals to our core sites. At the same time, such a shift would have allowed SPM advected by the Jutland Current to supply Zn and Pb from the southern North Sea to the core sites. Consequently, the heavy metal signal derived from the

Falun mining district was replaced by the heavy metal coming from the southern North Sea at approximately AD 1660, resulting in the described pattern of increasing Zn intensities, decreasing Cu intensities, and comparatively constant Pb intensities.

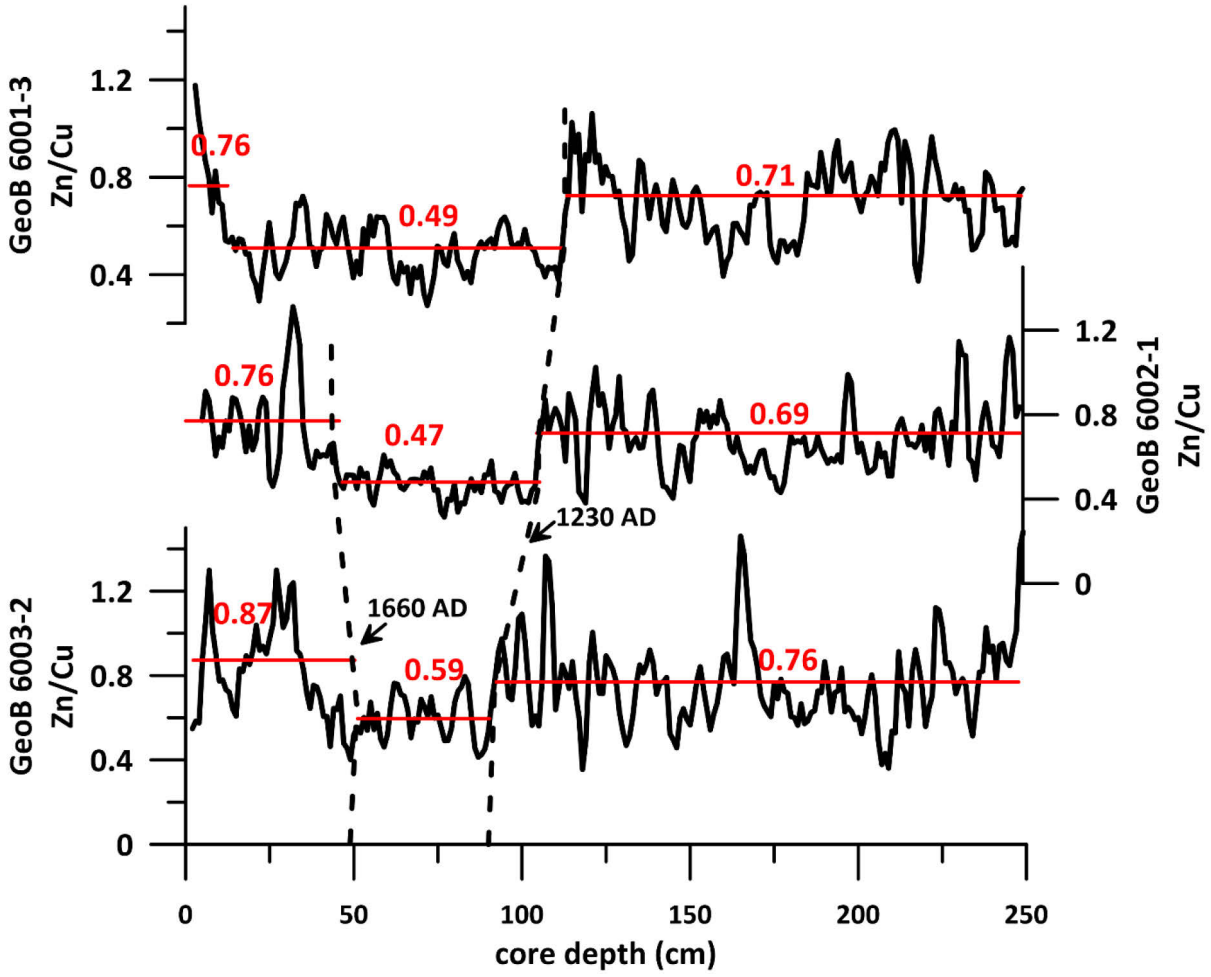

Fig. 6.5 *3-point running average of Zn/Cu ratios of the upper 250 cm of the three sediment cores indicating three different levels of Zn/Cu ratios. The first major decrease in the Zn/Cu ratios at ~AD 1230 coincides with the increased Cu and Pb net intensities, whereas the increase in the Zn/Cu ratios at ~AD 1660 marks the increase of Zn net intensities.*

However, after the initial Zn increase at ~ AD 1660, the Zn intensities are generally enriched compared to the background values, but indicate significant variations (Fig. 6.4). The partly opposing trends of the Zn and Cu intensities in the uppermost sediments of the cores GeoB 6002-1 and GeoB 6003-2 probably reflect varying contributions by the vortex and by the Jutland Current. Times of rather high Cu and Pb intensities and rather low Zn intensities are characterised by the dominance of SPM coming from the Falun area via the Norwegian Coastal Current, whereas times of high Zn and Pb intensities and rather low Cu intensities are dominated by SPM inputs from the southern North Sea. Thus, since the onset of additional

inputs from the southern North Sea at ~ AD 1660, the anthropogenic heavy metal inputs to the southern Skagerrak consists of a mixture of heavy metal supply from the Falun mining district and the southern North Sea in varying proportions.

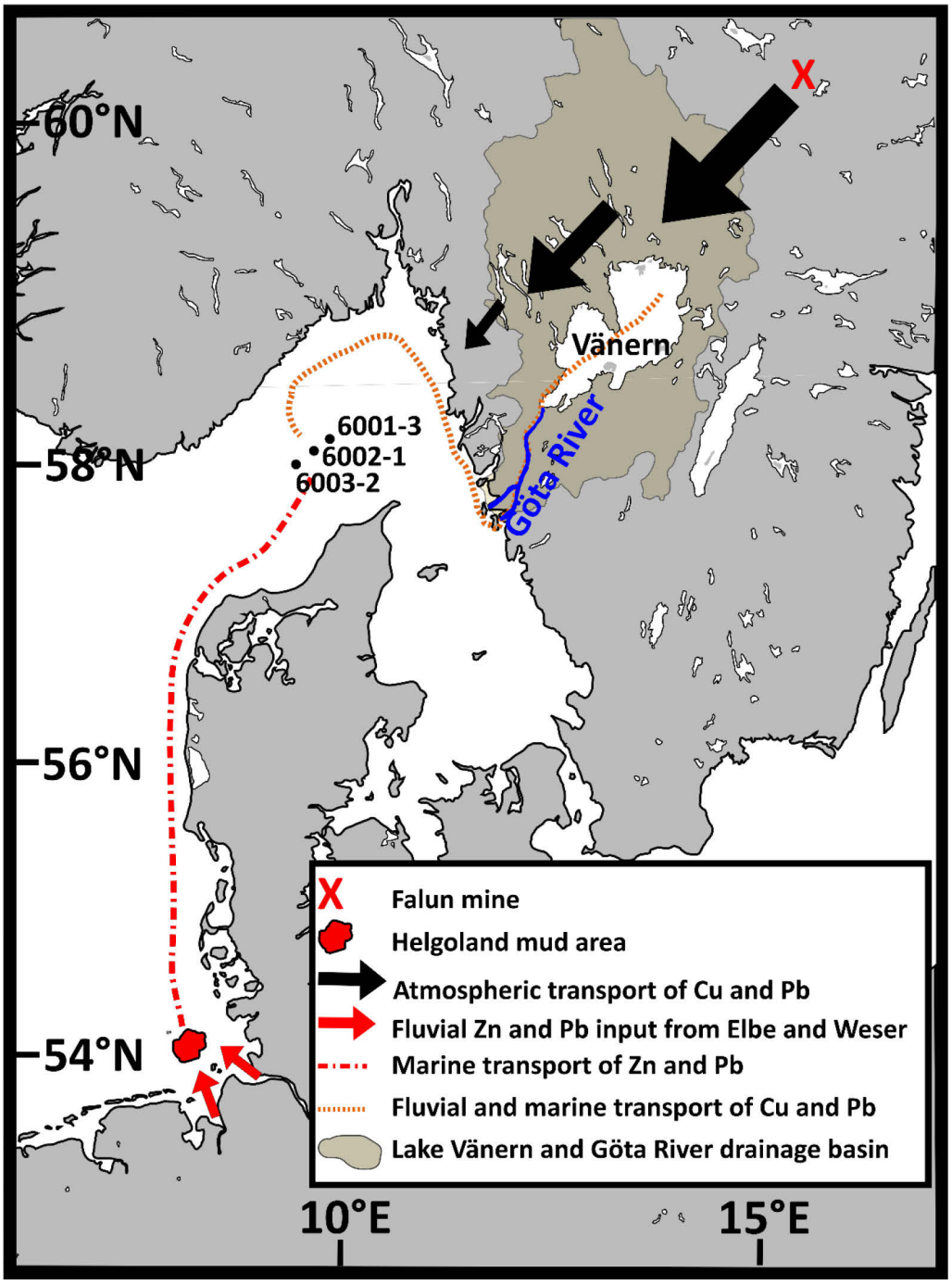

Fig. 6.6 *Possible scenario of heavy metal transport to the study area. During easterly winds, medieval Cu and Pb emissions from the Falun mine get transported through the atmosphere towards Lake Vänern and its catchment since ~ AD 1230. In the further course, these heavy metals might be transported to the northern Kattegat by the Göta River, and further transported to the core sites through the Baltic Current and the Norwegian Coastal Current. The direct atmospheric transport from the Falun area to the study sites might have contributed to the heavy metal inputs of the Skagerrak. Since approximately AD 1660, additional Zn and Pb inputs reach the study area via marine transport from the southern North Sea along the Danish west coast.*

6.6 Conclusion

An anthropogenic induced heavy metal input to the southern Skagerrak in historical times could clearly be shown by the presence of elevated Cu, Pb, and Zn levels in the sediments. Levels of Cu and Pb began to increase at approximately AD 1230 and are assumed to predominantly reflect early mining and smelting activities in the Falun mining district in central Sweden, with the heavy metal signal having been transported to the study sites direct atmospheric transport and via fluvial and marine transport. The later additional onset of Zn and Pb inputs at approximately AD 1660 can likely be attributed to mining and smelting activities in northern and eastern Germany, transported via major rivers to the southern North Sea and onwards by the Jutland Currents to the Skagerrak. This change in the source area of the heavy metals to the southern Skagerrak is assumed to reflect small scale oceanographic changes resulting in an increasing SPM supply from the southern North Sea and a decreasing SPM supply from the Norwegian Coastal Current.

7. Sediment deposition in the central Hauraki Gulf, New Zealand

Florian Boxberg[1], Brice Blossier[1], Willem P. de Lange[2], Bethany Fox[2], Dierk Hebbeln[1]

[1]MARUM - Centre for Marine Environmental Sciences, University of Bremen, Bremen, Germany

[2]School of Science, University of Waikato, Hamilton, New Zealand

7.1 Abstract

Based on the analysis of 14 short sediment cores, we present new insights in the distribution of surficial sediments in the central Hauraki Gulf, a semi-enclosed coastal embayment on the northeast coast of New Zealand`s North island, and identify and discuss the effects of interaction of modern wind-generated waves and currents with regards to deposition and reworking of sediments in the Gulf. The modern hydrodynamic regime is controlled by tidal currents, oceanic inflows, and wave-induced currents and it is responsible for a N-S gradient in sediment texture and elemental concentrations in the central Hauraki Gulf sediments. The present-day sediment input into the system is generally low and consists of fine-grained fluvial sediments mostly deposited in the southern study area and comparatively high inputs of relict carbonate material to the northern study sites. The central Hauraki Gulf sediments, which show numerous age reversals in the sedimentary record, can be characterized as palimpsest sediments, as a consequence of continuous reworking and storm-induced sediment transport. In view of the new data, a previously assumed significant post-transgression accumulation of sediments of >10 m in the central Hauraki Gulf appears to be very unlikely.

Key Words: Hauraki Gulf; sediment deposition; hydrodynamics; palimpsest sediment

7.2 Introduction

In recent times, the management, conservation, and sustainable use of near-coastal marine ecosystems has become increasingly important due to the ongoing anthropogenic modification and utilisation of these ecosystems (e.g. Waycott et al., 2009). Especially in highly populated areas with severe human impacts as e.g. the runoff of pollutants and nutrients into coastal waters (e.g. Howarth et al., 2000; Smith, 2003), the conversation of pristine coastal marine ecosystems or the restoration of human modified ecosystems, respectively, is an important issue. The sustainable use of these ecosystems requires a detailed knowledge of the seafloor setting and the processes controlling it.

The Hauraki Gulf, a shallow and semi-enclosed coastal embayment on the northeast coast of the North Island of New Zealand (Fig. 7.1), is an example for such a near-coastal marine ecosystem affected by anthropogenic activities at least since early European settlements in the area ~ 1800 AD. The Gulf plays an important role for New Zealand because it a) covers the largest shelf embayment of New Zealand, and b) borders the largest population centre of New Zealand, Auckland, and, hence, is important for both commercial and recreational activities for approximately one third of New Zealand's population. Even though the Gulf has been subject to a large number of studies, the seafloor setting and the processes controlling it have only partly be covered and are not fully understood yet. For instance, the knowledge of the processes controlling sedimentation patterns in the Gulf is lacking or is controversially described in the literature, respectively. The conceptual model of partly event-driven near-bed sediment transport by Manighetti and Carter (1999) would result in different sedimentation patterns as the model invoking the dominant control of "normal" residual or net circulation pattern in the Hauraki Gulf described by Proctor and Greig (1989). To which extent these two conceptual models control sedimentation patterns in the central Hauraki Gulf, however, is not known.

Based on the analysis of 14 short sediment cores focusing on a small area in the central Hauraki Gulf, this study aims to a) improve the understanding of surficial sediment distribution in the central Hauraki Gulf and b) identify and discuss the effects of the interaction of wind-generated waves and currents with regards to deposition and reworking of sediments in the Gulf, in order to assess which of the two conceptual models mentioned above has the greatest influence in the sediment deposition in the central Hauraki Gulf. It turned out that

sedimentation patterns in the Gulf are more complex than previously thought, and, hence, previously described patterns of deposition and dispersal of sediments in the central Hauraki Gulf might need some reconsideration.

7.2.1 Regional Setting

The Hauraki Gulf is bounded to the east by the Coromandel Peninsula and to the south and west by the mainland of New Zealand. To the north it is partially open to the Pacific Ocean (Fig. 7.1). Water depths in the Gulf increase northwards with values of <40 m in the inner Gulf south of Tiritiri Matangi Island, 40 – 50 m in the central Gulf between Tiritiri Matangi Island and Cape Rodney, and 50 – 100 m north of Cape Rodney to the Hen and Chicken Islands (Fig. 7.1). The southern end of the Hauraki Gulf consist of the wide and relatively shallow Firth of Thames with water depths < 20 m (Manighetti and Carter, 1999). The Gulf has been subject to a broad range of studies including sediment distribution (e.g. Eade, 1974; Carter and Eade, 1980; Greig, 1982; Manighetti and Carter, 1999), water circulation within the Gulf (e.g. Greig and Proctor, 1988; Proctor and Greig, 1989; Greig, 1990; Black et al., 2000; Zeldis et al. 2004), geophysical investigation of sub-seabed structures (e.g. Hochstein and Nixon, 1979; Hochstein et al., 1986; Thrasher, 1986), organic matter distribution (e.g. Uhle et al., 2007; Sikes et al., 2009) and paleoenvironmental analyses (Greig, 1982; Pocknall et al., 1989).

Sediments in the Hauraki Gulf

Sedimentary characteristics and structures in the Hauraki Gulf have been studied by Manighetti and Carter (1999) and Sikes et al. (2009), amongst others. The seafloor is characterised as a smooth and flat surface (Manighetti and Carter, 1999). Sediments in the sheltered Firth of Thames (Fig. 7.1) are predominantly fine grained; consisting of sandy and calcareous mud (Eade, 1974; Carter and Eade, 1980; Greig, 1982). Towards the north sediments generally become coarser, ranging from sandy mud to muddy sand. In general, grain sizes have been interpreted as being controlled by wave and current distribution rather than by depth (Sikes et al., 2009), as indicated by the presence of finer sediment in the more sheltered areas. Due to the divergence and weakening of the currents in the southern central Gulf, sedimentation rates were inferred to be generally higher, associated with the comparably higher accumulation of finer sediments compared to the higher energy settings in the outer Gulf (Sikes et al., 2009).

The modern-day terrigenous input is low, consisting of mud and fine sands supplied by several small rivers (Manighetti and Carter, 1999). Even though erosion rates in the catchment and, hence, the possible terrestrial sediment discharge, are thought to have dramatically increased in response to deforestation after the arrival of early Polynesian and European settlers, the bulk of the terrigenous sediment gets trapped within sheltered embayments such as the Firth of Thames and in estuaries (Carter and Eade, 1980; Greig, 1982). Nevertheless, for the central Hauraki Gulf, the uppermost Holocene post transgressive sediment thickness, forming since the flooding during the last marine transgression, has been estimated by Manighetti and Carter (1999) to be up to 12 m within relatively confined depocenters. After the last glacial period, the deglacial marine transgression reached the outer shelf at ~ 15 ka B.P. (Carter et al., 1986). The study area, with present-day water depths of ~ 45 m, was inundated by the rising sea level between 12 ka and 9.5 ka B.P. (Smith, 1992) and present-day sea level was reached at approximately 8.1-7.3 ka B.P. (Clement et al, 2015). Subsequently, sea level continued to rise, reaching a high-stand up to 2 m above present at ~ 4 ka B.P. before falling back to the present-day level at ~ 1 ka B.P. (Dougherty and Dickson, 2012).

In the past, the sedimentary history of the Hauraki Gulf was strongly connected to the Waikato River (Fig. 7.1), presently New Zealand's longest river with a total length of ~425 km. Until approximately 22.5 kyr ago, the Waikato River, draining the central volcanic region of New Zealand`s North Island, was the major supplier of sediments to the Hauraki Gulf over much of its history. However, at that time the river changed its course. Where previously it flowed into the glacial alluvial plain of the modern Hauraki Gulf, it now flows into the Tasman Sea (Manville and Wilson, 2004). Based on mineralogy, it has been suggested that a significant proportion of the coastal sands found presently along the western side of the Hauraki Gulf were derived by reworking and onshore movement of older Waikato River deposits on the continental shelf during the Holocene, and possibly earlier, marine transgressions (Schofield, 1970).

Circulation in the Hauraki Gulf

The water exchange between the Gulf and the Pacific Ocean takes place through three major channels: Jellicoe Channel between Little Barrier Island and the mainland (Cape Rodney), Cradock Channel between Great Barrier Island and Little Barrier Island, and Colville Channel between Great Barrier Island and the northern tip of the Coromandel Peninsula (Fig. 7.1). Water circulation and currents in the Hauraki Gulf are driven by the interaction of tidal flows

and the seafloor topography, which concentrates flow through the channels, and by winds creating pressure gradients within the Gulf, which vary in strength with wind direction and magnitude (Black et al., 2000).

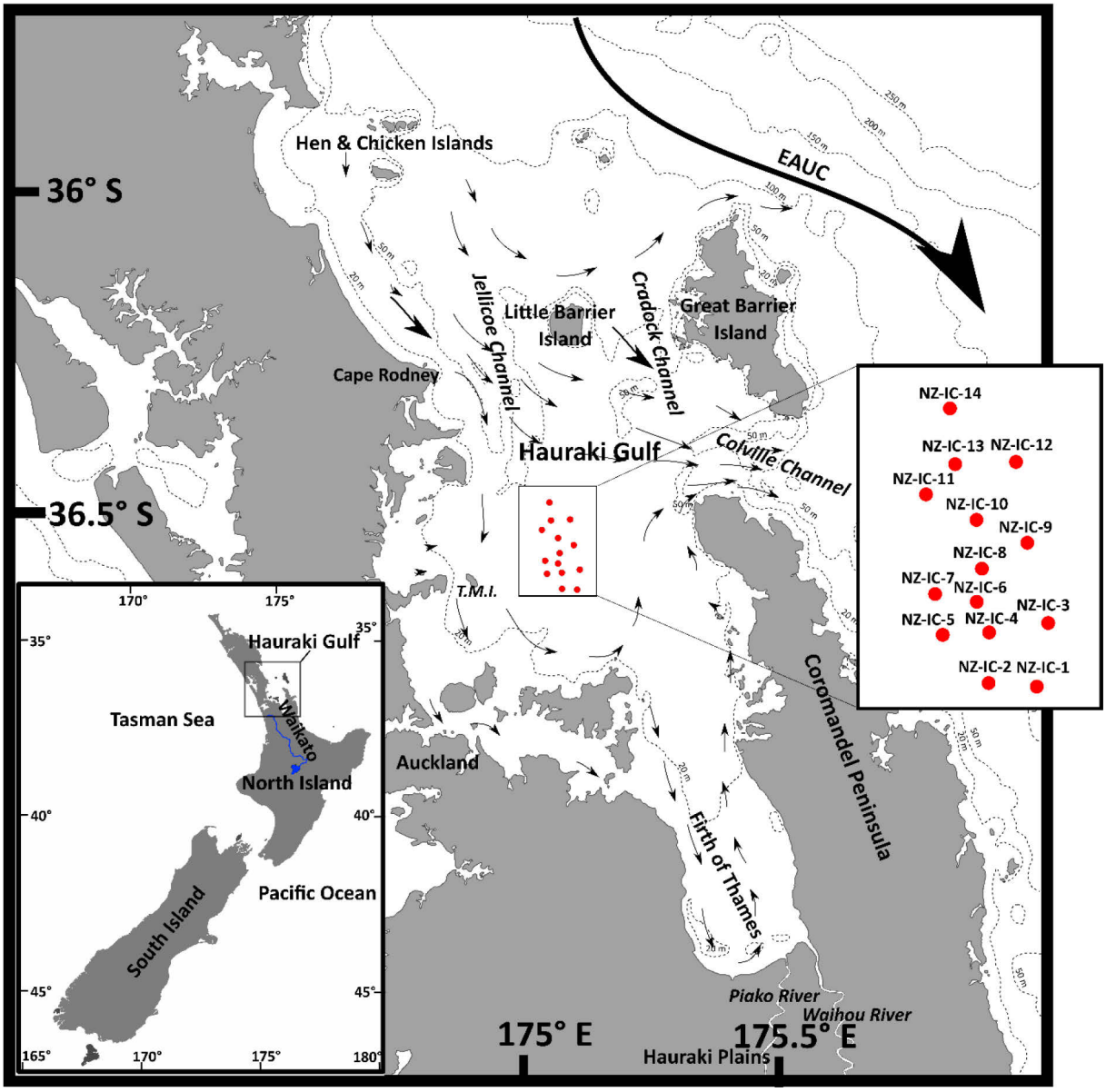

Fig. 7.1 *Location of the study area in the Hauraki Gulf. The left inset map shows the study area on the North Island of New Zealand. Red dots in the main map mark the core locations (NZ-IC-1 to NZ-IC-14; right inset map). Black arrows indicate the prevailing surface currents in and outside the Gulf according to Black et al (2000) (T.M.I. – Tiritiri Matangi Island; EAUC – East Auckland Current).*

In general, water enters the Gulf through Jellicoe Channel, flows anti-clockwise across the central/inner Gulf, and leaves the Gulf via Colville Channel (Greig, 1990). Waters entering the Gulf through Cradock Channel usually pass out of the Gulf directly through Colville Channel. The net circulation in the Hauraki Gulf is estimated to go from north to south, driven by

residual tidal currents (Greig and Proctor, 1988; Proctor and Greig, 1989; Sharples, 1997; Black et al., 2000; Zeldis et al., 2004). The tidal amplitude in the Gulf ranges from ~1.35 m in the southern Firth of Thames to ~0.85 m in the outer Gulf north of the Barrier Islands (Greig and Proctor, 1988). Tidal currents are strongest in the three Channels (Greig, 1990). The non-tidal circulation is mainly driven by wind with different wind directions resulting in different current directions. Surface currents are mainly in wind direction, whereas subsurface currents indicate closed circulation cells/gyres in near-coastal areas under SE and NE winds. (Proctor and Greig, 1989). Proctor and Greig (1989) modelled a steady inflow from the north, representing a mass flux into the Gulf and caused by winds acting on the shelf north of the Gulf.

Manighetti and Carter (1999) considered that the wind and tidally-driven near-bottom currents, interacting with waves and oceanic incursions of the East Auckland Current were the main factor causing sediment redistribution in the Hauraki Gulf. According to their model, under calm weather conditions, the circulation is dominated by the tide and the sand-sized sediments are mostly stable. However, under meteorological forcing, large storm waves with the potential to interact with the seafloor down to 100 m water depth lead to reworking of the sediments (Manighetti and Carter, 1999). The combination of wave entrainment of sediments and the advection by other wind-induced and tidal currents produces a transport of sand across the shelf to the central Gulf. This in turn leads to a net gain of sediments in the central Gulf (sediments from the mainland north of Cape Rodney) and a net loss of sediments from the Western Coromandel Peninsula through Cradock and Colville Channels (Manighetti and Carter, 1999).

7.3 Methods

Sampling

A set of 14 sediment cores was collected in the inner/central Hauraki Gulf (Fig. 7.1 and Table 7.1) using a Rumohr-type gravity corer with a total weight of ~80 kg and a tube diameter of 100 mm. The Rumohr corer is especially designed to take short, undisturbed sediment cores from the very top sediment layers. The 15-57 cm long sediment cores were subsampled at centimetre increments by slicing the cores. Approximately 2 g of each sample was used for particle size analysis. The remaining bulk sediment samples (475 in total) were dried in an oven at 50°C for 24 hours for further analysis.

Particle size analysis

Particle size analysis on each sample was performed with a Laser Diffraction Particle Size Analyser (Malvern Mastersizer 2000). Prior to the measurement, the terrigenous sediment fractions were isolated by removing organic carbon and calcium carbonate. Organic carbon was removed by adding 10 ml of 10% hydrogen peroxide (H_2O_2). This step was repeated every few hours until the reaction stopped. If multiple additions were required, the sample beakers were placed on a hot plate and warmed gently to speed up the reaction. Subsequent to the organic matter removal, the samples were diluted with filtered, demineralized water until a pH-value of ~7 was achieved. The calcium carbonate was then removed with 1 ml of 25% solution of hydrochloric acid (HCl). This step was repeated until the reaction stopped. After the carbonate removal, the sample was again diluted with filtered, demineralized water to a pH-value of ~7. Finally, the samples were dispersed with ~1 ml of 10% calgon and stirred. Measurements were carried out with demineralized and filtered water in the Malvern Mastersizer 2000 (Malvern Instruments). The results obtained show the particle-size distribution from 0.05 to 2000 µm subdivided into 100 size classes.

Table 7.1 *Site information for the 14 sediment cores from the central Hauraki Gulf taken from aboard the MV Macy Gray (Western Work Boats) on January 28, 2015.*

Core	GPS coordinates		Water depth	Core length
NZ-IC-	S	E	m	cm
1	36° 36.795'	175° 04.107'	44.5	57
2	36° 36.897'	175° 05.963'	45.8	42
3	36° 35.019'	175° 06.256'	47.1	40
4	36° 35.308'	175° 04.131'	44.1	31
5	36° 35.514'	175° 02.321'	45.3	57
6	36° 34.490'	175° 03.724'	44.9	34
7	36° 34.225'	175° 02.237'	45.6	30
8	36° 33.444`	175° 04.054'	45.1	42
9	36° 32.719'	175° 05.646'	46.5	34
10	36° 32.097'	175° 03.689'	45.5	32
11	36° 31.397'	175° 01.767'	46.2	20.5
12	36° 30.308'	175° 05.244'	45.5	13
13	36° 30.374'	175° 02.969'	46.9	23
14	36° 28.697'	175° 02.744'	47.7	20

XRF analysis

Approximately 1 g of the dried sub-samples of each sediment slice were grounded and homogenized using a mortar and pestle. The powdered sample was loaded into a sample cup and covered with a thin Mylar film. The samples were measured using an Olympus Innov-X Delta 50 keV Handheld XRF Analyser gun (Olympus Innov-X 50KV DP4050CX) set to "Soil Mode" and mounted in a benchtop stand. Concentrations of major and trace elements were recorded by Innov-X Delta Advanced PC software. The following elements were analysed: P, S, Cl, K, Ca, Ti, V, Cr, Mn, Fe, Co, Ni, Cu, Zn, As, Se, Rb, Sr, Y, Zr, Nb, Mo, Ag, Cd, Sn, Sb, Te, W , Au, Hg, Pb, Bi, Th, and U, however, only the Ca and Ti data are discussed in this study. Limits of detection for elements analysed are all in the ppm range, except for P (<0.5%). Scanning time was approximately 90 seconds per sample. To determine accuracy and precision of the method, an international reference material (Green River Shale, SGR-1) was measured after every 10 samples, with the results indicating constant values. In this study, only the relative variability of Ca/Ti is shown and discussed, and, thus, a good comparability of the concentrations is given.

Radiocarbon dating

To constrain the depositional history of the central Hauraki Gulf within a stratigraphic framework, discrete samples from different depths were selected for accelerator mass spectrometer (AMS ^{14}C) radiocarbon dating. Initially, 11 samples of macroscopic carbonate bivalve and gastropod shells were sent to the Poznań Radiocarbon Laboratory in Poznań, Poland (Table 7.2). In addition, for 9 samples approximately 10 mg of mixed benthic foraminifera were picked from the fraction 150-500 µm after wet-sieving and sent to the Poznań Radiocarbon Laboratory in Poznań and to the Beta Analytics Limited radiocarbon lab in London, UK (Table 7.2). Radiocarbon measurements were performed on cores NZ-IC-1, NZ-IC-3, NZ-IC-5; NZ-IC-6, NZ-IC-7, NZ-IC-8, NZ-IC-9 and NZ-IC-14. All AMS ^{14}C ages were corrected for isotopic fractionation using $\delta^{13}C$ values. The resulting conventional radiocarbon ages were converted into calendar years using the Calib 7.1 software (Stuiver et al. 2017) with the Marine 13 calibration curve (Reimer et al. 2013) considering a global mean reservoir age of 400 years (Bard, 1998), which has been confirmed as appropriate for nearby New Zealand east coast marine waters (Higham and Hogg, 1995). Results are given as the median probability calendar ages accompanied by the 1σ- (68.3 % probability) and 2σ-ranges (95.4 % probability) (Table 7.2).

SWAN simulation of wave parameters in the Hauraki Gulf

To evaluate the potential role of waves in the distribution of surficial sediments in the Hauraki Gulf, a regional nonstationary SWAN model was set up (Zijlema et al. 2010). It simulates the wave field for the northeast region of the North Island over the period 1989 – 2009. An unstructured grid (27673 cells) was used with a grid cell size that varies from 50 km² (offshore, more than 1000 m depth) to 0.5 km² in the vicinity of the Hauraki Gulf (depth less than 100 m).

Similar to the approach followed by Blossier et al. (2016), the model was nested into the global WaveWatch III (WW3) Ocean Wave hindcast model (National Oceanic and Atmospheric Administration, NOAA). Hourly 0.5° spatial resolution winds (Climate Forecast System Reanalysis Reforecast – CFSRR), provided by the NCEP (National Center for Environmental Prediction)) drove the global model and were included in the local nested model. Spectral wave conditions applied to the SWAN model boundaries were extracted from the nearest WW3 output locations (seven points). The nonstationary model time step was 30 min and wave field data were generated every hour. Regional bathymetry was provided by NIWA (National Institute for Water and Atmospheric Research, NZ) for New Zealand (Mitchell et al., 2012) and the Hauraki Gulf (Mackay et al., 2012). The wave model was validated based on the data collected by a wave buoy located near Motiti Island and maintained by the Bay of Plenty Regional Council. Reasonable hindcasting skill was found for significant wave height H_s (R^2 = 0.85 and RMSE (Root-Mean-Square Error) = 0.2) and mean wave period Tm (R^2 = 0.75 and RMSE = 0.9). Wave direction was fairly simulated as well (R^2 = 0.60 increasing to 0.75 for higher waves (H_s > 0.7 m) that are of interest in the present paper).

7.4 Results

Radiocarbon AMS ^{14}C dating

Twenty radiocarbon dates based on carbonate shells (mussels and snails, n=11) and mixed benthic foraminifera assemblages (n=9) have been established on 8 out of the total of 14 cores. The individual cores are frequently characterised by various age reversals. The oldest obtained ages go back as far as 10,900 cal yrs BP (Table 7.2). In general, the ages from the northern part of the study area span “only” the last ~2,300 years, whereas ages in samples from the southern part reveal frequently ages older as 7,000 years (Fig. 7.3 and Table 7.2).

However, due to the numerous age reversals, an estimation of sedimentation rates is rather difficult.

Table 7.2 *Overview of the AMS-^{14}C dates in the sediments based on the analysis of mixed benthic foraminifera (MBF) and carbonate shells (CS).*

Core no. NZ-IC	Depth (cm)	Lab. Identification	Conventional radiocarbon age (BP)	Sample type	1σ range of calender years BP	2σ range of calender years BP	Median Probability Age (calendar years BP)
1	**13-14**	Poz-78719	3240 ± 50	MBF	3253-3037	3366-2940	**3,149**
1	**26-27**	Poz-78720	2705 ± 30	MBF	2543–2373	2729-2369	**2,514**
1	**27-28**	Poz-75129	8440 ± 40	CS	9238-9051	9353-8957	**9,146**
1	**44-45**	Poz-78721	7140 ± 50	MBF	7768-7623	7854-7553	**7,697**
1	**50-51**	Poz-75130	9880 ±50	CS	11041-10797	11152-10717	**10,924**
3	**9-10**	Poz-78713	1455 ± 30	MBF	1161-1010	1242-963	**1,093**
3	**9-10**	Poz-75207	485 ± 30	CS	295-127; 78-modern	319–modern	**198**
3	**18-19**	Poz-78714	1900 ± 40	MBF	1575-1447	1693-1369	**1,533**
3	**36-37**	Poz-78715	2830 ± 40	MBF	2773-2578	2812-2450	**2,663**
3	**38-39**	Poz-75161	4045 ± 35	CS	4263-4056	4371-3960	**4,166**
5	**12-13**	Poz-75162	8950 ± 30	CS	9772-9595	9917-9559	**9,703**
5	**33-34**	Poz-75163	7120 ± 35	CS	7738-7618	7815-7549	**7,678**
6	**13-14**	Poz-75164	485 ± 30	CS	295-127; 68-modern	319-modern	**198**
7	**21-22**	Poz-75166	108.54 ± 0.31 pMC	CS	modern	modern	**> 1950 AD**
8	**9-10**	Beta – 455044	1290 ± 30	MBF	982-846	1044-768	**914**
8	**36-37**	Beta - 455043	2530 ± 30	MBF	2366-2211	2418-2102	**2,283**
9	**13-14**	Poz-75167	575 ± 30	CS	361-201	460-201; 77-modern	**288**
9	**28-29**	Poz-75168	1830 ± 30	CS	1537-1389	1599-1340	**1,464**
14	**6-7**	Beta - 455045	2180 ± 30	MBF	1936-1877	2017-2346	**1,861**
14	**18-19**	Poz-75169	770 ± 30	CS	556-429	580-359	**487**

Particle size analysis

The terrigenous fraction of the sediments in the study area generally consists of very fine to fine sands with varying amounts of finer and coarser particles (Fig. 7.2). No general trend in particle size with core depth is evident within individual cores and, hence, there is no consistent trend through time (Fig. 7.3). However, even though the general distribution curve follows the same distribution pattern for all the cores (Fig. 7.2a), differences in both the fine fractions <10 µm and in the coarse fraction (>200 µm) reveal a clear distinction between the southern (NZ-IC-1 – NZ-IC-7) and the northern cores (NZ-IC-8 – NZ-IC-14). The average sediment distribution of all sediments (Fig. 7.2b) further illustrates this differentiation with generally finer sediments in the south and coarser sediments in the north. Interestingly, in contrast to the fine fractions, where only the amount of material varies between the northern and the southern cores, coarse material >600 µm is solely present in the northern cores.

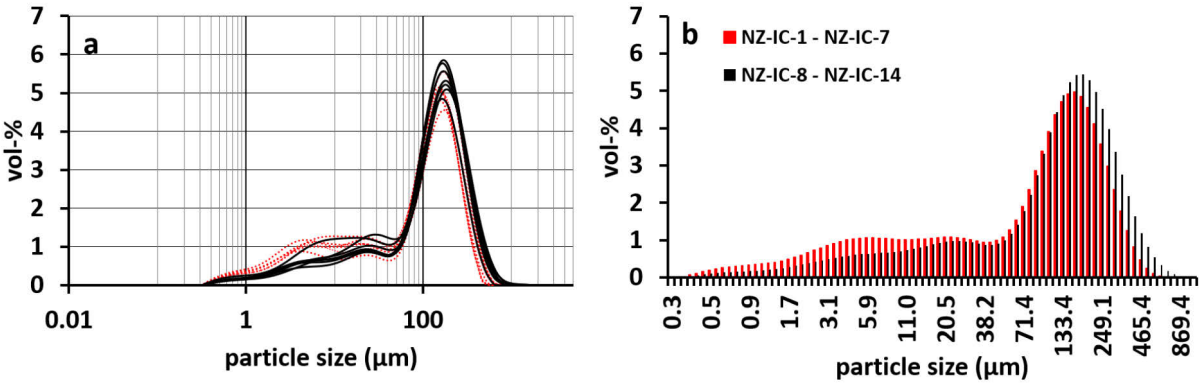

Fig. 7.2 a) *Average particle size distributions in each of the 14 sediment cores. Red dotted lines indicate the southern (NZ-IC-1 – NZ-IC-7), black lines the northern sediment cores (NZ-IC-8 – NZ-IC-14). Sediments of the southern cores generally contain a greater proportion of the fine fraction <20 µm and a lower proportion of coarser fractions >200µm.* ***b)*** *Bar chart indicating the average grain size distributions of all southern cores (NZ-IC-1 – NZ-IC-7) (in red) and all northern cores (NZ-IC-8 – NZ-IC-14) (in black). In addition, here, major differences are visible in the particle size fractions <20 µm and >200 µm.*

The difference between the northern and southern sites can be well illustrated by the <10 µm fraction that varies between 11.5 vol-% and 40.0 vol-% with a mean of 20.3 vol-% in the southern cores (NZ-IC-1 – NZ-IC-7) and between 6.6 vol-% and 14 vol-% with a mean of 12.0 vol-% in the northern cores (Fig. 7.3). In addition, also the coarse fraction >300 µm reveals significant changes between southern and northern sediments with contents from 0.8 vol-% to 10.0 vol-% (mean of 5.0 vol-%) in the southern cores and from 4.9 vol-% to 16.0 vol-% (mean of 10.7 vol-%) in the northern cores.

XRF analysis

The XRF-analysis indicates no coherent patterns for the cores with depth. However, as noted above for the particle size analysis, differences can be observed between the sediments in the southern and northern parts of the study area. These differences are particularly evident for the Ca/Ti ratio that is often used to distinguish between terrigenous and marine inputs (Fig. 4). The Ca/Ti ratios of the northern sediments are twice as high as those of sediments in the southern study area, with mean values of 75.8 and 38.2, respectively. This shows that a distinct N-S offset is not solely a feature of the particle size distribution, but also of the elemental compositions. However, the offset in the Ca/Ti ratio seems to be largest between core NZ-IC-5 and NZ-IC-6, which differs from the abrupt change in the fine sediment fraction > 10 µm between the cores NZ-IC-7 and NZ-IC-8. (Fig. 7.3).

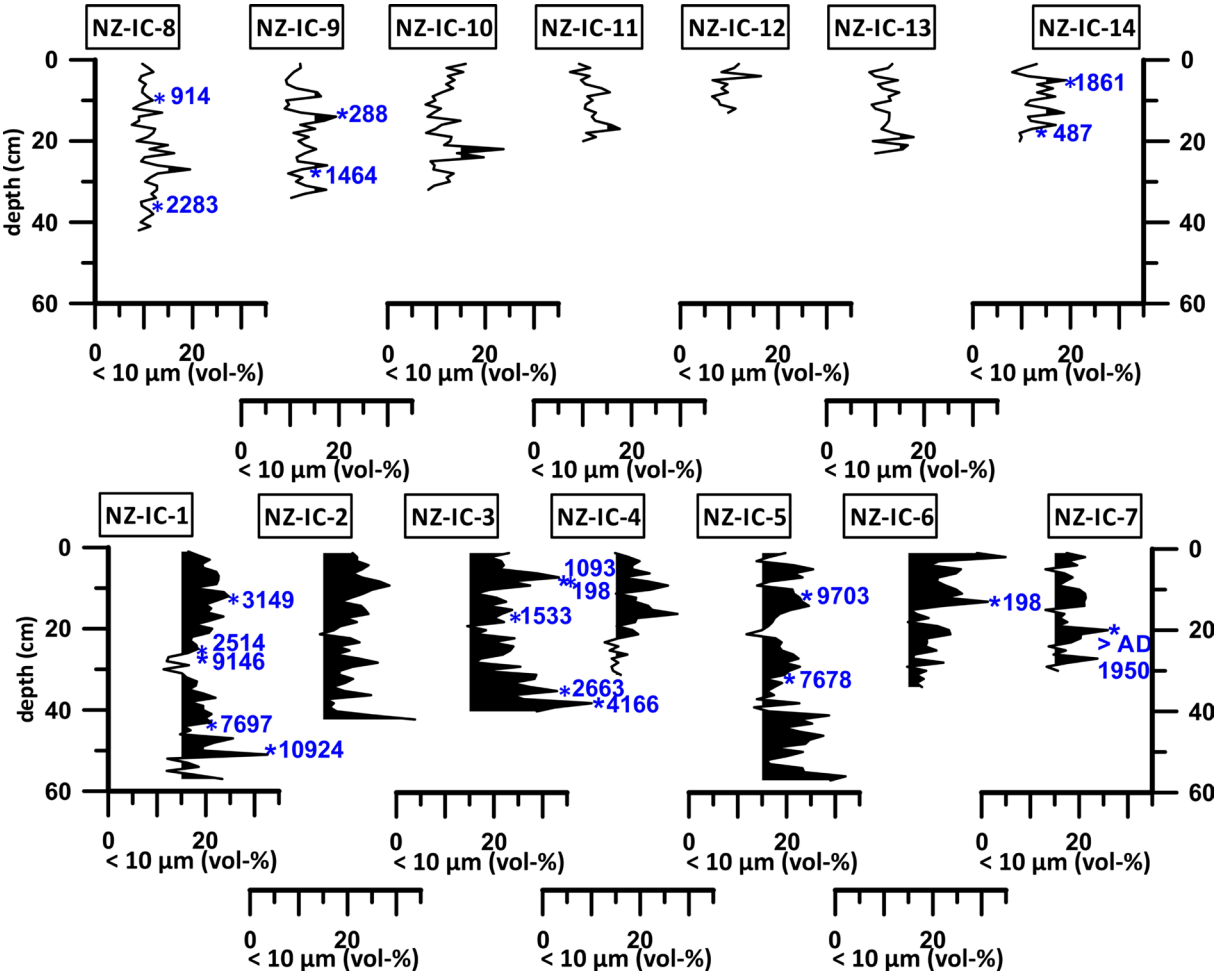

Fig. 7.3 *Contents of the terrigenous particle size fraction <10 µm indicating generally higher proportions of this fine fraction in the southern (NZ-IC-1 to NZ-IC-7) compared to the northern cores (NZ-IC-8 to NZ-IC-14). Black shading of the curves indicates contents above 15 vol%. Calendar ages BP are shown in blue.*

SWAN simulation

The results of the SWAN simulation of wave patterns carried out for the years 1989-2009 indicate that the highest average H_s over this period occurred in the open Pacific Ocean outside the Hauraki Gulf, with a maximum of ~2.3 m in the north-eastern corner of the simulated region (Fig. 7.5a). Within the Hauraki Gulf, mean H_s decreases southward towards the relatively shallow Firth of Thames. Values range from ~1.1 m in the northern part of the central Hauraki Gulf and the major channels to a minimum of ~0.3 m in the southern end of the Firth of Thames and in sheltered estuaries. Average H_s at the coring sites varied between 0.95 m (NZ-IC-14) and 0.81 m (NZ-IC-2) consistent with this southerly decreasing trend (Fig. 7.5a). Under strong wind forcing, H_s in the coring sites can reach much higher values. Whereas strong NE and SW winds can result in H_s of 3 to 4 m (Fig. 7.5b, c), maximum values between 4.7 m (NZ-IC-1) and 5.0 m (NZ-IC-14) appear to be related to easterly storm winds (Fig. 7.5d). A gradual decrease towards the south can be observed for the average but also for the storm conditions (Fig. 7.5), except for SW storms when newly generated waves are rather uniform within the study area (Fig. 7.5c). The three major channels connecting the Hauraki Gulf with the Pacific Ocean –Jellicoe, Cradock, and Colville Channels —generally experience higher average H_s than other areas in the Hauraki Gulf (Fig. 7.5). Shadow zones with low mean H_s occur in the lee of the larger Hauraki Gulf Islands (e.g. Little and Great Barrier Island) and on the west coast of the Coromandel Peninsula. Overall, H_s in the study area varied between 0.1 m and 5.0 m throughout the simulation period.

Highest H_S in the study area linked to easterly storm winds are characterised by largest waves entering the Hauraki Gulf through Colville Channel, producing H_s of up to ~ 5.0 m in the northern study area, with a strong reduction of H_s towards the south. Differences in H_s between the southernmost and the northernmost coring sites can exceed 1 m (e.g. on the 10th of July 2007, Fig. 7.5d). After entering the Gulf through Colville Channel, waves slowly rotate clockwise towards the northern and anti-clockwise towards the southern Hauraki Gulf. Since the wave energy (mean wave energy density per unit area (J/M^2)) is solely dependent on the wave height, the H_s translates directly into the wave energy.

7.5 Discussion

Low Holocene sediment thickness

The sediment cores studied here were taken from the main modern depocenter in the Hauraki Gulf as indicated by Manighetti and Carter (1999), who estimated post-transgressive sediment thicknesses of up to 10 m in this location. This suggests that, following the inundation of these probably between ~9.5 ka and 12 ka BP (Carter et al., 1986), they should have experienced average sedimentation rates in the order of ~1 m/kyr. However, the new age determinations, characterised by numerous age reversals in the cores (Fig. 7.3), reveal that sedimentation in the Hauraki Gulf is not continuous, but characterised by intensive reworking/resedimentation.

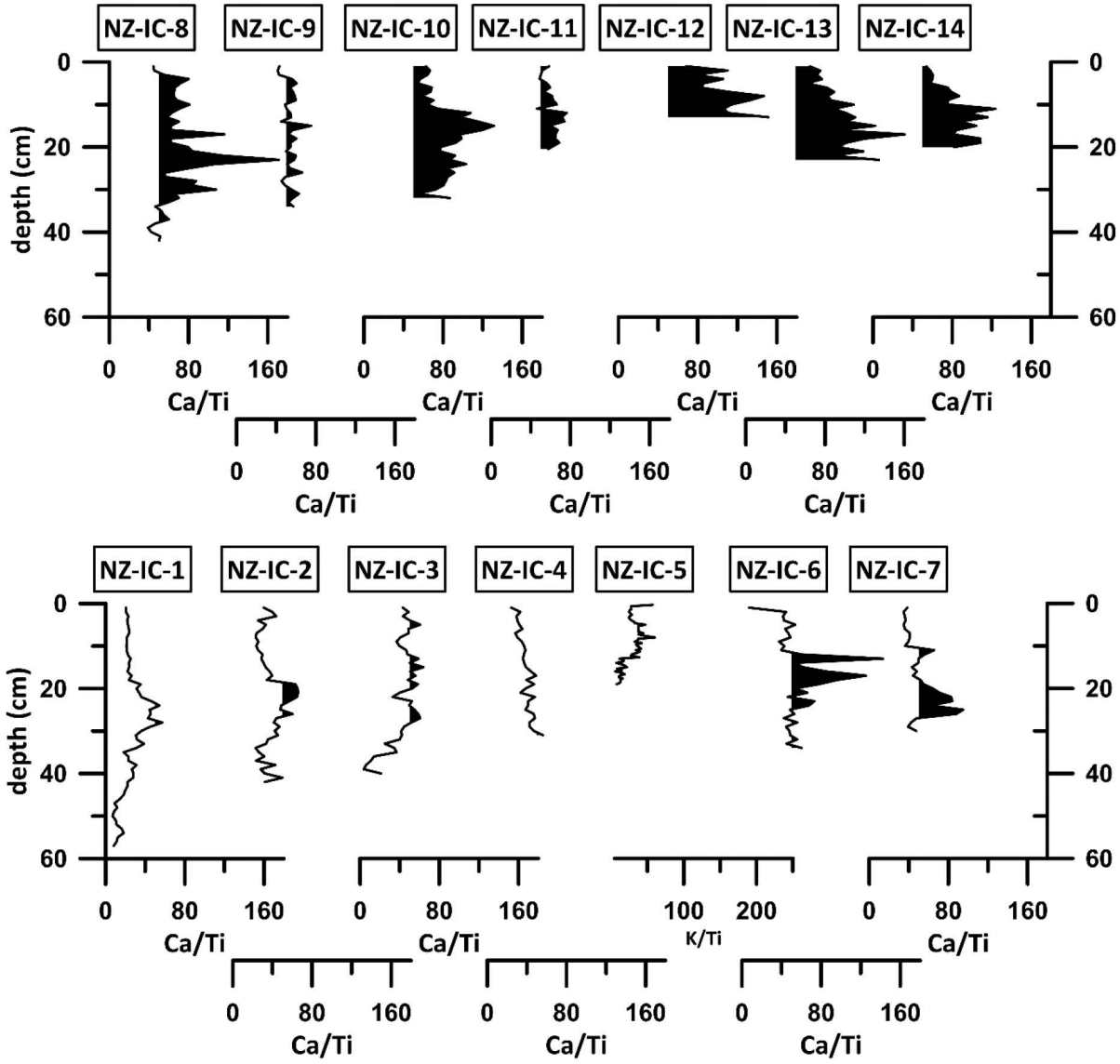

Fig. 7.4 *Ca/Ti ratio of the sediments indicating higher ratios in the northern cores. Black shading of the curves display Ca/Ti ratios over 50.*

Furthermore, the presence of datable material with ages of up to ~11 kyr found in the uppermost 60 cm of the cores does not support the assumption of long-term sedimentation rates in the order of ~1 m/kyr. Although the oldest ages are obtained from carbonate shell fragments, that easily can be reworked, ages obtained on foraminifera also yield ages of >7 kyr and display several age reversals (without considering the shell fragments). With estimated sedimentation rates of ~1 m/kyr, ages of several thousands of years are usually not expected that close to the sediment surface. Of course, the observations described here are no proof, but the combined evidence of foraminiferal and shell fragment ages and the observation that here the rate of burial appears to be generally less than the rate of disturbance, strongly point to low average sedimentation rates in the Hauraki Gulf. This conclusion is in line with a low modern-day sediment input into the Hauraki Gulf system, mainly contributed by several small rivers (Manighetti and Carter, 1999).

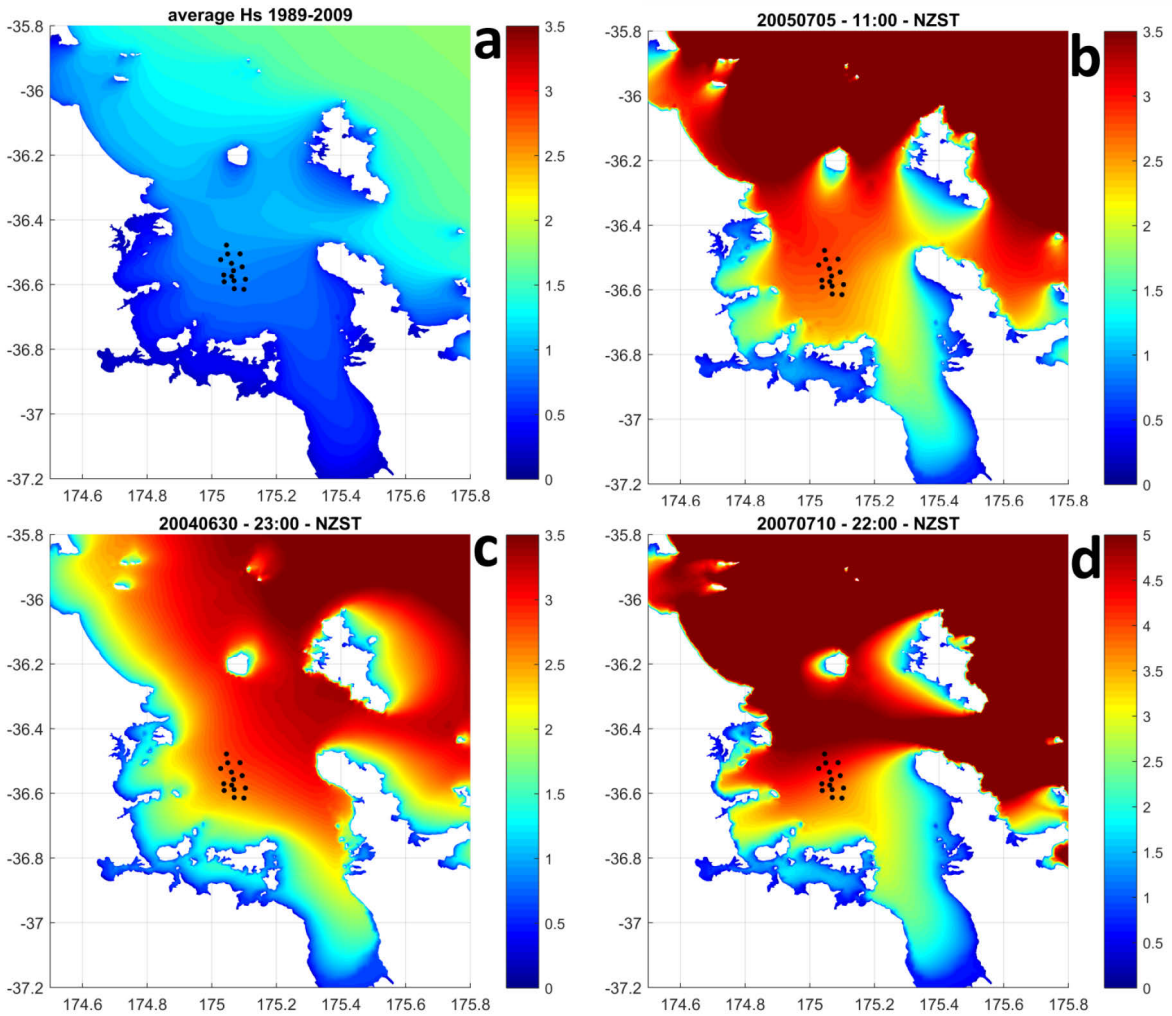

Fig. 7.5 *Maps showing significant wave heights* H_s (in m) *at different times. a) average* H_s *of the simulated years 1989-2009, b)* H_s *on 5th of July 2005 with waves predominantly coming from the north-east, c) on 30Th of June 2004 with* H_s *increasing in NE direction d)* H_s *on 10th July 2007 with waves mainly entering via Colville Channel.*

Today, these small river systems discharge ~100 m^3s^{-1} to the inner Gulf (Sikes et al., 2009), with the largest suppliers of terrestrial material being the Piako and Waihou Rivers, both draining igneous and volcanic regions, and the predominantly agricultural Hauraki Plains, into the southern end of the Firth of Thames (Fig. 7.1). Interestingly, before the arrival of first the Polynesian settlers (~1000 yr BP) and later on of the European settlers (~1800 AD), sediment input to the Hauraki Gulf was probably even much lower, as land clearance by these settlers resulted in a significant increase in soil erosion rates in New Zealand (e.g. Bussell, 1988; McGlone and Wilmshurst, 1999). However, the majority of the soils eroded following these clearances were trapped in estuaries and sheltered near-coastal areas, and, thus, not reached the central Gulf (Carter and Eade, 1980; Greig, 1982).

These observations, pointing to overall sedimentation rates probably much lower than ~1m/kyr, indicate that the depocenter described by Manighetti and Carter (1999) probably consist only of a small component of post-transgressive sediments, and that most of the up to 10 m thick sediment package most likely is older. Assuming that a significantly higher sediment input is needed to result in the deposition of these sediments, in the past, other sediment sources must have contributed. The prime candidate here is the Waikato River, which until 22 ka BP entered the Hauraki Gulf before switching to the Tasman Sea in the west (Fig. 7.1). Its present-day mean discharge of 340 m^3s^{-1} (Duncan and Woods, 2004) indicates its potential to deliver several times the amount of sediment than all the modern smaller rivers entering into the Hauraki Gulf taken together. In the case the Waikato River has been such an additional sediment source in the past, two scenarios could explain the presumably older deposits observed in the hydroacoustic data by Manighetti and Carter (1999): these were deposited (a) as flood plain deposits under Pleistocene sea level low stand conditions, e.g., during the last glacial when the Waikato River last drained into the Hauraki Gulf region or (b) as marine sediments during the last interglacial when, in contrast to today, sediment input to the Gulf was much higher, and was predominantly supplied by the Waikato River.

North-to-south gradient in sediment composition

The latitudinal N-S pattern, visible in both sediment texture and elemental concentrations, most likely reflects the influence of the present-day hydrodynamic regime in the study area as a combination of tidal currents, oceanic inflows and wave-induced currents. The net overall circulation is described as dominated by waters entering the Gulf through Jellicoe Channel, flowing anti-clockwise across the Gulf and passing out through Colville Channel in the east

(Greig and Proctor, 1988; Greig, 1990). The dominant influence of the major channels connecting the Hauraki Gulf to the Pacific Ocean can be seen in the SWAN simulations as well (Fig. 7.5). Wave energies in the Gulf are strongest in the channels (Jellicoe, Cradock, and Colville) and then generally decrease from north to south, indicated by on average (for the period 1989-2009) lower mean H_s and, consequently, lower mean absolute wave energies (Fig. 7.5).

It has been shown previously that storm waves with H_s of ~5 m in the Gulf can potentially stir fine sands on the seafloor down to depths of ~100 m (Manighetti and Carter, 1999). Interestingly, especially under strong storm forcing through Colville Channel (Fig. 7.5d), when H_s is highest, a rather steep N-S gradient in wave energy through our sampling area has the potential to modify the seafloor sediments towards the pattern observed in the grainsize and Ca/Ti-ratio data (Fig. 7.3 and 7.4). Higher wave energies in the north, thus, could result in the advection of coarser shell fragments increasing the Ca/Ti ratio (Fig. 7.4), and in the resuspension/erosion of finer particles and/or delivery of coarser particles resulting in a comparably coarser sediment (Fig. 7.3).

Indeed, strong correlations between latitude, H_s, grain sizes and elemental composition can be observed (Table 7.3). This clearly hints to wave action as the most important process affecting grainsize distribution and elemental concentrations of the sediments in the central Hauraki Gulf. In such a scenario with waves partly stirring up the sediments at the seafloor, the deposition of continuous, undisturbed sedimentary sequences is largely precluded.

Table 7.3 *Selected correlation coefficients of various sediment parameters, latitude, and H_s. Strong positive correlation coefficients > 0.5 are marked in yellow, strong negative correlation coefficients > -0.5 are marked in grey. The data show a strong positive correlation between latitude and the proportion of coarser particles > 300 µm, average H_s, and Ca concentrations and a strong negative correlation between latitude and the proportion of the fine particles < 10 µm pointing to sediment sorting due to the hydrodynamic regime. (Data used for the correlation: each cm in each cores (n=475) for particle sizes and Ca content; one value for each core for average Hs and latitude (n=14)).*

	latitude	**<10 µm** vol.-%	**>300 µm** vol.-%	**average H_s** m	**Ca** ppm
latitude	-				
<10 µm vol.-%	-0.59	-			
>300 µm vol.-%	0.70	-0.23	-		
average H_s m	1.00	-0.58	0.68	-	
Ca ppm	0.73	-0.52	0.60	0.71	-

Present-day sediment dispersal

Dispersal of sediments in the southern part of the Hauraki Gulf is affected by tidal eddies and water flowing out of the Firth of Thames, whereas in the northern study area it is often impacted by waters coming through Colville Channel, usually during times of enhanced hydrodynamic forcing (Black et al., 2000). Sikes et al. (2009) assumed that most of the present-day terrigenous sediment input into the Gulf consists of fine-grained material supplied by the Waihou and Piako Rivers, from where tidal eddies can transport it to the southern study area. This might explain higher proportions of fine-grained sediment in this area. However, it would not explain the abrupt change in the fraction <10 µm observed between the southern and the northern study sites, unless the boundary between the cores NZ-IC-7 and NZ-IC-8 marks the northern-most point to which these fluvial sediments are transported

Even though an estimation of sedimentation rates based on the radiocarbon dates is difficult due to the numerous age reversals in our sediment cores, a pattern emerges indicating the sediments at the northern study sites to be younger, spanning “only” the last 2,300 years (288 yrs to 2.283 yrs, n=6), whereas sediments at the southern study sites span the last 10,900 years (recent to 10.924 yrs, n=14, 50% of the ages are >4.000 yrs, Table 7.2). This points to a peculiar pattern of lower “average sedimentation rates” in the southern part of the study area, where higher relative contributions of finer sediments are interpreted to reflect the deposition of sediments from fluvial sources, compared to the northern sites, where these finer sediments are missing, but where the radiocarbon dates point to higher “average sedimentation rates”.

This at first glance contradictory observation might be explained by the existence of another sediment source for the northern sites. A hint at the identification of such a source is given by the presence of coarse terrigenous materials > 500 µm, which are absent in the southern sediments (Fig. 7.2) and which occur in combination with much higher Ca contents. Visual inspection of the untreated sediment fraction >500 µm from a northern (NZ-IC-3) and a southern (NZ-IC-8) sediment sample reveals a much higher content of large shell debris in the north (Fig. 7.6), which is in agreement with the higher coarse fraction contents in the terrigenous sediment fraction in the northern cores (Fig. 7.2). Thus, higher “average sedimentation rates” in the north might be a result of enhanced deposition of coarse materials consisting largely of carbonates. In addition to local carbonate bio-productivity (foraminifera, bivalve, and gastropods), which probably affects the northern study sites in a similar way to

the southern sites, a large proportion of the carbonate shell debris in the north may be relict material transported to the study site. Manighetti and Carter (1999) described regions of high carbonate contents (up to >92%) in Hauraki Gulf surface sediments from the Jellicoe and Colville Channels, from southeast of Kawau Island, and from directly southwest of our southern coring sites. Especially in the Jellicoe and Colville Channels, these sediments consist to a large part of shell hash with dominant size modes of up to 350 µm.

During larger storms with waves entering the Gulf through Colville and/or Jellicoe Channel (Fig. 7.5b, d), carbonate shell hash and also coarse terrigenous particles may be taken up from the seafloor and transported to the study area resulting there in a gain of coarse material (carbonates and terrigenous material). The ability of storm waves in the Hauraki Gulf to rework coarse carbonate shell fragments especially in the main channels has already been outlined in detail by Manighetti and Carter (1999). Within our study area, the southward weakening of wave energies results in the predominant deposition of this coarse material in its northern part. A strong N-S gradient in wave energy, as e.g. observed in the study area on 10th July 2007 with waves mainly entering via Colville Channel (Fig. 7.5d), might hint to easterly storms as the main driver of coarse sediment input to the central Hauraki Gulf, as this gradient would be very well in line with the observed N-S differences in sediment composition in the study area. Nevertheless, some regional differences in the major changes in sediment composition occur, e.g., the shift from higher to lower Ca/Ti ratios between cores NZ-IC-5 and NZ-IC-6 and the shift from lower to higher <10 µm contents between cores NZ-IC-7 and NZ-IC-8. However, this offset might be explained by an additional input of fine-grained carbonate material to cores NZ-IC-6 and NZ-IC-7 from the southwest, where surface sediments are characterised by high carbonate (>50%) and clay (>30%) contents (Manighetti and Carter , 1999), during periods of strong westerly offshore winds (Fig. 5c).

In terms of sediment accumulation in the central Hauraki Gulf, the on average younger sediments in the northern study area indicate that the amount of coarse (carbonate and terrigenous) material supplied to the northern study sites is higher than the amount of fluvial input of fine terrigenous material supplied to the southern study sites, resulting in higher “average sedimentation rates” in the north. Nevertheless, also the sediments in the southern part are significantly reworked as indicated by numerous age reversals.

7.6 Conclusion

Revisiting the main sediment depocenter in the central Hauraki Gulf as identified by Manighetti and Carter (1999) and focusing on the area with the assumed highest accumulation of >10 m of post-transgressional sediments, revealed that this region is rather controlled by event-driven sediment reworking and input than by continuous deposition. This is indicated, e.g., by radiocarbon ages of >10,000 yrs obtained on carbonate shell fragments and of >7,000 years obtained on foraminifera within the uppermost 60 cm of the sediment. While age reversals in the sedimentary records characterise the entire study area, the sediment composition allows differentiating between coarser sediments in the north and finer sediments in the south. Most likely, the coarser sediments in the north are supplied under easterly storm forcing from the Colville Channel, whereas the finer sediments in the south are provided by fluvial input. In terms of average sediment accumulation, the on average younger sediments in the north indicate that the amount of coarse (carbonate and terrigenous) material supplied to the northern study sites is higher than the amount of fluvial input of fine terrigenous material supplied to the southern study sites, resulting in higher "average sedimentation rates" in the north. However, also in the south a dominance of reworking over sedimentation is indicated by numerous age reversals in the individual cores. The distinct boundary between these two types of sediment is in line with wave energy patterns that can be related to strong easterly storms and, thus, the resulting sediments (at least in the north) can be defined as palimpsest sediments.

While the existing conceptual models proposed in the literature argue for modern day sediment input coming either predominantly from the north or from the south, our new data suggests a combination of both models. Fine fluvial sediments from the south contribute to the sedimentation in the southern study sites and higher inputs of relict carbonate and coarse terrigenous material coming from sources in the east (and in the north) contributes to sedimentation in the northern study sites.

By focusing on a small area with a high spatial resolution in sampling, this study reveals that the general pattern of sedimentation patterns in the Hauraki Gulf previously outlined by Manighetti and Carter (1999) might in parts need some reconsideration in order to fully understand sedimentation and sediment dispersal patterns in the Hauraki Gulf. In times when the sustainable use of coastal ecosystems and partly even their protection require a detailed

knowledge about the seabed setting and about the processes controlling it, for the Hauraki Gulf such knowledge appears to be still largely lacking. Thus, future research efforts should target the sedimentary system of the Hauraki Gulf, the largest shelf embayment of New Zealand.

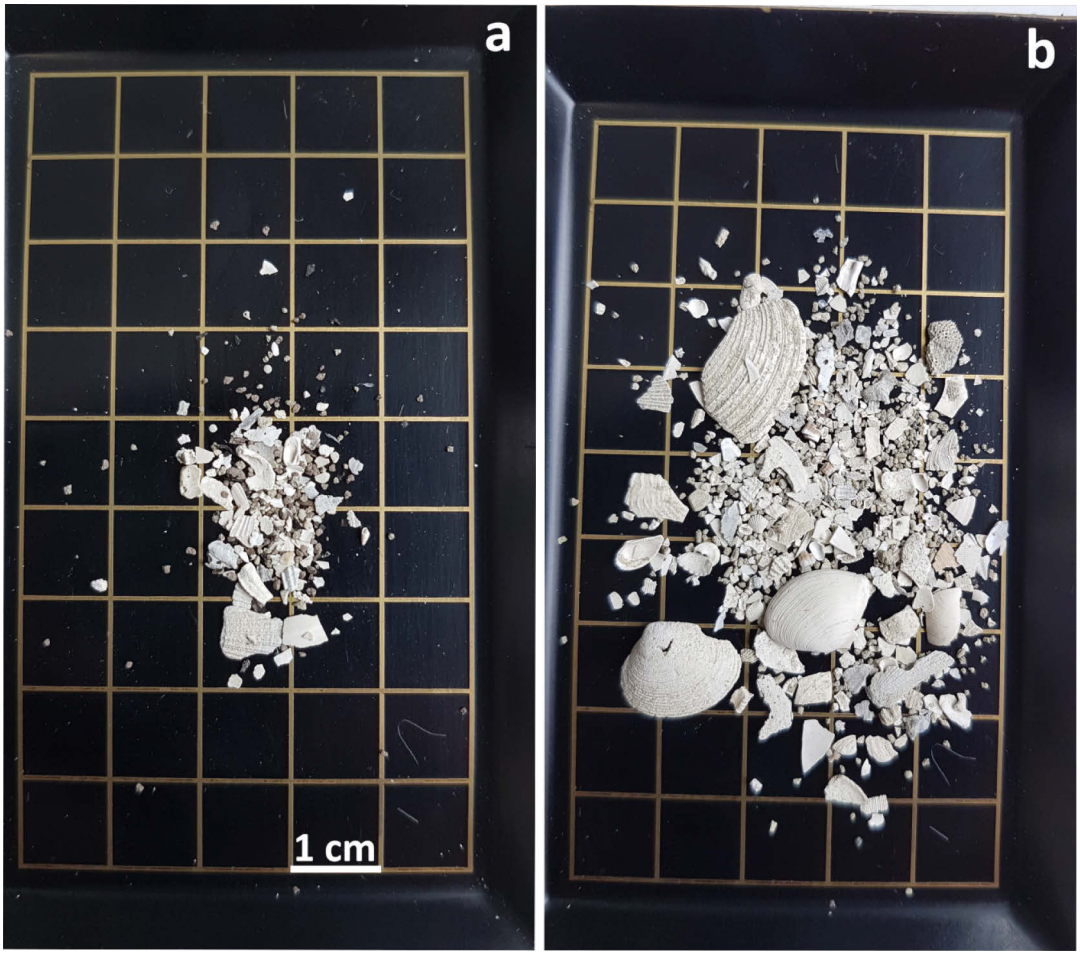

Fig. 7.6 *Examples of wet-sieved particle size fractions > 500 µm in a) a southern core (NZ-IC-3; 36-37 cm core depth) and b) northern core (NZ-IC-8; 36-37 cm core depth)) indicating the different composition of the coarse fractions between the southern and northern sediments.*

8. Synthesis

The principal aim of the thesis was a) to decipher the historical, anthropogenic induced, heavy metal inputs to sediments in near-coastal marine depocenters in the North Sea and the Hauraki Gulf, b) to identify possible source areas of the heavy metal inputs, and c) to understand the transport mechanisms of the heavy metals to these near-coastal marine depocenters. Based on the analysis of 23 sediment cores, most of the research questions outlined in chapter 1.2 could be answered.

Within two individual studies it was shown that man-made heavy metal enrichments occurred in sediments of the Helgoland mud area and the Skagerrak. Due to the low present-day sediment input in combination with strong sediment reworking and mixing, no heavy metal enrichments related to anthropogenic activities could have been detected in the sediments from the Hauraki Gulf. However, the Hauraki Gulf study provided new insights into the distribution of surficial sediments in the central Hauraki Gulf and identified and discussed the effects of the interaction of modern wind-generated waves and currents with regards to deposition and reworking of sediments in the Hauraki Gulf. The surficial sediment distribution is palimpsest, a consequence of generally low sediment input to the region and continuous sediment reworking under strong wind and wave forcing.

The Hauraki Gulf sediments revealed a generally low anthropogenic modification of the Hauraki Gulf seafloor and, thus, stands in contrast to heavy metal contaminated sediments in estuaries and natural harbours around the city of Auckland as e.g. the Tamaki estuary and Manukau and Waitemata Harbours (e.g. Glasby et al., 1988; Taylor and Smith, 1997; Abrahim and Parker, 2002; Abrahim and Parker, 2008; Kelly et al., 2014), which are associated with industrial activities in the highly industrialised Auckland region. Other areas of heavy metal contaminated sediments in the greater Hauraki Gulf were found in the south-eastern Firth of Thames and are primarily related to mining on the Coromandel Peninsula (e.g. Kim, 2007; Kelly et al., 2014). Sediments in the central Hauraki Gulf studied here were, hence, expected to be heavy metal contaminated as well. However, due to the generally low sediment accumulation and the continuous reworking of the sediments, it could be shown that elevated heavy metal concentrations might have been trapped in the estuaries and did not reach the central Hauraki Gulf. In addition, it might be that anthropogenic induced heavy metal were transported to the central Hauraki Gulf, but the signal was diluted by the continuous reworking of the sediments.

In summary it can be said that mining activities on the Coromandel Peninsula and industrial activities in the Auckland region are only recorded locally. Heavy metals are mostly deposited in shallow, near-coastal areas close to the pollution sites and did not reach the deeper settings in the Hauraki Gulf to a detectable amount.

In contrast, heavy metal enrichments (Zn and Pb) in the Helgoland mud area date back to ~ AD 750, ~1000 years earlier than estimated in previous studies. Whereas the temporal development and the source of the heavy metals were controversially discussed in the literature, it could clearly be shown that the heavy metal enrichments started in pre-industrial times and, thus, are most likely attributed to early mining and smelting activities in medieval mining centres in northern and eastern Germany. Heavy metals were transported from the mining areas mostly in the aquatic milieu through Elbe and Weser rivers. Upon reaching the North Sea, their deposition was most likely facilitated by a stationary, vertical eddy situated above the Helgoland mud area.

A less pronounced heavy metal enrichment (Cu, Pb, and Zn) could be shown in sediments of the southern slope of the Skagerrak. Early Cu and Pb enrichments, which could be traced back to an onset at ~ AD 1230, most likely reflected medieval mining and smelting activities in the Falun mining district in central Sweden. Assumingly, these heavy metals were transported through the atmosphere and through the aquatic milieu to the sampling sites. The later onset of Zn enrichment at ~ AD 1660 was estimated to reflect the heavy metal signal known from the Helgoland mud area. Sediments in these two depocenters of the North Sea are connected through the North- and South Jutland Current, which are most likely responsible for the northward transportation of heavy metals from the SE North Sea towards the Skagerrak.

The results of the three individual study sites partly shed new light on the strong and long-term heavy metal inputs to the sediments of the Helgoland mud area and the Skagerrak, whereas, due to the modes of sediment dispersal in the Hauraki Gulf, such heavy metal contributions to the sediments in the central Hauraki Gulf were not detectable. This absence of anthropogenic induced heavy metal enrichments in the Hauraki Gulf was not expected but could be explained by limiting factors as e.g., sediment trapping in the estuaries, low sediment input to the central Gulf and continuous sediment reworking.

The individual studies showed the importance of near-coastal sediment depocenters for paleo-reconstruction studies on historical time scales. Near-coastal sediment depocenters

often provide undisturbed sediment records with annual- to decadal-scale temporal resolution. And even if they do not provide undisturbed sediment records, their sediment records can provide important insights into the general sedimentation and sediment dispersal patterns in these near-coastal sediment depocenters. In times, when the sustainable use of coastal ecosystems and their protection requires a detailed knowledge of the general sedimentary setting and the processes controlling it, these informations appear to be really important, highlighting the importance of these sedimentary records.

9. Outlook

The spatial and temporal distribution of heavy metal inputs to the Helgoland mud area indicate a time-transgressive pattern of early heavy metal enrichments in the south-eastern mud area that is/was slowly progressing in north-western direction and can be dated back to an early onset at ~ AD 750. Prior to this study, the source and the temporal history of heavy metal input to this area were controversially discussed. For instance, Irion et al. (1987) assumed that anthropogenic Zn input to the Helgoland mud area commenced in post-war times due to the dumping of contaminated harbour muds, whereas Hebbeln et al. (2003) estimated an onset as early as AD 1750, reflecting historic mining activities in the Harz Mountains and the Erzgebirge. Even though the new results provide new knowledge about the temporal development of heavy metal inputs, the pattern is not yet completely understood. A promising future step would be a better stratigraphic resolution of the cores in combination with the analysis of additional sediment cores. The existing age models are based on few radiocarbon ages in each core and revealed some gaps and age reversals. A better stratigraphic resolution of the existing and additional sediment cores would help to understand the described time-transgressive pattern of heavy metal inputs, to support and improve the existing age models and, thus, to improve our understanding of the timing of anthropogenic heavy metal inputs to the German Bight.

Also for the southern flank of the Skagerrak in the northern North Sea, an anthropogenic induced heavy metal signal could be observed in the upper sediment layers. However, even though possible source areas for the elevated heavy metal levels were proposed and discussed, the sources could not be clearly identified. A potential future step helping to understand the general pattern, might be a provenance analysis of clay minerals and their elemental compositions similar to e.g. Zuther et al. (2000) and Pache et al. (2008) to understand the origin and pathways of clay minerals and the associated heavy metals in the sediment cores. Pache et al. (2008) identified a close genetic relationship between sediments of the Helgoland mud area and Elbe River sediments by comparing K/Rb data of clay minerals. By measuring the K/Rb data of clay minerals in the studied sediment cores and comparing them to the sediments of the Helgoland mud area and the Elbe River a possible genetic relationship between sediments in the Helgoland mud area and Skagerrak sediments could be determined. The same method could be applied to sediments further south-(east) in the northern Kattegat and sediments of the Göta River upstream towards Lake Vänern to further

increase the knowledge of clay mineral provenances and, hence, heavy metal provenances associated to the clay minerals.

On the other side of the globe, sediments from the central Hauraki Gulf did not reveal any signal of anthropogenic induced heavy metal inputs. The observed low sedimentation rates in the area came as a surprise, as previously a >10 m thick package of Holocene post-transgressive sediments thickness was assumed to cover it (Manighetti and Carter, 1999). A high-resolution hydroacoustic analysis of the central Hauraki Gulf deposits combined with the collection of longer sediment cores would help to improve the understanding of the sedimentary structures and their ages and, hence, might improve the knowledge about the general sedimentary setting of the Hauraki Gulf and it's sedimentary.

In order to observe a stronger heavy metal signal and identify the temporal development of anthropogenic heavy metal inputs in the Hauraki Gulf, future studies have to focus on more sheltered areas closer to the heavy metal sources. An interesting new approach would be the analysis of sediments in close proximity to different point sources of heavy metal contamination on the western coast of the Coromandel Peninsula. This heavy metal signal might potentially be traced through the Firth of Thames in northern direction. Generally, the Firth of Thames at the southern end of the Hauraki Gulf seems to be more promising due to the generally finer grained sediments and a potentially higher sediment accumulation in combination with significantly lower exposure to wave energies.

In summary, it can be said that even though this study provides many new insights into the spatial and temporal development of anthropogenic induced heavy metal inputs to near-coastal sediment depocenters and into the general sedimentological setting of those depocenters, there are still gaps in the understanding of those systems, which might be targeted in future studies.

10. Bibliography

Abrahim, G.M.S., Parker, R., 2002. Heavy-metal contaminants in Tamaki Estuary: impact of city development and growth, Auckland, New Zealand. Environmental Geology 42 (8), 883-890.

Abrahim, G.M.S., Parker, R.J., 2008. Assessment of heavy metal enrichment factors and the degree of contamination in marine sediments from Tamaki Estuary, Auckland, New Zealand. Environmental monitoring and assessment 136 (1). 227-238.

Adriano D.C., 1986. Trace Elements in the Terrestrial Environment. Springer, New York.

Alloway, B.J., 2013. Sources of heavy metals and metalloids in soils. In: Heavy metals in soils. Springer Netherlands.

Andres, M.S., Bernasconi, S.M., McKenzie, J.A., Röhl, U., 2003. Southern Ocean deglacial record supports global younger Dryas. Earth and Planetary Science Letters 216 (4), 515-525.

Arz, H.W., Pätzold, J., Moammar, M.O., 2001. Late Quaternary climate records from the Northern Red Sea: reults on gravity cores retrieved during R/V METEOR Cruise M44/3. Marine Sciences 12 (1).

Bak, J., Jensen, J., Larsen, M.M., Pritzl, G., Scott-Fordsmand, J., 1997. A heavy metal monitoring-programme in Denmark." Science of the Total Environment 207 (2-3), 179-186.

Bard, E., 1998. Geochemical and geophysical implications of the radiocarbon calibration. Geochimica et Cosmochimica Acta 62 (12), 2025–2038.

Bartels, C., 1996. Mittelalterlicher und frühneuzeitlicher Bergbau im Harz und seine Einflüsse auf die Umwelt. Naturwissenschaften 83 (11), 483-491.

Beckhoff, B., Kanngieser, B., Langhoff, N., Wedell, R., Wolff, H., 2006. Handbook of Practical X-ray Fluoresecence Analysis, Springer Verlag, Berlin, Heidelberg.

Bengtsson, H., Stevens, R.L., 1996. Heavy-mineral provinces in southern Skagerrak and northern Kattegat. Norges Geologiscke Undersøkelse Bulletin 430, 47-55.

Black, K. P., Bell, R. G., Oldman, J. W., Carter, G. S., Hume, T. S., 2000 Features of 3-dimensional barotropic and baroclinic circulation in the Hauraki Gulf, New Zealand. New Zealand Journal of Marine and Freshwater Research 34 (1), 1-28.

Blossier, B., Bryan, K.R., Daly, C.J., Winter, C., 2016. Nearshore sandbar rotation at single-barred embayed beaches. Journal of Geophysical Research: Oceans 121 (4), 2286-2313.

Bowman, S., 1990. Radiocarbon dating (Vol.1). University of California Press.

Boxberg, F., Asendorf, S., Bartholomä, A., Schnetger, B., de Lange, W.P., Hebbeln, D., in preparation. Historical anthropogenic heavy metal input to the south-eastern North Sea.

Bozzano, G., Kuhlmann, H., Alonso, B., 2002. Storminess control over African dust input to the Moroccon Atlantic margin (NW Africa) at the time of maxima boreal summer insolation: a record of the last 220 kyr. Paleogeography, Paleoclimatology, Paleoecology 183 (1), 155-168.

Brack, K., Stevens, R., 2002. Historical pollution trends in disturbed, estuarine sedimentary environment, SW Sweden. Environmental Geology 40 (8), 1017-1029.

Bradl, H. (eds.), 2012. Heavy Metals in the Environment: Origin, Interaction and Remediation Volume 6. Academic Press. London.

Brännvall, M.-L., Bindler, R., Emteryd, O., Nilsson, M., Renberg, I., 1997. Stable isotope and concentration records of atmospheric lead pollution in peat and lake sediments in Sweden. Water, Air, and Soil Pollution 100 (3-4), 243–252.

Brännvall, M.-L., Bindler, R., Emteryd, O., Renberg, I., 2001. Four thousand years of atmospheric lead pollution in northern Europe: A summary from Swedish lake sediments. Journal of Paleolimnology 25 (4), 421-435.

Bussell, M.R., 1988. Mid and late Holocene pollen diagrams and Polynesian deforestation, Wanganui district, New Zealand. New Zealand Journal of Botany 26 (3), 431-451.

Callender, E., 2003. Heavy metals in the environment-historical trends. Treatise on geochemistry 9, 612.

Candeias, C., Melo, R., Ávila, P.F., da Silva, E.F., Salgueiro, A.R., Teixeira, J.P., 2014. Heavy metal pollution in mine-soil-plant systems in S. Francisco de Assis-Panasqueira mine (Portugal). Applied Geochemistry 44, 12-26.

Carter, L., Eade, J. V., 1980 Hauraki Sediments. New Zealand Oceanographic Institute Chart, Coastal Series 1:200,000.

Carter, R.M., Carter, L., Johnson, D.P., 1986. Submergent shorelines in the SW Pacific: evidence for an episodic post-glacial transgression. Sedimentology 33 (5), 629-649.

Clement, A. J. H., Whitehouse, P. L., Sloss, C. R. 2015. An examination of spatial variability in the timing and magnitude of Holocene relative sea-level changes in the New Zealand archipelago. Quaternary Science Reviews 131, 73-101.

Clement, A.J., Nováková, T., Hudson-Edwards, K.A., Fuller, I.C., Macklin, M.G., Fox, E.G., Zapico, I., 2017. The environmental and geomorphical impacts of historical mining in the Ohinemuri and Waihou river catchments, Coromandel, New Zealand. Geomorphology 295, 159-175.

Cooke; C.A., Bindler, R., 2015. Lake sediment records of preindustrial metal pollution. In: Environmental Contaminants (pp. 101-119). Springer Netherlands.

Copat, C., Arena, G., Fiore, M., Ledda, C., Fallico, R., Sciacca, S., Ferrante, M., 2013. Heavy metals concentrations in fish and shellfish from eastern Mediterranean Sea: consumption advisories. Food and Chemical Toxicology 53, 33-37.

Cortizas, A.M., López-Merino, L., Bindler, R., Mighall, T., Kylander, M.E., 2016. Early atmospheric metal pollution provides evidence for Chalcolithic/Bronze Age mining and metallurgy in Southwestern Europe. Science of the Total Environment 545, 398-406.

Costa Caramé, M.E., Díaz-Zorita Bonilla, M., García Sanjuán, L., Wheatley, D.W., 2010. The Copper Age settlement of Valencina de la Concepción (Seville, Spain): demography, metallurgy and spatial organization. Trabajos de Prehistoria 67 (1), 85-117.

Croudace, I.W., Rothwell, R.G., 2015. Micro-XRF Studies of Sediment Cores: Applications of a non-destructive tool for the environmental sciences. Springer Science + Media Dordrecht.

Danielssen, D.S., Eder, L., Fogelquist, E., Fneslius, S.H., Foyn, L., Hernroth, I., Hakansson, B., Olsson, I., Svendsen, E., 1991. SKAGEX: Some preliminary results. Interntational Council for the Exploration of the Sea, CM 1991, C (2), 14pp.

De Boer, G.B.J., De Weerd, C., Thoenes, D., Goosens, H.W.J., 1987. Laser diffraction spectrometry: Fraunhofer versus Mie scattering. Particle & Particle Systems Characterization 4 (1-4), 14-19.

Dellwig, O., Hinrichs, J., Hild, A., Brumsack, H.J., 2000. Changing sedimentation in tidal flat sediments of the southern North Sea from the Holocene to the present: a geochemical approach. Journal of Sea Research, 44 (3), 195-208.

Dhanakumar, S., Solaraj, G., Mohanraj, R., 2015. Heavy metal partitioning in sediments and bioaccumulation in commercial fish species of three major reservoirs of river Cauvery delta region, India. Ecotoxicology and environmental safety, 113, 145-151.

Dominik, J., Förstner, U., Mangini, A., Reineck, H.E., 1978. 210Pb and 137Cs chronology of heavy metal pollution in a sediment core from the German Bight (North Sea). Senckenbergiana maritima 10, 213-227.

Dougherty, A. J., Dickson, M.E., 2012. Sea level and storm control on the evolution of a chenier plain, Firth of Thames, New Zealand. Marine Geology 307, 58-72.

Duncan, M., Woods, R., 2004. Flow regimes. In: Harding, J.S., Mosley, M.P., Pearson, C.P., Sorrell, B.K. (eds.). Freshwaters of New Zealand, 7.1-7.14. New Zealand Hydrological Society and New Zealand Limnological Society, Christchurch.

Eade, J. V., 1974 Poor Knights Sediments. New Zealand Oceanographic Institute Chart, Coastal Series 1:200,000.

Eisma, D., 1981. Supply and deposition of suspended matter in the North Sea. Holocene Marine Sedimentation in the North Sea Basin, 415-428.

Eisma, D., Kalf, J., 1987. Dispersal, concentration and deposition of suspended matter in the North Sea. Journal of the Geological Society 144 (1), 161-178.

Ek, A. S., Renberg, I., 2001. Heavy metal pollution and lake acidity changes caused by one thousand years of copper mining at Falun, central Sweden. Journal of paleolimnology 26 (1), 89-107.

Eriksson, J. A., Qvarfort, U., 1996. Age determination of the Falun copper mine by 14C-datings and palynology. GFF 118 (1), 43-47.

Fergusson, J.E. (ed.), 1990. The Heavy Elements: Chemistry, Environmental Impact and Health Effects. Pergamon Press, Oxford

FGG Elbe, 2010. Elbebericht 2008 – Ergebnisse des nationalen Überwachungsprogramms Elbe und der Bundesländer über den ökologischen Zustand der Elbe nach EG-WRRl sowie der Trendentwicklung von Stoffen und Schadstoffgruppen. Flussgemeinschaft Elbe, Hamburg.

Figge, K., 1981. Karte der Sedimentverteilung in der Deutschen Bucht (No. 2900). Deutsches Hydrographisches Institut, Hamburg.

Förstner, U., Müller, G., 1973. Heavy metal accumulation in river sediments: a response to environmental pollution. Geoforum 4 (2), 53-61.

Förstner, U., Reineck, H.E., 1974. Die Anreicherung von Spurenelementen in den rezenten Sedimenten eines Profilkerns aus der Deutschen Bucht. Senckenbergiana maritima 6, 175-184.

Glasby, G.P., Stoppers, P., Walter, P., Davis, K.R., Renner, R. M., 1988. Heavy-metal pollution in Manukau and Waitemata Harbours, New Zealand. New Zealand journal of marine and freshwater research, 22(4), 595-611.

Godwin, H., 1962. Half-life of radiocarbon. Nature 195 (4845).

Geyh, M.A., Schleicher, H., 2012. Absolute age determination: physical and chemical dating methods and their application. Springer Science & Business Media.

Greig, D. A., 1982 Sediments and recent geological history of the Hauraki Gulf, Firth of Thames and Colville Channel, North Island, New Zealand. PhD Thesis, University of Auckland.

Greig, M.J., Proctor, R., 1988. A numerical model for the Hauraki Gulf, New Zealand. New Zealand Journal of marine and freshwater research 22 (3), 379-390.

Greig, M.J., 1990. Circulation in the Hauraki Gulf, New Zealand. New Zealand journal of marine and freshwater research 24 (1), 141-150.

Guyard, H., Chapron, E., St-Onge, G., Abselmetti, F., Amaud, F., Magand, O., Francus, P., Mèlières, M.A., 2007. High-altitude varve records of abrupt environmental changes and

mining activity over the last 4000 years in the Western French Alps (Lake Bramant, Grandes Rousses Massif). Quaternary Science Reviews 26 (19), 2644-2660.

Haas, H.C., 1993. Depositional processes under changing climate: Upper Subatlantic granulometric records from the Skagerrak (NE-North Sea). Marine Geology 111 (3-4), 361-378.

Hamburg Port Authority, 2015. Umgang mit Baggergut aus dem Hamburger. Teilbericht. Umlagerung von Baggergut nach Neßsand, Jahresbericht 2014 Hafen, Freie und Hansestadt Hamburg, Hamburg.

Hanebuth, T.J.J., Lantzsch, H., 2008. A Late Quaternary sedimentary shelf system under hyperarid conditions: unravelling climatic, oceanographic, and sea-level controls (Golfe dÀrguin, Mauritania, NW Africa) Marine Geology 256 (1), 77-89.

Hanebuth, T.J.J., Henrich, R., 2009. Recurrent decadal-scale dust events over Holocene western Aftrica and their control on canyon turbidite activity (Mauritania). Quaternary Science Reviews 28 (3), 261-270.

Haug, G.H., Hughen, K.A., Sigman, D.M., Peterson, L.C., Röhl, U., 2001. Southward migration of the intertropical convergence zone through the Holocene. Science 293 (5533), 1304-1308.

Hauraki Gulf Forum, 2011. State of our Gulf – Tikapa Moana – Hauraki Gulf State of the Environment Report. Auckland: Hauraki Gulf Forum.

He, Z.L., Yang, X.E., Stoffella, P.J., 2005. Trace elements in agroecosystems and impacts on the environment. Journal of Trace Elements in Medicine and Biology 19 (2), 125-140.

Hebbeln, D., Scheurle, C., Lamy, F., 2003. Depositional history of the Helgoland mud area, German Bight, North Sea. Geo-Marine Letters 23 (2), 81–90.

Hebbeln, D, Knudsen, K.-L., Gyllencreutz, R., Kristensen, P., Klitgaard-Kristensen, D., Backman, J., Scheurle, C., Jiang, H., Gil, I., Smelror, M., Jones, P.D., Sejrup, H.-P., 2006. Late Holocene coastal hydrographic and climate changes in the eastern North Sea. The Holocene 16 (7), 987-1001.

Heier-Nielsen, S., Heinemeier, J., Nielsen, H.L., Rud, N., 1995. Recent reservoir ages for Danish fjords and marine waters. Radiocarbon37 (3), 875-882.

Hertweck, G., 1983. Das Schlickgebiet in der inneren Deutschen Bucht. Aufnahme mit dem Sedimentechographen. Senckenbergiana maritima 15 (4/6), 219–249.

Higham, T. F. G., Hogg, A.G., 1995 Radiocarbon dating of prehistoric shell from New Zealand and calculations of the ΔR value using fish otoliths. Radiocarbon 37 (2), 409-416.

Hinrichs, J., Dellwig, O., Brumsack, H.J., 2002. Lead in sediments and suspended particulate matter of the German Bight: natural versus anthropogenic origin. Applied Geochemisty 17 (5), 621-632.

Hochstein, M.P., Nixon, I.M., 1979. Geophysical study of the Hauraki Depression, North Island, New Zealand, New Zealand Journal of Geology and Geophysics 22 (1),1-19.

Hochstein, M.P., Tearney, K., Rawson, S., Davey, F.J., Davidge, S., Henry, S., Backshall, D., 1986. Structure of the Hauraki Rift (New Zealand. Royal Society of New Zealand Bulletin 24, 333-348.

Holzwarth, U., Meggers, H., Esper, O., Kuhlmann, H., Freudenthal, T., Hense, C., Zonneveld, K.A., 2010. NW African climate variations during the last 47, 000 years: evidence from organic-walled dinoflagellate cysts. Paleogeography, Paleoclimatology, Palaeocology 291 (3), 443-455.

Hong, S.M., Candelone, J.P., Patterson, C.C., Boutron, C.F., 1994. Greenland ice evidence of hemispheric lead pollution 2 millennia ago by Greek and Roman civilizations. Science 265 (5180), 1841-1843.

Hong, S., Candelone, J.-P., Patterson, C.C., Boutron, C.F., 1996. History of ancient copper smelting pollution during Roman and medieval times recorded in Greenland ice. Science 272 (5259), 246-249.

Hong, S., Candelone, J.P., Boutrom, C.F., 1997. Changes in zinc and cadmium concentrations in Greenland ice during the past 7760 years. Atmospheric Environment 31 (15), 2235-2242.

Howarth, R.W., Anderson, D.B., Cloern, J.E., Elfring, C., Hopkinson, C.S., Lapointe, B., Maloney, T.J., Marcus, N., McGlathery, K., Sharpley, A.N., Walker, D., 2000. Issues in ecology: Nutrient pollution in coastal rivers, bays, and seas.

Hurrell, J., 1995. Decadal trends in the North Atlantic Oscillation: regional temperatures and precipitation. Science-AAS-WEEKLY Paper Edition 269 (5224), 676-679.

Itambi, A.C., con Dobeneck, T., Mulitza, S., Bickert, T., Heslop, D., 2009. Millennial-scale northwest African droughts related to heinrich events and Dansgaard-Oeschger cycles: evidence in marine sediments from offshore Senegal. Paleoceanography 24 (1).

Irion, G., Wunderlich, F., Schwedhelm, E. 1987. Transport of clay minerals and anthropogenic compounds into the German Bight and the provenance of fine-grained sediments SE of Helgoland. Journal of the Geological Society of London 144 (1), 153–160.

Jaffe, D., Cerundolo, B., Rickers, J., Stolzberg, R., Baklanov, A., 1995. Deposition of sulphate and heavy metals on the Kola Peninsula. Science of the Total Environment 160, 127-134.

Jahn, B., Schneider, R.R., Mueller, P.J., Donner, B., Röhl, U., (2005). Response of tropical African and East Atlantic climates to orbital forcing over the last 1.7 Ma. Geological Society, London. Special Publications 247 (1), 65-84.

Jansen, H.F., van der Gaast, S.J., Koster, B., Vaars, A.J., 1998. CORTEX, shipboard XRF-scanner for element analyses in split sediment cores. Marine Geology 151 (1), 143-153.

Jansen, K., 2003. X-Ray Fluorescence Analysis. Handbook of Spectroscopy, 363-420.

Kelley, J. A., Jaffe, D.J., Baklanov, A., Mahura, A., 1995. Heavy metals on the Kola Peninsula: aerosol size distribution. Science of the total environment 160, 135-138.

Kelly, S., Sim-Smith, C., Faire, S., Pierre, J., Hikuroa, D., 2014. State of our Gulf 2014. Hauraki Gulf-Tikapa Moana/Te Moananui s Toi. State of the Environment Report 2014. Hauraki Gulf Forum.

Kersten, M., Dicke, M., Kriews, M., Naumann, K., Schmidt, D., Schulz, M., Schwokowski, M., Steiger, M., 1993. Distribution and fate of heavy metals in the North Sea. In: Pollution of the North Sea (pp 300-347). Springer Berlin Heidelberg.

Kido, Y., Koshikawa, T., Tada, R., 2006. Rapid and quantitative major element analysis method for wet fine-grained sediments using an XRF microscanner. Marine Geology 229 (3), 209–225.

Kienlin, T. L., Bischoff, E., Opielka, H., 2006. Copper and bronze during the Eneolithic and Early Bronze Age: a metallographic examination of axes from the Northalpine region. Archaeometry 48(3), 453-468.

Kim, N., 2007. Trace elements in sediments of the lower eastern coast of the Firth of Thames. Environment Waikato Technical Report 2007/08, Environment Waikato, Hamilton.

Kissel, C., Laj, C., Kienast, M., Bolliet, T., Holbourn, A., Hill, P., Kuhnt, W., Braconnot, P., 2010. Monsoon variability and deep oceanic circulation in the western equatorial Pacific over the last climatic cycle: Insights from sedimentary magnetic properties and sortable silt. Paleoceanography 25 (3).

Knudsen, K.L., Conradsen, K., Heier-Nielsen, S., Seidenkrantz, M.S., 1996. Paleoenvironments in the Skagerrak-Kattegat basin in the eastern North Sea during the last deglaciation. Boreas 25 (2), 65-77.

Kuijpers, A., Dennegård, B., Albinson, Y. and Jensen, A., 1993a. Sediment transport pathways in the Skagerrak and Kattegatt as indicated by sediment Chernobyl radioactivity and heavy metal concentrations. In: Liebezeit, G., van Weering, T.C.E., Rumohr, J (eds.), Holocene Sedimentation in the Skagerrak. Marine Geology 111 (3-4), 231-244.

Kuijpers, A., Werner, F., Rumohr, J., 1993b. Sandwaves and other large-scale bedforms as indicators of non-tidal surge currents in the Skagerrak off northern Denmark. In: Liebezeit, G., van Weering, T.C.E., Rumohr, J. T (Editors), Holocene Sedimentation in the Skagerrak. Marine Geology 111 (3-4), 209-221.

Leblanc, M., Morales, J. A., Borrego, J., Elbaz-Poulichet, F., 2000. 4,500-year-old mining pollution in southwestern Spain: long-term implications for modern mining pollution. Economic Geology, 95 (3), 655-662.

Lee, S.V., Cundy, A.B., 2001. Heavy metal contamination and mixing processes in sediments from the Humber Estuary, Eastern England. Estuarine, Coastal and Shelf Science 53 (5), 619-636.

Lepland, A., Andersen, T.J., Lepland, A., Arp, H.P.H., Breedveld, G.D., Rindby, A., 2010. Sedimentation and chronology of heavy metal pollution is Oslo Harbor, Norway. Marine pollution bulletin 60 (9), 1512-1522.

Leung, H.M., Leung, A.O.W., Wang, H.S., Ma, K.K., Liang, Y., Ho, K.C., Cheung, K.C., Tohidi, F., Yung, K.K.L., 2014. Assessment of heavy metals/metalloid (As, Pb, Cd, Ni, Zn, Cr, Cu, Mn) concentrations in edible fish species tissue in the Pearl River Delta (PRD), China. Marine pollution bulletin, 78(1), 235-245.

Li, M.S., Luo, Y.P., Su, Z. Y., 2007. Heavy metal concentrations in soils and plant accumulation in a restored manganese mineland in Guangxi, South China. Environmental pollution, 147 (1), 168-175.

Li, Z., Ma, Z., van der Kuijp, T.J., Yuan, Z., Huang, L., 2014. A review of soil heavy metal pollution from mines in China: pollution and health risk assessment. Science of the Total Environment 468, 843-853.

Lohse, L., Malschaert, J.F.P., Slomp, C.P., Helder, W., van Raaphorst, W., 1995. Sediment-water fluxes of inorganic nitrogen compounds along the transport route of organic matter in the North Sea. Ophelia 41 (1), 173-197.

Longva, O., Thorsnes, T. (Eds.), 1997. Skagerrak in the past and at the present: an integrated study of geology, chemistry, hydrography and microfossils ecology (No. 8). Norges Geologiske Undersøkelse.

Lotze, K., Reise, K., Worm, B., van Beusekom, J., Busch, M., Ehler, A., Heinrich, D., Hoffmann, R.C., Holm, P., Jensen, C., Knottnerus, O.S., Langhanki, N., Prummel, W., Vollmer, M., Wolff, W.J.. 2005. Human transformations of the Wadden Sea ecosystem through time: a synthesis. Helgoland Marine Research 59 (1), 84-95.

Lowe, D.J., Newnham, R.M., McFadgen, B.G., Higham, T.F.G., 2000. Tephras and New Zealand archaeology. Journal of Archaeological Science 27 (10), 859-870.

Lowe, J.J., Walker, M.J.C., 2014. Reconstructing Quaternary Environments. Routledge.

Lundqvist, G., 1963. Falu gruvas ålder i geologisk och arkeologisk belysning. Almqvist & Wiksell, Uppsala, Sweden, 77 pp. (in Swedish).

Mackay, K.A., Mackay, E.J., Neil, H.L., Mitchell, J.S., Bardsley, S.A., 2012. Hauraki Gulf. NIWA Chart, Miscellaneous Series 91.

Madsen, P.P., Larsen, B., 1986. Accumulation of mud sediments and trace metals in the Kattegat and the Belt Sea. Miljøstyrelsens Havforureningslaboratorium.

Manighetti, B., Carter, L., 1999 Across-shelf sediment dispersal, Hauraki Gulf, New Zealand. Marine Geology 160 (3), 271-300.

Manville, V., Wilson, C. J. N. 2004. The 26.5 ka Oruanui eruption, New Zealand: A review of the roles of volcanism and climate in the post-eruptive sedimentary response. New Zealand Journal of Geology and Geophysics 47(3), 525-547.

Marshall, J., Kushnir, Y., Battisti, D., Chang, P., Czaja, A., Dickson, R., Hurrell, J., McCartney, M., Saravanan, R., Visbeck, M., 2001. North Atlantic climate variability: phenomena, impacts and mechanisms. International Journal of Climatology 21 (15), 1863-1898.

Matschullat, J., Ellminger, F., Agdemir, N., Cramer, S., Ließmann, W., Niehoff, N , 1997. Overbank sediment profiles – evidence of early mining and smelting activities in the Harz Mountains, Germany. Applied Geochemistry 12 (1), 105-114.

Mayer, B. (1995). Ein dreidimensionales, numerisches Schwebstoff-Transportmodell mit Anwendung auf die Deutsche Bucht. Dissertation, Universität Hamburg.

McCave, I.N., Bryant, R.J., Cook, H.F., Coughanowr, C.A., 1986. Evaluation of laser-diffraction-size analyser for use with natural sediments. Journal of Sedimentary Research 56 (4).

McGlone, M.S., Wilmshurst, J.M., 1999. Dating initial Maori environmental impact in New Zealand, Quaternary International 59 (1), 5-16.

Miller, H., Croudace, I.W., Bull, J.M., Cotterill, C.J., Dix, J.K., Taylor, R.N., 2014. A 500 year sediment lake record of anthopogenic and natural inputs to Windermere (English lake District) using double-spike lead isotopes, radiochronology, and sediment microanalysis, Environmental Science and Technology 48 (13), 7254-7263.

Milliman, J.D., Eade, R.H., 1983. World-wide delivery of river sediment to the oceans. The Journal of Geology, 91 (1), 1-21.

Mitchell, J.S., Mackay, K.A., Neil, H.L., Mackay, E.J., Pallentin, A., Notman, P., 2012. Undersea New Zealand, 1:5,000,000. NIWA Chart, Miscellaneous Series 92.

Monna, F., Hamer, K., Lévêque, J., Sauer, M., 2000. Lead isotopes as a reliable marker of early mining and smelting in the Northern Harz province (Lower Saxony, Germany) Journal of Geochemical Exploration 68 (3), 201-210.

Nilsson, N., 1998. Falu koppargruvas ålder och föroreningsbelastning av koppar och bly i sjön Runn under 1000 år, Miljö- och hälsoskydd. MH1998:20. Umeå universitet, Umeå

Nolting, R. F., Eisma, D., 1988. Elementary composition of suspended particulate matter in the North Sea. Netherlands Journal of Sea Research 22 (3), 219-236.

Nordberg, K. 1991. Oceanography in the Kattegat and Skagerrak over the past 8000 years. Paleoceanography 6 (4), 461-484.

Nriagu J.O., 1990. Global metal pollution: poisoning the biosphere? Environment: Science and Policy for Sustainable Development 32 (7), 7–33.

Ortlam, D. 1989. Geologie, Schwermetalle und Salzwasserfronten im Untergrund von Bremen und ihre Auswirkungen. Neues Jahrbuch für Geologie und Paläontologie Mh 8 , 489-512.

Olausson, E., 1975. Man-made effect on sediments from Kattegat and Skagerrak. GFF 97 (1), 3-12.

OSPAR Commission, 2000. Quality Status Report 2000, Region II – Greater North Sea. OSPAR Commission, London. 136 + xiii pp.

Pache, T., Brockamp, O., Clauer, N. 2008. Varied pathways of river-borne clay minerals in a near-shore marine region: A case study of sediments from the Elbe- and Weser rivers, and the SE North Sea. Estuarine, Coastal and Shelf Science 78 (3), 563-575.

Pederstad, K., Roaldset, E., Rønningsland, T.M., 1993. Sedimentation and environmental conditions in the inner Skagerrak-outer Oslofjord. Marine Geology 111(3-4) 245-268.

Pinedo, S., Jordana, E., Flagella, M.M., Ballesteros, E., 2014. Relationships between heavy metals contamination in shallow marine sediments with industrial and urban development in Catalonia (Northwestern Mediterranean Sea). Water, Air & Soil Pollution.

Pittauerová, D., 2013. Gamma spectrometry for chronology of recent sediments (Doctoral dissertation, Staats- und Universitätsbibliothek, Bremen.

Pocknall, D. T., Gregory, M. R., Greig, D. A., 1989 Palynology of core 80/20 and its implications for understanding Holocene sea level changes in the Firth of Thames, New Zealand. Journal of the Royal Society of New Zealand 19 (2), 171-179.

Proctor, R., Greig, M.J., 1989. A numerical model investigation of the residual circulation in the Hauraki Gulf, New Zealand. New Zealand journal of marine and freshwater 23 (3), 421-442.

Puls, W., Pohlmann, T.H., Sündermann, J., 1997. Suspended Particulate Matter in the Southern North Sea: Application of a Numerical Model to Extend NERC North Sea Project Data Interpretation. Deutsche Hydrografische Zeitschrift 49 (2-3), 307-327.

Qvale, G., van Weering, T.C.E., 1985. Relationship of surface sediments and benthic foraminiferal distribution patterns in the Norwegian Channel (northern North Sea. Marine Micropaleontology 9 (6), 469-488.

Qvarfort, U., 1984. The influence of mining on Lake Tisken and Lake Runn. Bulletin of the geological Institution of the University Upsala 10, 111-130.

Reimer, P.J., Reimer, R.W., 2001. A marine reservoir correction database and on-line interface. Radiocarbon 43 (2a), 461-463.

Reimer, P.J., Bard, E., Bayliss, A., Beck, J.W., Blackwell, P.G., Bronk Ramsey, C., Buck, C.E., Cheng, H., Edwards, R.L., Friedrich, M., Grootes, P.M., Guilderson, T.P., Haflidason, H., Hajdas, I., Hatte, C., Heaton, T.J., Hoffmann, D.L., Hogg, A.G., Hughen, K.A., Kaiser, K.F., Kromer, B., Manning, S.W., Niu, M., Reimer, R.W., Richards, D.A., Scott, E.M., Southon, J.R., Staff, R.A., Turney, C.S.M., van der Plicht, J., 2013. IntCal13 and Marine13 Radiocarbon Age Calibration Curves 0–50,000 Years cal BP. Radiocarbon 55 (4), 1869-1887.

Reineck, H.E., 1963. Sedimentgefüge im Bereich der südlichen Nordsee. Abhandlungen der Senckenbergischen Naturforschenden Gesellschaft 505, 1-138.

Reineck, H.E., Gutmann, W.F., Hertweck,G., 1967. Das Schlickgebiet südlich Helgoland als Beispiel rezenter Schelfablagerungen. Senckenbergiana lethaea 48, 219-275.

Renberg, I., Wik-Persson, M., Emteryd, O., 1994. Pre-industrial atmospheric lead contamination detected in Swedish lake sediments. Nature 368 (6469), 323-326.

Renberg, I., Brännvall, M.-L., Bindler, R., Emteryd, O., 2001. Atmospheric lead pollution history during four millennia (2000 BC to 2000 AD) in Sweden. AMBIO: A Journal of the Human Environment 29 (3), 150-156.

Rijnsdorp, A.D., Buys, A.M., Storbeck, F., Visser, E.G., 1998. Micro-scale distribution of beam trawl effort in the southern North Sea between 1993 and 1996 in relation to the trawling frequency of the sea bed and the impact on benthic organisms. International Council for Exploration of the Seas, Journal of Marine Sciences 55 (3), 403-419.

Rodhe, J., 1987. The large-scale circulation in the Skagerrak; interpretation of some observations. Tellus, 39 (3), 245-253.

Rodhe, 1996. On the dynamics of the large-scale circulation of the Skagerrak. Journal of Sea Research 35 (1-3), 9-21.

Rodhe, J., Holt, N., 1996. Observations of the transport of suspended matter into the Skagerrak along the western and northern coast of Jutland. Journal of Sea Research 35 (1-3), 91-98.

Rodhe, J., 1998. The Baltic and North Seas: A process-oriented review of the physical oceanography. In: Robinson, A.R., and Brink, K.H. (eds.): The Sea. John Wiley & Sons, Inc., 699-732.

Röhl, U., Bralower, T.J., Norris, R.D., Wefer, G., 2000. New chronology for the late Paleocene thermal maximum and its environmental implications. Geology 28, 927-930.

Rotstigen, A.B., 2009. Benthic foraminifera as a proxy for natural versus anthropogenic environmental change in the German Bight, North Sea: a record over the last 1000 years. Master of Geosciences, University of Oslo, Oslo.

Salomons, W., Forstner, U., Mader, P. (eds.), 2012. Heavy metals: problems and solutions. Springer Science & Business Media.

Scheurle, C., Hebbeln, D., 2003. Stable oxygen isotopes as recorders of salinity and river discharge in the German Bight, North Sea. Geo-Marine Letters 23 (2), 130-136.

Scheurle, C., Hebbeln, D., Jones, P., 2005. An 800-year reconstruction of Elbe river discharge and German Bight sea-surface salinity. Holocene 15 (3), 429-434.

Schofield, J. C. 1970. Coastal sands of Northland and Auckland. New Zealand Journal of Geology and Geophysics 13 (3), 767-824.

Schulz, H.D., 1981. Die Kupferverhüttung auf Helgoland im Mittelalter. Offa, Berichte und Mitteilungen zur Urgeschichte, Frühgeschichte und Mittelalterarchäologie 38, 365-376.

Serna, A., Pätsch, J., Dähnke, K., Wiesner, M.G., Hass, C.H., Zeiler, M., Hebbeln, D., Emeis, K.C. 2010. History of anthropogenic nitrogen input to the German Bight/SE North Sea as reflected by nitrogen isotopes in surface sediments, sediment cores and hindcast models. Continental Shelf Research 30 (15), 1626-1638.

Sharples, J., 1997. Cross-shelf intrusion of subtropical water into the coastal zone of Northern New Zealand. Continental shelf research 17 (7), 835–857.

Sikes, E.L., Nodder, S.D., Howard, M.E., 2009. Sources of organic matter in a coastal marine environment: Evidence from n-alkanes and their δ13C distributions in the Hauraki Gulf, New Zealand. Marine Chemistry 113 (3), 149-163.

Smith, A.M., 1992. Aspects of the sedimentology of New Zealand bryozoans and mixed carbonate–clastic deposits: a contribution to the Temperate Shelf Carbonate model. Unpublished PhD Thesis, University of Waikato.

Smith, V.H., 2003. Eutrophication of freshwater and coastal marine ecosystems a global problem. Environmental Science and Pollution Research 10 (2), 126-139.

Smolders, A.J.P., Lock, R. A. C., Van der Velde, G., Hoyos, R.M., & Roelofs, J.G.M., 2003. Effects of mining activities on heavy metal concentrations in water, sediment, and macroinvertebrates in different reaches of the Pilcomayo River, South America. Archives of Environmental Contamination and Toxicology, 44 (3), 0314-0323.

Stuiver, M., Polach, H.A., 1977. Discussing reporting of ^{14}C data. Radiocarbon 19 (3), 355-363.

Stuiver, M., Reimer, P.J., and Reimer, R.W., 2017, CALIB 7.1 [WWW program] at http://calib.org.

Sutton, D. G. (Ed.), 1994. Origins of the First New Zealanders. Auckland: Auckland University Press.

Svansson, A., 1975. Physical and chemical oceanography of the Skagerrak and the Kattegat, I: Open sea conditions. Fischery Board Sweden, Institute of Marine Research Report, 1, 1-88.

Svendsen, E., Bemtsen, J., Skogen, M., Ådlandsvik, B., Martinsen, E., 1996. Model simulation of the Skagerrak circulation and hydrography during SKAGEX. Journal of Marine Systems, 8 (3-4), 219-236.

Syvitski, J.P.M., 1991. Principles, methods and application of particle size analysis, Cambridge University Press, Cambridge.

Taylor, R., Smith, I., 1997. The state of New Zealand's environment 1997. Environment.

Tchounwou, P.B., Yedjou, C.G., Patlolla, A. K., Sutton, D.J., 2012. Heavy metal toxicity and the environment. In Molecular, clinical and environmental toxicology (pp. 133-164). Springer Basel.

Thrasher, G.P., 1986. Basement structure and sediment thickness beneath the continental shelf of the Hauraki Gulf and offshore Coromandel region, New Zealand, New Zealand Journal of Geology and Geophysics, 29 (1), 41-50.

Tjallingii, R., Röhl, U., Kölling, M., Bickert, T., 2007. Influence of the water content on X-ray fluorescence core scanning measurements in soft marine sediments. Geochemistry, Geophysics, Geosystems. 8 (2), 1-12.

Uhle, M.E., Sikes, E.L., Nodder, S.D., Pilditch, C.A., 2007. Sources and diagenetic status of organic matter in the Hauraki Gulf, New Zealand: Evidence from the carbon isotopic composition of D- and L-amino acids. Organic Geochemistry 38 (3), 440-457.

Van Weering, T.C.E., 1981. Recent sediments and sediment transport in the North Sea: surface sediments of the Skagerrak. In: S.D. Nio, R.T.E. Schittenhelm and T.C.E. van Weering (Editors), Holocene Marine Sedimentation in the North

Van Weering, T.C.E., Qvale, G., 1983. Recent sediments and foraminiferal distribution in the Skagerrak, north-eastern North Sea. Marine Geology 52 (1-2), 75-99.

Van Weering, T.C.E., Rumohr, J., Liebezeit, G., 1993a. Holocene sedimentation in the Skagerrak: A review. Marine Geology 111.3-4, 379-391.

Van Weering, T.C.E., Berger, G.W., Okkels, E., 1993b. Sediment transport, resuspension and accumulation rates in the north-eastern Skagerrak. Marine Geology 111 (3-4), 269-285.

Vink, R.J., Behrendt, H., Salomons, W., 1999a. Point and diffuse source analysis of heavy metals in the Elbe drainage area: comparing heavy metal emissions with transported river loads. In: Man and River Systems (pp. 307-314). Springer Netherlands.

Vink, R., Behrendt, H., Salomons, W., 1999b. Development of the heavy metal pollution trends in several European rivers: an analysis of point and diffuse sources. Water Science and Technology 39 (12), 215-233.

Von Haugwitz, W., Wong, H.K., Salge, U., 1988. The mud area southeast of Helgoland: A reflection seismic study. Mitteilungen aus dem Geologisch-Paläontologischen Institut der Universität Hamburg 65, 409–422.

Von Storch, H., Costa-Cabral, M., Hagner, C., Feser, F., Pacyna, J., Pacyna, E., Kolb, S., 2003. Four decades of gasoline emissions and control policies in Europe: a retrospective assessment. Science of the Total Environment 311 (1), 151-176.

Waycott, M., Duarte, C.M., Carruthers, T.J., Orth, J.R., Dennison, W.C., Olyarnik, S., Calladine, A., Fourqurean, J.W., Heck, K.L., Hughes, A.R., Kendrick, G.A., Kenworthy, W.J., Short, F.T., Williams, S.L., 2009.Accelerating loss of seagrasses across the globe threatens coastal ecosystems. Proceedings of the National Academy of Sciences 106 (30), 12377-12381.

Weltje, G.J., Tjallingii, R., 2008. Calibration of XRF core scanners for quantitative geochemical logging of sediment cores: theory and application. Earth and Planetary Science Letters 274 (3), 423-438.

Wirth, H.A.N.S., Wiesner, M.G., 1988. Sedimentary facies in the North Sea. Mitteilungen des Geologisch-Paläontolgischen Instituts der Universität Hamburg, 65, 269-287.

Xu, Y., Sun, Q., Yi, L., Yin, X., Wang, A., Li, Y., Chen, J., 2014. The source of natural and anthropgenic heavy metals in the sediments of the Minjiang River Estuary (SE China): implications for historical pollution. Science of the Total Environment 493, 729-736.

Zeiler, M., Schulz-Ohlberg, J., Figge, K., 2000. Mobile Sand deposits and shore-face sediment dynamics in the inner German Bight (North Sea). Marine Geology 170 (3), 363-380.

Zeldis, J. R., R. A. Walters, M. J. N. Greig, and K. Image, 2004. Circulation over the north-eastern New Zealand continental slope, shelf and adjacent Hauraki Gulf, during spring and summer. Continental Shelf Research 24 (4), 543-561.

Zijlema, M., 2010. Computation of wind-wave spectra in coastal waters with SWAN on unstructured grids. Coastal Engineering 57 (3), 267-277.

Zöllmer, V., Irion, G., 1993. Clay mineral and heavy metal distributions in the north-eastern North Sea. Marine Geology 111 (3-4), 223-230.

Zuther, M., Brockamp, O., Clauer, N., 2000. Composition and origin of clay minerals in Holocene sediments from the south-eastern North Sea. Sedimentology 47 (1), 119-134.